令和 2 年度

長岡技術科学大学大学院　工学研究科

博士後期課程　博士論文

Effects of Residual Stress and Coating Thickness on Fatigue Behavior of TiAlN Coated Titanium Alloys

TiAlN コーティングで被覆したチタン合金の疲労挙動に及ぼす残留応力および皮膜厚さの影響

令和 3 年 1 月 29 日

長岡技術科学大学大学院工学研究科

情報・制御工学専攻
学籍番号　16700286
NithyaGnana Poorani Sivagnanam Chandra

指導教員　大塚 雄市 准教授
Supervisor Associate Professor OTSUKA Yuichi

長岡技術科学大学
Nagaoka University of Technology

Graduate School of Engineering
Nagaoka University of Technology

Abstract

Student ID: 16700286

Name: NithyaGnana Poorani Sivagnanam Chandra

Fatigue behavior of titanium alloys such as Ti6242S and gamma TiAl was investigated as they are widely used as high performance material in gas turbine engine components due its high specific strength, oxidation resistance and erosion resistance. To further improve their fatigue life in those applications, surface modification was carried out by coating those materials with TiAlN which has enhanced oxidation, wear and erosion resistance. Initially the fatigue test was conducted at room temperature for uncoated and then for coated specimens. TiAlN coating was done under different substrate bias voltages. In the first part of this study, coating done under lower bias voltages exhibits degraded fatigue life than that of uncoated specimen where the fatigue crack initiate from the coating layer surface. Whereas the coated specimen under higher bias voltages exhibits enhanced fatigue life than uncoated specimen where the fatigue crack initiate from the subsurface of the substrate. The compressive residual stress induced in the coating layer was significantly increased with increasing bias voltage, which dominantly influence the fatigue behavior and fatigue mechanism of coated specimens by supressing the crack to initiate from the coating layer thereby improves the fatigue life especially in the case of high bias voltage coating. In the second part of this study, the optimum coating thickness that enhances the fatigue life is investigated for two titanium alloys coated with TiAlN under lower and higher bias voltages, in which the specimens were coated with various types of thickness for each bias voltage. Under the same applied stress amplitude, the optimum thickness for the longest fatigue life was unchanged regardless of the bias voltage. The conclusion obtained in the present study is that there exists optimum thickness and the reason is explained based on the variation of fatigue crack initiation mechanisms of the coated specimen depending on the coating thickness. As a third part of study, the fatigue strength tests of TiAlN coated Ti-alloys were carried out to investigate the suitable coating process condition for avoiding the degradation of fatigue strength and ensuring the enhanced fatigue strength of TiAlN coated Ti-alloys. For that, a critical

relationship between the applied stress and bias voltage is formulated for proper selection of bias voltage. The coating process condition that avoids degradation of fatigue life of coated specimen was recommended by the investigation results. Overall from the study, the titanium alloy specimens coated with TiAlN under higher negative bias voltages with a moderate coating thickness exhibits enhanced fatigue life in which compressive residual stress plays a dominant role in their enhanced fatigue behavior. Based on the critical relationship between normalized applied stress amplitude and bias voltages, a suitable selection method of bias voltage for avoiding the fatigue life degradation of TiAlN coated Ti-alloy were discussed.

.

Table of Contents

List of Figures

Chapter 1 Introduction

1.1 GENERAL CONSIDERATIONS

Future gas turbine engine components and aircraft engines need high performance materials that can withstand high operating temperatures. The primary consideration in selecting the new materials for such applications is to keep the weight minimum. In the high pressure section of gas turbine engine components, Ti6242S titanium alloy is broadly used with an operating temperature of 538°C [1]. At room and high temperature, these applications demand good combination of high specific strength and adequate errosion/oxidation resistance. In aeroengine applications, higher thrust and improved fuel efficiency are the major requirements, which focuses the attraction towards TiAl-based alloys. In the compressor part and low pressure part of gas turbine engines in aerospace applications these intermetallic alloys are considered as a candidate to replace for conventional titanium alloys and Ni-based superalloys respectively, because of their high temperature strength, less density and good oxidation resistance. For the past two decades research activities were targeted in developing gamma alloy, In automotive engines, γ -TiAl alloys are preferred as suitable material for rotors of turbocharger [2] and for turbine blades in General Electric's GENx engines[3].Till now the greatest achievement in TiAl technology is that the cast Ti-47Al-2Cr-2Nb alloy, successfully passed the certification of FAR33 in 2007 for GEnx engines that power the B787.The strength of these titanium alloys under fatigue can be enhanced in both room and elevated temperature by applying a protective coating over it. The role of coating processing conditions on the strength of those titanium alloys under fatigue have been regarded as promising with respect to the development of coated high performance materials for room temperature and high temperature applications.

1.2 Ti6242S TITANIUM ALLOY

Ti6242S titanium alloy exhibits bimodal microstructure comprising of α phase with crystal structure of hexagonal close packed and β phase with the crystal structure of body centered cubic. At about 993 $^\circ$ C, $\alpha - \beta$ transformation temperature or β- transus occurs in Ti6242S. The α stabilizer Al and interstitials (C,O and N) raise the β –transus. Mo is a β stabilizer [4]. By solid solution strengthening mechanism, Zr and Sn strengthen the α phase with slight effect on β –transus [4]. Compared to the β phase, α phase has low ductility and greater strength [5] and hence act as a main strengthening phase in this alloy. By the formation of a protective TiO2 oxide film, Ti offers better oxidation and corrosion resistance in different oxidising/corrosive environment [4] . In Ti6242S titanium alloy, the α stabilizer Al, increases the tensile strength, creep strength and moduli while the alloy density is decreased. Al exhibits maximum solid solution strengthening limitedly because about 7% of Al enhances ordering and formation of Ti3Al associated with embrittlement. Tin is an α stabilizer with less potential and is a solid solution strengthener which is used in conjunction with Al to obtain greater strength without embrittlement. Zirconium is a weak beta stabilising element that forms a continuous solid solution with titanium. At low and intermediate temperatures, Zirconium offers better strength. The ductility and creep strength may be decreased by the use of Zirconium at above 5-6%. The prime beta stabilizer in these titanium alloys is Molybdenum,that increases the heat treatment response of the alloys noticeably. The alloys that aimed at long term creep strength like Ti6242S have lower molybdenum content. In high temperature titanium alloys, Silicon is a vital element, as it increases strength at all temperatures and also has a noticeable advantageous effect on resistance over creep. Small amount of silicon i.e., from 0.1% to 0.5%Si decreases the stacking fault energy of the alloy comparing with other alloy systems. By hindering the cross slip the addition of Si declines the mobility of the dislocations under stress.

1.3 TITANIUM ALUMINIDE BASE INTERMETALLIC COMPOUND

Intermetallic compounds are a phase formed at intermediate composition between two pure metallic elements. The crystal structure of these intermediate phase is different from both pure metallic elements. They exhibits good high temperature strength, lightness and stiffness. Among various classic intermetallic compounds, titanium aluminide base materials highlights in many applications due to their high specific strength. The investigations on TiAl and TiAl3 are more recent research works. Most of the research works were carried out on Ti3Al base intermetallic compound. The possible operating temperatures of titanium aluminide base materials are up to 1000°C and may eventually find applications in aero engine components and automotive turbocharger working in this temperature range. An attractive combination of elevated temperature oxidation and creep resistance, coupled with high specific strength and modulus, has led to intense interest in major structural and rotating components such as in engine components, these properties could increase the engine thrust to weight ratio.Several alloying elements can be introduced to obtain a better overall balance of properties.

1.4 PHYSICAL VAPOUR DEPOSITION OF COATING

he PVD (Physical Vapour Deposition) method is a coating method using an evaporation technique. By evaporating the coating material from a solid material, a flux of atomistic coating materials can be produced and then deposited over the object to be surface modified. The erosion and wear behavior of tools could be improved by hard coatings like borides, carbides or nitrides of the transitional metals. CVD or PVD methods of coating is preferred based on the temperature that exists during reaction that are permitted to avoid unwanted treatment that happens to the substrates. Ion bombardment occurs in all process of PVD except with simple thermal evaporation, which greatly influences higher residual stresses that can be observed during the deposition of coating material over the substrate. Every PVD process has three basic steps [6]: • Formation of vapour phase: This needs conversion of solid

state of material to be coat to vapour phase by evaporation, ion bombardment. • Movement of vapour from the target source to the substrate: The atoms emitted from the target will be moved through molecular flow conditions. • Growth of film on material surface: The moved molecule will start to nucleate around the substrate and grow by number of process. The incipient growth of the coating film determines the interfacial strength between substrate and coating.

1.4.1 Cathodic arc ion plating deposition of coating

Applications such as cutting tools, metal mold, etc. were subjected to coating technique of Cathodic arc plasma which is one of the potential ion plating technique in physical vapour deposition methods. With the technique of cathodic arc plasma TiAlN, TiN and CrN films are coated over cutting tools in industries to enhance their operationability. A cathode spot is created while an arc discharge is formed under medium and higher vacuum environment. There will be no formation of anodic spot .The coating material is evaporated by the cathode spot which is very active with higher temperature. A very dense plasma is formed at the cathode spot region, and evaporates the cathode material. The evaporated cathode material gets ionized and these ionized material gets deposited over the surface to be coated as a solid film. In physical vapour depositions (PVDs) , arc deposition plays a vital role that bears merits of higher ion energy, comparing to the other PVD techniques. In cathodic arc technique the ion source is in solid form so crucible is not required, therefore the solid source is fixed on the wall of chamber where process is undertaken. The ions generated in the vacuum environment are prone to react with the working gases due to their high energy. Arc Ion Plating technique deposits film on the substrate with fine structure and good adhesion, and it suits for wear and erosion resistant coatings. The applications such as cutting tools and sliding parts targets hard coating methods to meet the industrial requirements. For example of metals, ceramics, diamond like carbon, some semiconductors and superconductors , films are deposited by Cathodic arc deposition process which is handled either in a gaseous atmosphere of low pressure or at higher vacuum environment. To avoid the contaminants that are formed by micro droplet, the stream of plasma is filtered and the substrate bias controls

the energy of ions, this pays the path to transform the direct way of deposition method into hybrid one with other surface modification methods such as ion beam mixing, ion beam–assisted deposition, and implantation of ions. For the processing of highlighted surfaces, this coating method plays as a vital tool of plasma. For the deposition of tribological and wear/erosion/corrosion-resistant ceramic coatings, cathodic arc evaporation PVD method get attracted widely in industrial and structural application due to its simplicity in the control of process, sophisticated to deposit multiple component and multilayer coatings with adaptability to huge coating deposition methods (scaleability).At the cathode spots, molten droplets get emitted from molten cathode material which are considered as a drawback in cathodic arc evaporation process. The ejected droplets forms porosity by the impingement of these droplets into the deposited film, which initiates corrosion for active substrates in corrosive prone environment [7].The formation of micro droplets could be reduced by some factors such as using the cathodes at higher melting point, minimizing the arc current, deflection of the cathode spot motion either by magnetic or electrostatic, arc shielding and by the creation of a compound layer of cathode by the reaction of gaseous reagents with cathode which has higher melting point (cathode poisoning) [8]. Majority of these methods affect the deposition rate markedly.

1.4.2 Working Principle of Arc Ion Plating method

Arc Ion Plating technique is a technique of film deposition by utilization of vacuum arc discharge between a target (coating film material)which act as a cathode and an anode, evaporating the materials in the target and ionizing them, and finally depositing it on the substrate surface (the component to be coated) to which negative substrate bias voltage is biased. This method exhibits the film deposition with good density and adhesion because of its enhanced ratio of the evaporated materials ionization .With the coating technique for cutting tools applications, as represented by (Ti, Al) N coating, the film deposited by this method is now synonymous.Figure 1.1.Shows the schematic of an Arc Ion Plating technique system. On the lateral side of a vacuum chamber in the AI Plating system, multiple evaporation sources with a plate target are equipped on it and a table of substrate is fixed in the vacuum chamber. To assure the even distribution of film thickness in the vertical direction and to make wider coating surface area, the multiple evaporation sources are arranged in the vertical direction. To coat more number of substrates evenly along the circumference, a rotating mechanism is equipped in the table where the substrate is fixed.

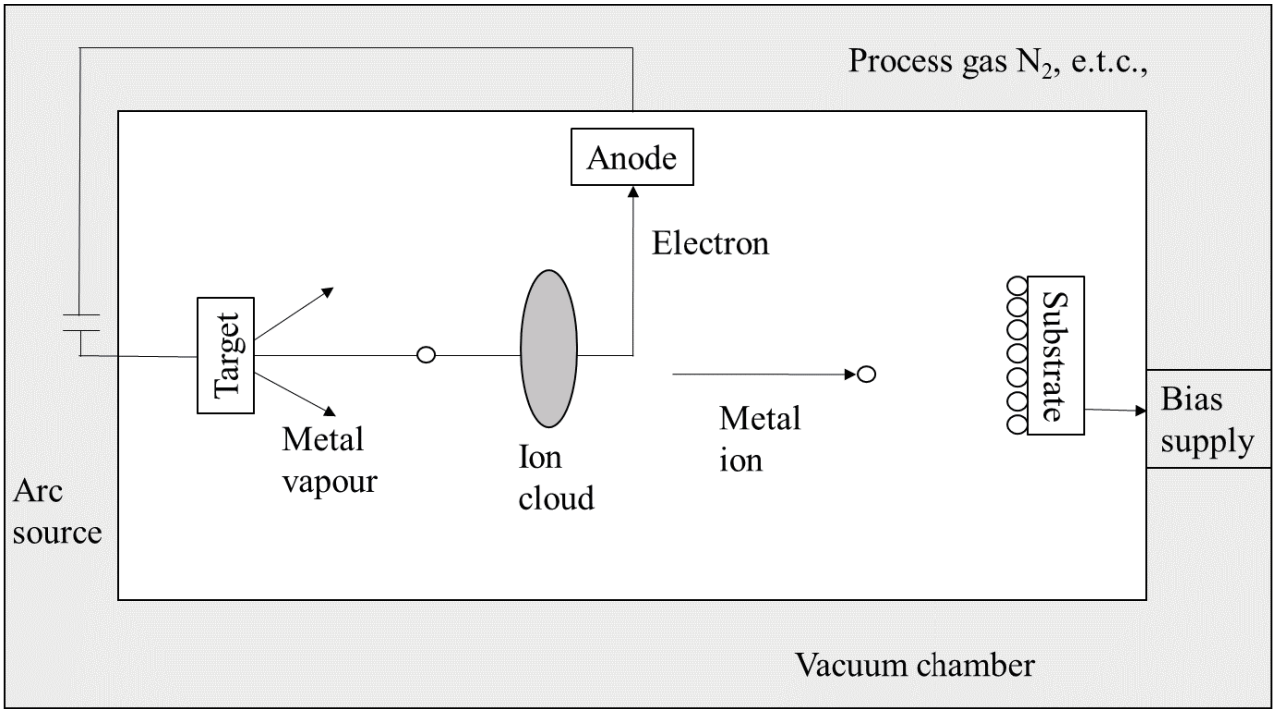

Fig. 1.1 Schematic of an AIP system.

1.4.3 Ion Energy Control

The energy of plasma ions in cathodic arc could be controlled which makes it meritable in many ways, provides a way for performing surface modification by ions similar to that of ion implantation , ion-beam-assisted deposition depending on the energy phase implemented. For controlling the ion energy, substrate bias is employed.

1.5 TITANIUM ALUMINIUM NITRIDE COATING

To enhance the surface behavior of industrial components, there exists major attraction on materials technology. By improving the surface properties of the materials, the behavior of resistance to wear, erosion and corrosion could be enhanced by the usage of transitional metal hard coatings. Thereby compounds of boron, nitrides and carbides are widely preferred in the industrial applications [9]. Their attractive properties like high hardness, good wear and chemical stability prolonged the study of transition metal nitrides thin films in detail. For improving the ternary and quaternary nitride coating properties multi/element nitrides had place in major consideration. As TiAlN thin film exhibits good resistance of oxidation [10] , greater hardness, lower frictional coefficient, and improved resistance of wear [11] it proves its place more genuine. In dry high speed machining and in conforming tools, TiAlN is considered as one of the prominent coatings [12] . Erosion, wear and corrosion resistant coatings are done over industrial components and cutting tools with Physical vapour deposition (PVD) [13] [14]. Many of the deposition methods such as physical vapour deposition (PVD) ion plating and chemical vapour deposition are utilized to make TiAlN films with the obtained film possessing the properties that markedly influenced by the parameters that are used during processing like (substrate temperature, working gas pressure, bias voltage of substrate, power of plasma, working gas flow rate). Figure 1.2 Illustrates the influence of surface modification for enhanced productivity with good quality and highly ecological.

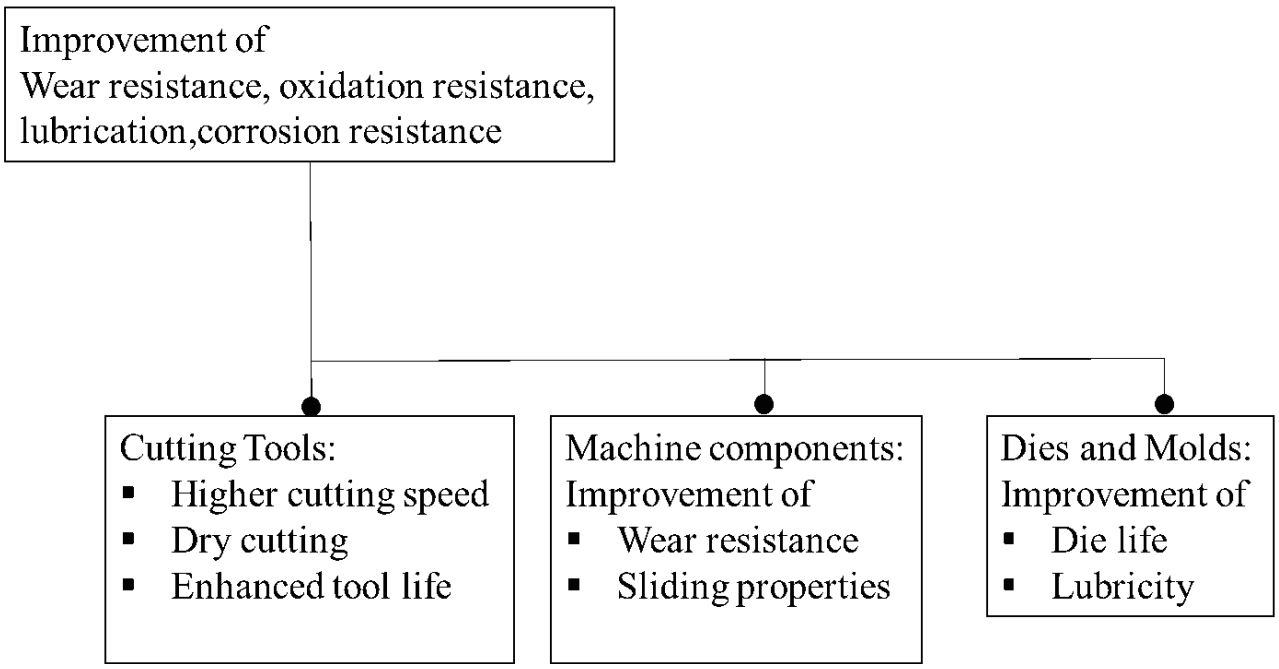

Fig. 1.2 Effect of surface modification.

1.6 SCOPE OF THIS WORK

Titanium alloy is a heat resistant and light weight material, which is used for high pressure compressor or low pressure turbine blade or impeller of turbo-charger, replacing heavy Ni based superalloy. The density of Nickel based superalloy is 9.0 g/ cm^3, whereas the density of α-TiAl is 3.9g/ cm^3 which highlights the consideration of titanium alloys in gas turbine engine applications with improved thrust to weight ratio in place of nickel based superalloys. Though titanium alloys exhibit excellent high temperature properties, wear and erosion resistance, as well as light weight, their wear and erosion resistance at high temperature have to be improved as the structural materials for turbine engine components. One of the promising technologies for this purpose is the TiAlN coating, as it exhibits improved oxidation resistance behavior in high temperature applications because of the reason that the aluminium oxide gets produced which in turn behave as a hindrance for the creation of oxidation in later timing. The characteristics of coating is greatly influence by the coating processing conditions such as substrate temperature, bias voltage, working gas pressure, deposition time, coating thickness e.t., However, so far no systematic investigation have yet examined and filed related on behavior of titanium alloys coated with TiAlN in fatigue regime, such as influence of coating process condition and effect of coating thickness, etc. To clarify the fatigue behavior of TiAlN coated titanium alloys is

essential for applying the TiAlN coated titanium alloy as a structural material to turbine engine components. There is, therefore, a need for investigating the coating processing conditions that can affect the fatigue characteristics of the titanium alloys coated with TiAlN . The aim of this study is to clarify the fundamental behavior of fatigue and mechanisms of fatigue on the titanium alloys coated with TiAlN and also to validate the significance of processing condition that have been handled during coating on the fatigue related characteristics of TiAlN coated titanium alloys in detail. The significant influence of coating proceeding variables such as bias voltage of substrate and coating thickness on the fatigue behavior of titanium alloys coated with TiAlN were investigated systematically. These kinds of systematic investigation have not been carried out and are new and original. The schematic framework of the present thesis work carried out is shown in Fig.1.3. In Chapter 2, to clarify the basic fatigue behavior and fatigue mechanisms of TiAlN coated titanium alloys, fatigue strength tests and detail fracture surface observation of the TiAlN coated Ti6242S titanium alloy were carried out. Surface crack initiation and propagation behavior was also measured by using the replica method. Based on the results, basic fatigue behavior, fatigue mechanisms and effect of bias voltage on them were discussed. In Chapter 3, since the coating thickness was kept to be 5 μm in the former chapters, fatigue strength tests of the TiAlN coated Ti6242S and γ-TiAl alloys with coating thicknesses of 1 μm, 5 μm and 15 μm have been used for the investigation on influence of thickness of coating over behavior of fatigue. Based on the results, the optimum thickness for the longest fatigue life and the reasons for the optimum thickness were discussed. In Chapter 4, since the fatigue behavior and fatigue strength of the coated titanium alloys was found to be intensively affected by the bias voltage in Chapter 2, to clarify the impact of substrate bias voltage on fatigue mechanism and its behavior for various substrate alloys, fatigue strength tests of TiAlN coated Ti6242 (as-rolled without solution treatment) and γ-TiAl alloys were carried out in addition to those of TiAlN coated Ti6242S alloy. Based on the results, the critical condition of bias voltage for avoiding fatigue strength degradation by TiAlN coating was also discussed. In Chapter 5, the general conclusions are summarized and future prospects are presented.

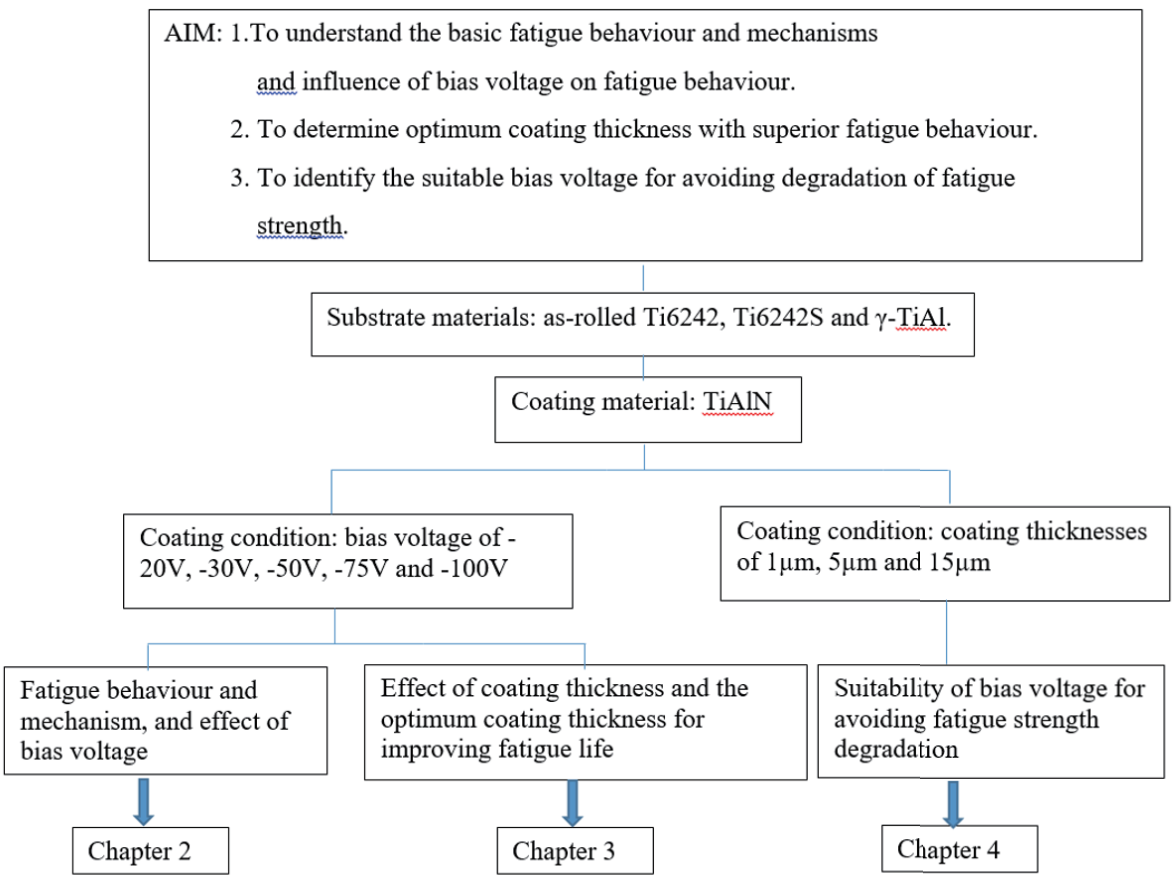

Fig. 1.3 Schematic framework of the thesis work carried out.

Chapter 2 Effect of bias voltages on fatigue behavior of TiAlN coated Ti6242S alloy

2.1 INTRODUCTION

Ti6242S titanium alloy with excellent high temperature strength compared to Ti64 alloy was developed in 1970s. It can be used at higher temperatures up to 565°C [15]. Since then, it has been extensively applied as one of the high specific strength heat resistant materials in jet engines, automotive parts and aerospace components. TiAlN coating on Ti6242S alloy has been recently applied for improving the resistance behaviour of Ti6242S components on corrosion and wear at high temperature. Titanium Aluminium Nitride kind of coatings are known as one of the most excellent coatings with excellent resistance to erosion, corrosion and wear accompanied with better resistance to oxidation at elevated temperatures. Synthesization of Titanium aluminium nitride type of coatings were carried out by many methodologies such as plating by arc ion [16], magnetron sputtering using direct current [17] and chemical vapour deposition with the assistance of plasma [18]. Industrial applications such as cutting tools, automotive parts, etc. have a great demand on usage of hard coatings and wear resistant coatings which are synthesized through cathodic arc ion plating. Modification on the properties of deposited films happens by the bias voltage that are biased to the substrate which induces the energy of ions. These modified deposited film properties were highly influenced by the magnitude, type and mode of bias voltage[19] [20] [21] [22].The coating processing conditions strongly influences the coating characteristics [23] [24] [25] [26]. TiAlN coating exhibits hardness to a maximum of 28-32GPa [27]. As the bias voltage increases, the hardness of TiAlN coatings approaches the highest value in which the coating layer possesses uniform and smooth columnar structure [28]. Additionally the composition of aluminium in the guarantees improved resistance to temperature until 800 degree celcius [29]. Aluminium oxide is formed as a dense, thin and good adhered layer of protection to behave as a hinderer for diffusion and thereby deteriorates wear that

occur by diffusion.[30] [31]. Fatigue behavior of Ti6242S alloy has been investigated. For example, fatigue mechanism and influence of dislocation interaction on crack nucleation in fatigue of Ti6242S alloy without coating have been investigated in [32] and [33], respectively. The fatigue life improvement of Ti6242S alloy at both room and elevated temperatures was achieved by applying the Pt ion plating on the surface of Ti6242S alloy [34] . However, publications investigating the fatigue behavior of TiAlN coated Ti6242S alloy could not be found. Therefore, detailed fatigue mechanism and properties as well as detailed effect of PVD condition such as bias voltage on fatigue strength of the TiAlN coated Ti6242S alloy have not yet been clarified. In the present chapter, as the first step of detailed investigation on fatigue behaviour of TiAlN coated titanium alloys, fatigue strength tests of STA-treated Ti6242S specimens with TiAlN coating deposited under various bias voltages have been carried out at room temperature to investigate basic fatigue characteristics and effect of bias voltage on fatigue strength. Measurements of hardness and residual stress of the coating layer, detail observations of crack nucleation and propagation behaviour on the surface of the coating as well as fatigue fracture surface observations were also carried out to discuss basic fatigue mechanisms of the TiAlN coated Ti6242S alloy.

2.2 EXPERIMENTAL PROCEDURE

2.2.1 Material

The substrate material used in the present chapter was an STA-treated Ti6242S titanium alloy, which was fabricated by casting and forging. Following STA heat treatment (Solution Treatment and Aging) was applied, where solution treatment was done at 979°C for 92min and then air cooling, and then aging was done at 593°C for 512min. Chemical composition of the material used is Al 6%, Sn 2%, Zr 4%, Mo 2%, Si 0.1% and Ti balance (in mass percentage). The ultimate tensile strength and yield strength of the material are considered as 1056MPa and 983MPa respectively [34]. Microstructure of the material is shown in Fig. 2.1.

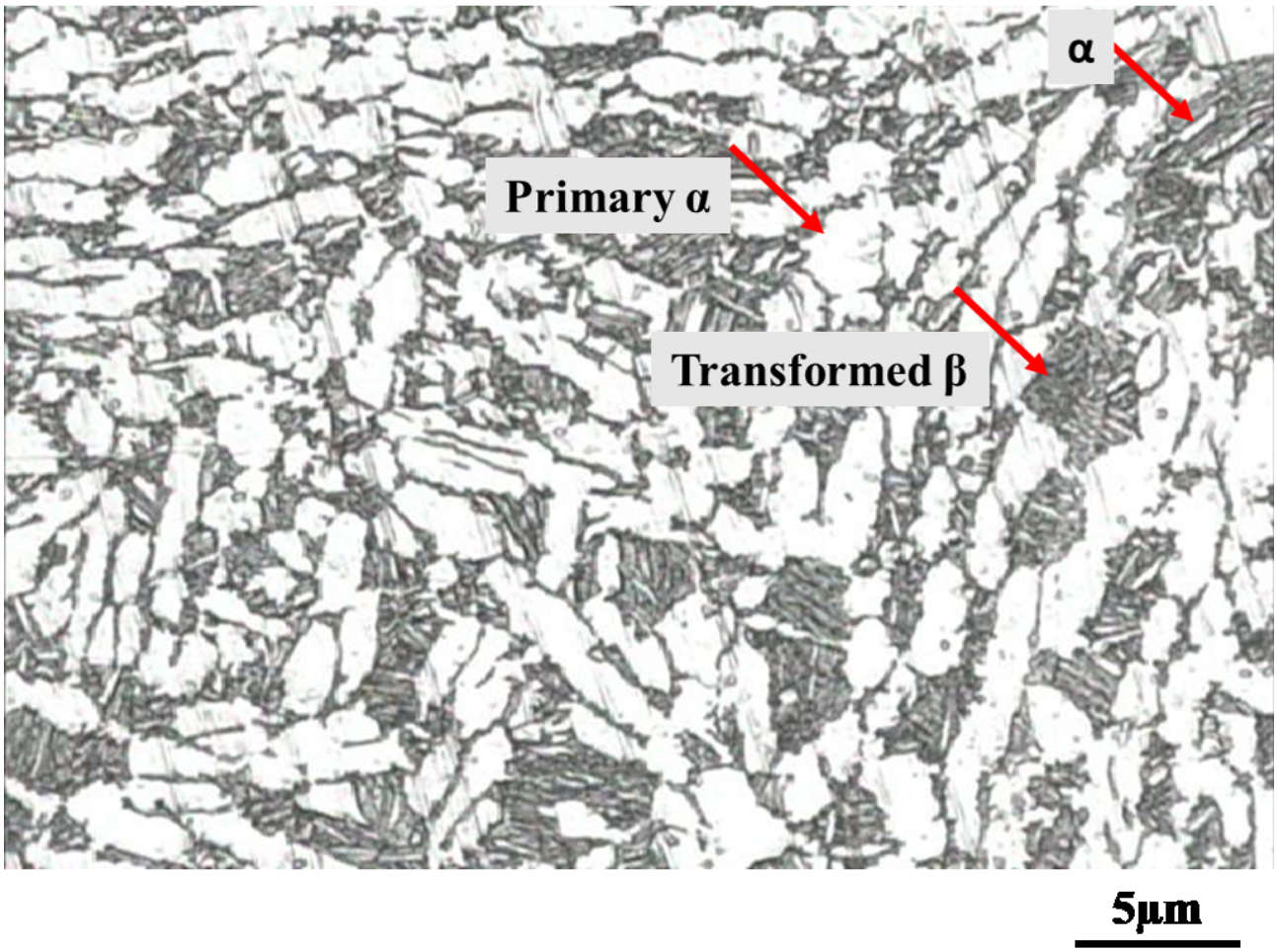

Fig. 2.1 Microstructure of STA-treated Ti6242S alloy.

2.2.2 Fatigue test specimen

The fatigue test specimen was a round bar tension type specimen, shape and dimensions of which are shown in Fig.2.2. In order to avoid any defects and micro cracks on the specimen surface that might be formed during machining processes, the specimen surface was successively polished by using #240,#320, #500,#800, # 1000,# 1500,# 2400, # 4000 SiC abrasive papers and buff polished using diamond pastes with particle sizes from 9μm to 1μm. Then the specimens were forwarded to the coating process. Some specimens were used for fatigue tests without coating. Before fatigue tests, the specimens were ultrasonically cleaned with acetone for 10 minutes.

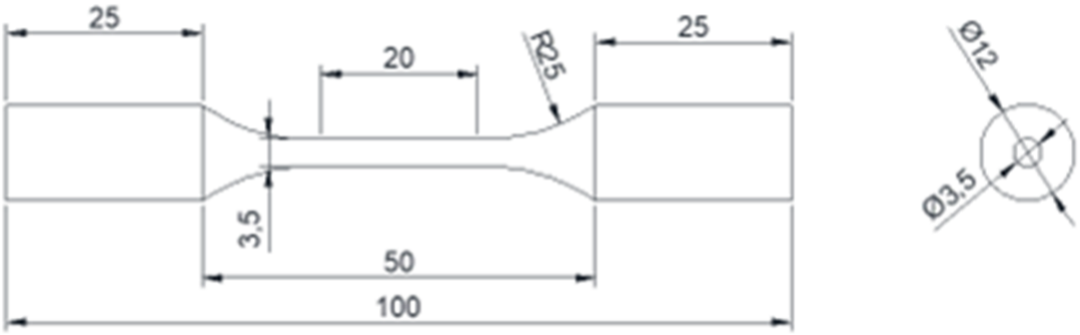

Fig. 2.2 Fatigue test specimen (All dimensions are in mm).

2.2.3 Coating Procedure

A cathodic arc ion plating system (AIP-SS002, Kobe Steel Ltd.) was used for the TiAlN coating. Ti50Al50 (at%) target was used for deposition. Prior to deposition, the substrate specimens were heated and plasma-etched using Ti metal ion bombardment. Pure reactive nitrogen atmosphere of 4Pa was used for the deposition process. The deposition was made at a temperature of 500°C under various substrate bias voltages to study their effects on fatigue behavior. No additional annealing effect on the hardness of the substrate material after the coating process could be found by the hardness measurements of the substrate material before and after coating process. The deposition duration was controlled to keep the coating thickness of approximately 5 μm for each bias voltage.

2.2.4 Fatigue test

Fatigue strength tests of STA-treated Ti6242S alloy specimens with and without TiAlN coating (hereinafter referred to as the coated specimen and the uncoated specimen, respectively) were carried out using a servo-hydraulic fatigue testing machine with a load capacity of 10 kN at room temperature in air under a stress ratio of 0.1 and a frequency of 20 Hz. The fatigue test was continued up to complete separation of the specimen. When the specimen was not fractured up to 10^7 cycles, the test was stopped. For the uncoated specimens, fatigue tests under various stress amplitudes were conducted to obtain basic S-N curve for STA-treated Ti6242S alloy. For the coated specimens, the fatigue tests were conducted at the same stress amplitude of 260 MPa to compare their fatigue lives with that of the uncoated specimen as well as to investigate effect of bias voltage on fatigue life. Surface crack observation by using a replica technique during the fatigue test was conducted to discuss crack nucleation and growth behavior. Replifix consisting of silicone rubber is used to take the replica of specimen surface. The test was repeatedly interrupted at every 5% of number of cycles to failure for taking the replica. The obtained replica was observed through a digital microscope for clear visualization to measure the surface crack length. Fractographic observation and elemental composition analysis were performed by using JEOL-scanning electron microscope (SEM) and energy dispersive X-ray spectrometry (EDX), respectively. Surface morphology of coating was also observed by using the SEM to identify the coating defects. Stylus Profilometer (Mitutoyo S-3000) was utilized to measure the surface roughness of the coating. Hardness of coating was evaluated by using Nano-indenter (Dynamic ultra-microhardness tester) with indentation load of 400 mN and indentation duration of 10 seconds. .

2.2.5 Measurement of residual stress

The stress induced in the coating layer during coating process creates intrinsic stress in it which is stated as residual stress.These stress have been measured through X ray Diffractometer multiple HKL method with X-ray tube Cu(Kα). The measurement of residual stress is done by $\sin^2 \phi$ technique [35] . This measurement of stress determination is carried out by calculating the spacing between interplanes of the vectors that scattered in various directions.These angular spacing is termed as ϕ and ψ. The diffraction method is done by averaging the mean value of spacing between interplanes for those grains which get reflected with the vector that scattered normal to crystal planes hkl. XRD method of diffraction calculation is carried out in the volume near to the surface. The measuring method is controlled by the extent of radiation absorption.

Residual stress was determined by measuring mutliple hkl reflections by glancing angle as shown in Figure 2.3.

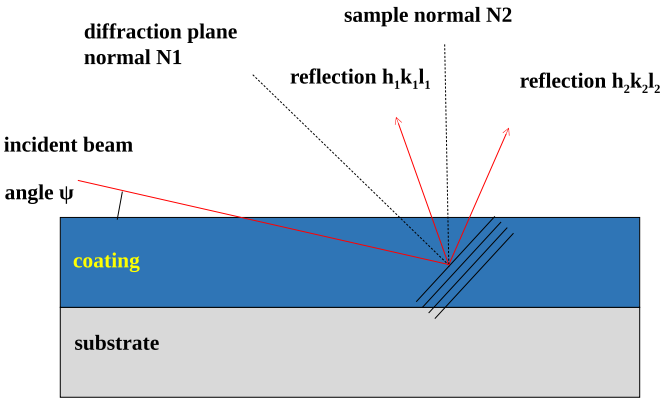

Fig. 2.3 Residual stress measurement.

2.2.6 Diffraction Analysis of Residual Stress State

The component that is normal to the surface of the specimen ε zz, is the evaluated component of residual elastic strain. The direction which is normal to the surface of the specimen is stated as

z- direction. Under the conditions of diffraction that occurs symmetrically,in which the diffracted rays and the incident x-rays exist at equal angles to the surface of specimen analysed, the interplanar spacing coplanar with the surface of specimen were determined. By comparing the d-spacing of a stressed region to that of an unstressed reference d-spacing, the elastic strain componenet ε zz can be assessed [36].

2.3 Result

2.3.1 Characteristics of the TiAlN coating layer

2.3.2 Surface morphology of TiAlN coating

The overall surface morphology of TiAlN coating looked smooth with some coating growth defects. It is known that the growth defects formed during coating process disturbs the uniformity of coating and would degrade the quality and strength of coating [37]. It can be found that the growth defects are not uniform in size. The distribution of defects in on the coating surface is was analysed by using binalization technique in VHX –Keyence digital microscope under x1000 magnification. The results of extreme statistical analysis of defect distribution of coatings deposited under different bias voltages are shown in Fig. 2.4. and Fig. 2.4. As seen from the figure, the maximum areas of defects distributed are reduced for the coating deposited under higher negative bias voltages. The average and maximum sizes of growth defect for each bias voltage have been measured from arbitrary ten locations with the area of 30 μm × 20 μm . The results are shown in Fig 2.5. As found from the figure, the average and maximum defect sizes decrease with increasing bias voltage. The maximum size of growth defect measured was found to be about 97.2 μm at the bias voltage of -20V.

The surface profile of TiAlN coating was evaluated by using a contact type stylus profilometer. The results showed that the average surface roughness values Ra for the bias voltages of -20V, -30V, -50V, -75V and -100V were 0.1 μm, 0.07 μm, 0.05 μm, 0.05 μm and 0.05 μm, respectively, which revealed that the average surface roughness slightly decreased with increasing bias voltage. It was

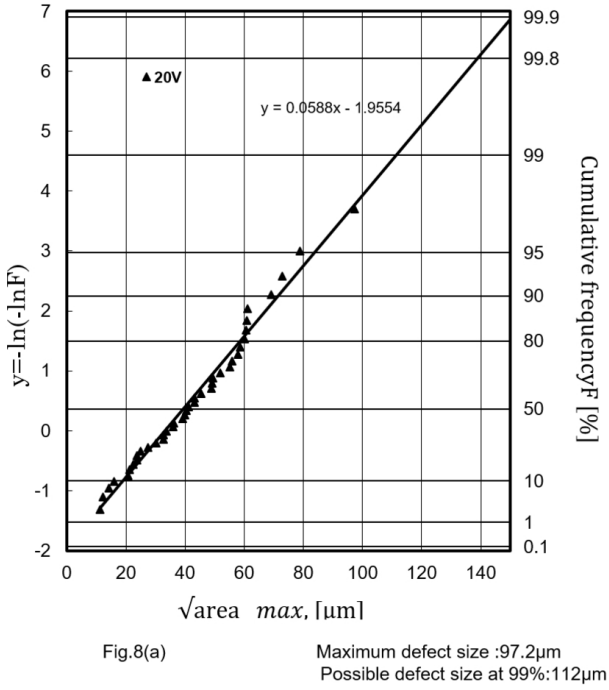

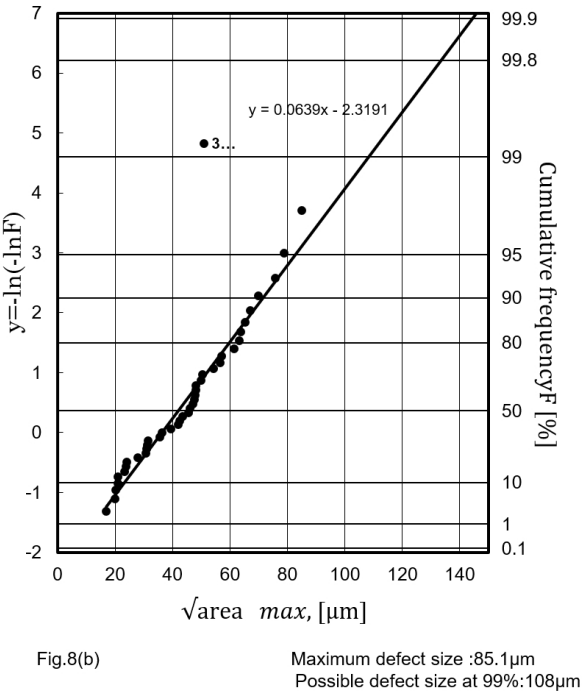

Fig. 2.4 Extreme statistic analysis of growth defects on the surface of coating layer deposited under various bias voltages on the STA-treated Ti6242S substrate (a)-20V,(b)-30V.

found from the EDX analysis that the chemical compositions of all TiAlN coatings in atomic percent were similar regardless of bias voltage, that is Ti in the range from 51.69 to 51.99 at%, Al in the range from 33.52 to 34.17 at% and N from 14.14 to 14.96 at%, and exhibited that the influence of bias voltage on chemical composition was not significant.

2.3.3 Residual stress in the coating layer

The compressive residual stress as a function of bias voltage is demonstrated in Fig. 2.6. As seen from the figure, the compressive residual stress significantly increased by 5.3 times from -1.5 to -8GPa (the minus sign indicates “compressive”) with increasing bias voltage from -20V to -100V. Similar increase in residual stress with increasing bias voltage for TiAlN coatings was reported in [38]. This increase of residual stress would be attributed to the ion peening effect as in the case of TiC coatings synthesized by a filtered cathodic arc technique [39] and in the case of magnetron sputtered TiN [40] and TiC[41] coatings. The input energy of irradiated ion, which produces the intrinsic stress in the coating layer, increases with increasing bias voltage. This increased intrinsic stress is the main reason

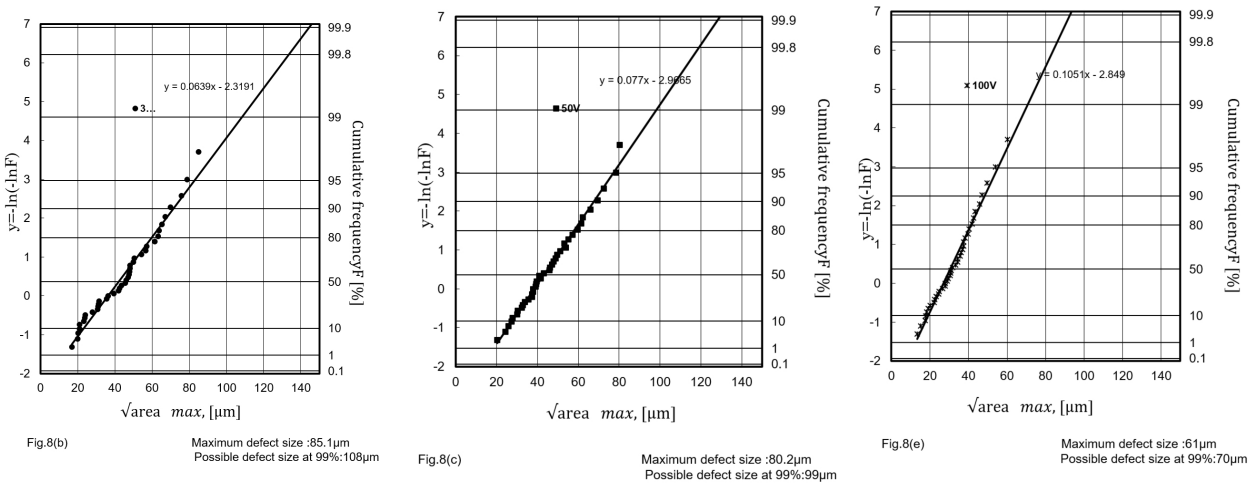

Fig. 2.5 Extreme statistic analysis of growth defects on the surface of coating layer deposited under various bias voltages on the STA-treated Ti6242S substrate (c)-50V and (d)-100V.

for the increased residual stress with increasing bias voltage.

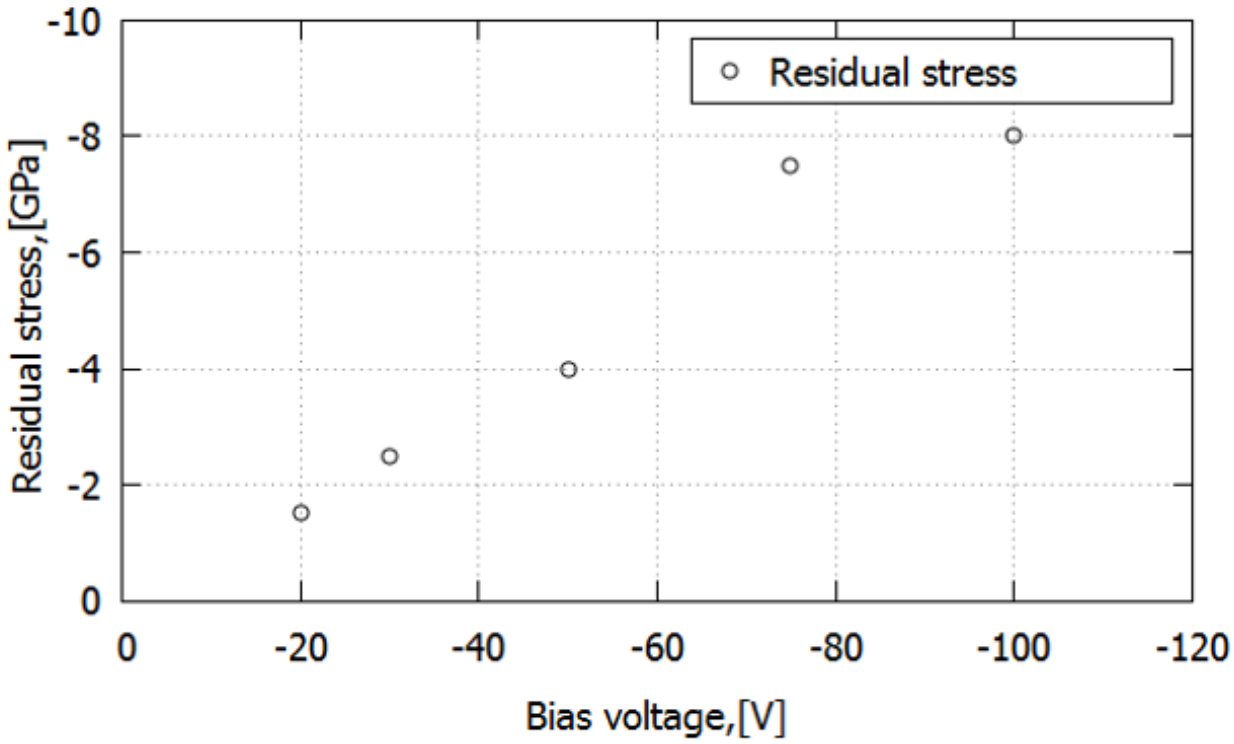

Fig. 2.6 Relationship between compressive residual stress of TiAlN coating layer and bias voltage.

2.3.4 Hardness of coating layer

The hardness values of TiAlN coating layer deposited under various bias voltages are plotted in Fig.2.7. As seen from the figure, the value of hardness increased by 1.3 times from 20.6GPa to

25.9GPa with increasing bias voltage from -20V to -100V. However, the increment of hardness with increasing bias voltage is not significant compared to the increment of compressive residual stress, as found by comparing Fig.2.7 with Fig. 2.6. Similar increase in hardness with increasing bias voltage for TiAlN coatings was reported in [28][38]. While the hardness variation would generally result from the grain size variation, the texture variation and the residual stress variation, it was concluded that the residual stress is the dominant factor for TiAlN coating [38][42]. Therefore, the higher hardness under higher bias voltage would mainly result from an increase of compressive residual stress at higher bias voltage. Consequently, the variation of intrinsic hardness due to the bias voltage would be much less than the variation of apparent hardness found in Fig..2.7

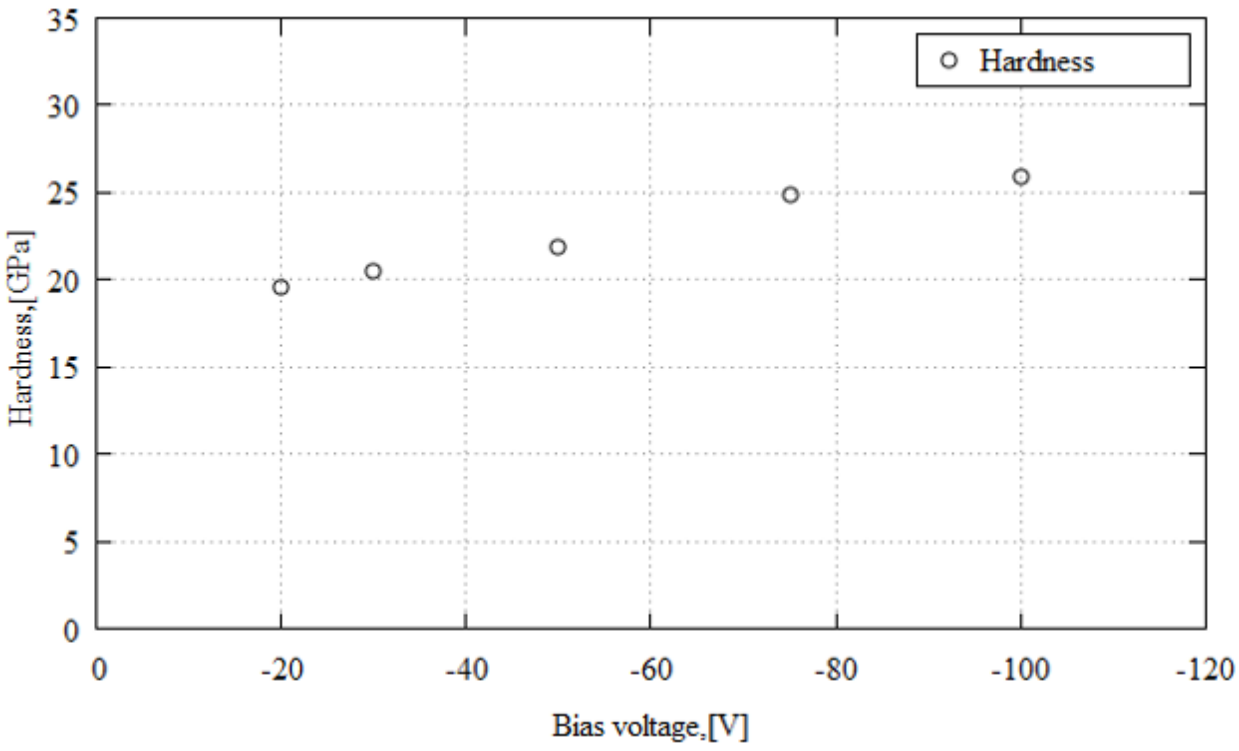

Fig. 2.7 Relationship between hardness of TiAlN coating and bias voltage.

2.3.5 Thickness of the coating layer

In order to confirm the thickness of the coating layer, the fracture surface topography of the coating layer deposited under various bias voltages was observed. All of coating layers tend to look more columnar, as shown in Fig.2.8. As seen from the same figure, the coating layer thickness was about 5

μm, which did not depend on the bias voltage. This same coating thickness regardless of bias voltage was realized by controlling the deposition duration.

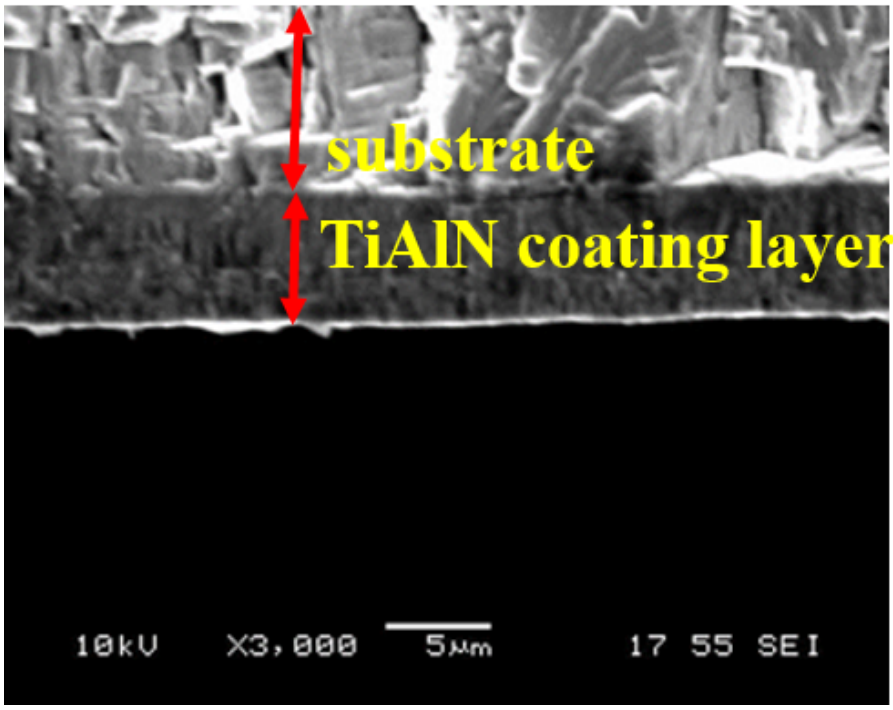

Fig. 2.8 SEM cross-sectional view of the TiAlN coating layer deposited under a bias voltage of -75V through secondary electron imaging.

2.3.6 Bias voltage

Negative bias voltage of substrate is a significant tool and an important coating process parameter to tailor the microstructure, structural morphology and mechanical properties of TiAlN coating. The control energy of the ions arriving at the substrate during the coating process is a greatly controlled by the negative bias voltage biased to the substrate. The coating properties and adhesion of coating to the substrate is greatly influenced by the applied bias voltage during a PVD process. The larger the bias voltage, the higher the film strength and endurance are. However, the film adhesion deteriorates by increasing the applied bias voltage to the substrate. At higher negative bias voltages, the ion bombardment induces the mobility of ad-atoms, which enhances the destruction of defects, increases the residual stress and consequently the hardness as well [43]. The substrate bias voltage could control the microstructure as the ion energy distribution changes. The microstructure of the TiAlN

coating deposited with negative bias voltage of -35 V exhibits a columnar structure with column widths of a few hundred nanometers. The change in substrate bias voltage to -70 V increases the ion energy during bombardment which results in a larger probability for re-nucleation of new grains and thus a smaller grain size [44].

From − 20 to − 50 V bias voltages, the process of generating defects seems to be the predominant one. In this bias range, the largest changes in mechanical and microstructure parameters could be observed. From − 50 to − 100 V bias voltages, the induced mobility of adatoms may have led to the annihilation of some defects, which is observed as not so a large change in mechanical and microstructural parameters. of -30V and -70V.

2.4 Fatigue strength of the uncoated and coated specimens

To obtain basic fatigue characteristics of the STA-treated Ti6242S substrate, fatigue strength tests of the uncoated specimens were carried out. The S-N curve for the uncoated specimen is shown in Fig 2.9. As seen from the figure, the fatigue strength at 10^7 cycles was about 200MPa. The fatigue test results of the coated specimens tested at 260 MPa, which was selected by referring the S-N curve of the uncoated specimen, are also shown in Fig. 2.9. As seen from the figure, the fatigue lives of the coated specimens deposited under low bias voltages of -20V and -30V were significantly degraded compared to that of the uncoated specimen. On the other hand, the coated specimens deposited under higher bias voltages of -50V, -75V and -100V exhibited the enhanced fatigue lives compared to that of the uncoated specimen.

2.5 Fracture surface observations for the uncoated and coated specimens

Overall fracture surfaces of the uncoated and coated specimens tested at 260MPa are shown in Fig. 2.10. Fatigue cracks seemed to nucleate from specimen surface for the uncoated specimen and the

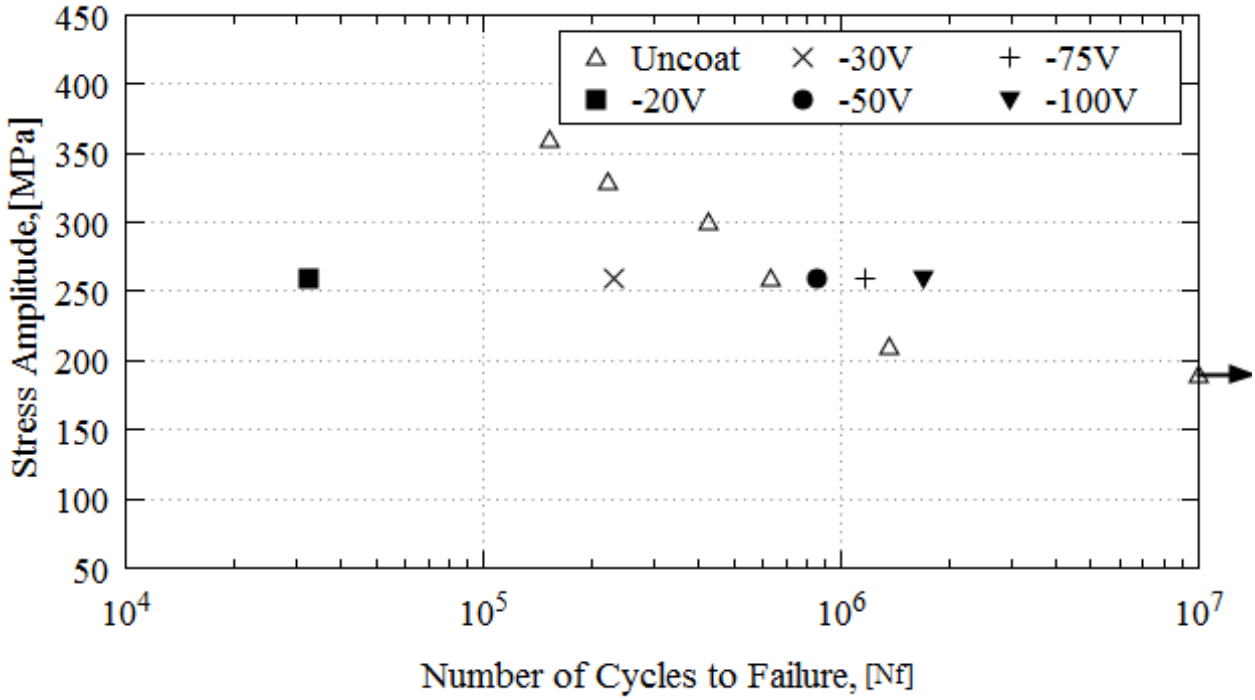

Fig. 2.9 Comparison of fatigue lives of the uncoated specimen and the coated specimens tested at a stress amplitude of 260MPa.

coated specimens deposited under bias voltages of -20V and -30V, while those for the coated specimens deposited under bias voltages of -50V, -75V and -100V seemed to nucleate from subsurface. To confirm the crack nucleation behavior in detail, higher magnification view of crack nucleation region for the coated specimens deposited under bias voltages of -20V and -100V are shown in Fig.2.11. From Fig.2.11 for the case of lower bias voltage -20V, flat and smooth surface without a step between coating layer and substrate was observed. The same flat and smooth surface was also observed for the bias voltage of -30V. On the other hand, from Fig. 2.11 for the case of higher bias voltage -100V, not-smooth surface with a step between coating layer and substrate was observed. The same not-smooth surface with a step was observed for the bias voltages of -50V and -75V. It is speculated that if the crack nucleates from surface of the coating and propagates into substrate, the crack propagates along the same flat plane without step between coating layer and substrate. It is also speculated that if the crack firstly nucleates and propagates inside the substrate and then the coating layer failed, a step between coating layer and substrate would be formed

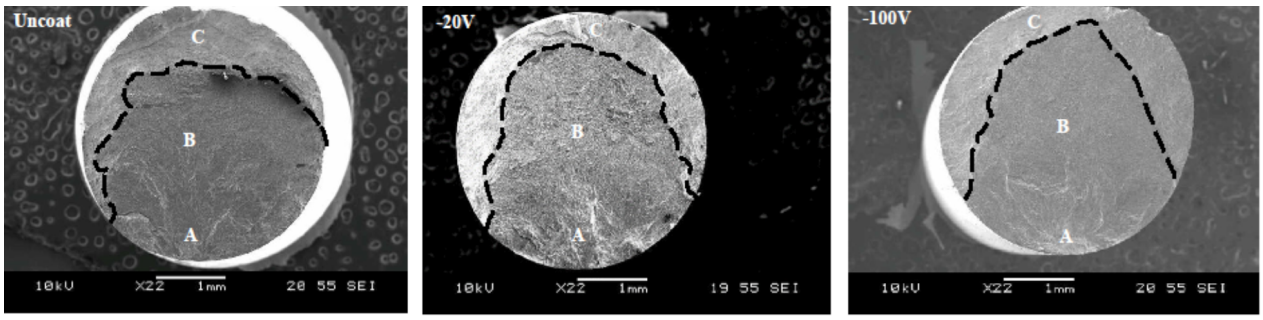

Fig. 2.10 Overall fracture surface view of the uncoated specimen and the coated specimens deposited under -20V and -100V.The marks A, B and C represent crack initiation region, crack propagation region and final fracture region, respectively.

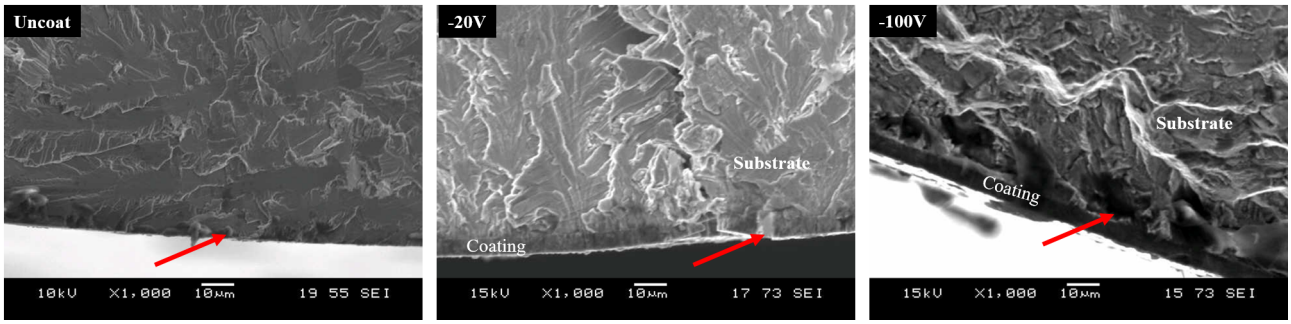

Fig. 2.11 Crack initiation region of the uncoated specimen and the coated specimens deposited under -20V and -100V.

2.6 Surface crack observations

Since fatigue crack nucleation mechanism might be different between the coated specimens deposited under lower and higher bias voltages, as discussed in the section 2.3.3, detail surface crack nucleation and propagation behavior was observed by the replica method. Since many micro-cracks were observed on the specimen surface and it was difficult to define which crack would be a main crack at early stage of crack nucleation, a main crack was firstly defined at later stage of crack propagation and then the main crack was inversely followed from the later stage to the early stage to confirm the crack propagation curve of the same main crack. Thus, the crack length of the main crack was measured on the replica taken at every 5 % of number of cycles to failure. From the results, relationships between crack length on the specimen surface and number of cycles are shown in Fig.2.12. In the figure, there is no data point for the coated specimen deposited under the bias voltage of -100V because no crack could be observed on the specimen surface until failure. From the figure, early crack nucleation was found for the coated specimens deposited under the bias voltages

of -20V and -30V compared to the uncoated specimen. On the other hand, the crack nucleation was delayed for the coated specimens deposited under the bias voltages of -50V, -75V and -100V compared to the uncoated specimen. From the results of surface crack observation shown in Fig.2.13, the relationship between the ratio of crack nucleation life and failure life, Ni /Nf and bias voltage is shown in Fig.2.13 . In the figure, the ratio of the uncoated specimen is shown at the bias voltage of 0V. From the figure, for the cases of bias voltages of -20V and -30V, the Ni/Nf values were almost equal or rather small compared to the uncoated specimen, which means fatigue crack nucleation of these coated specimens takes place in the early stage of life like the uncoated specimen. This result also suggests that the cracks nucleate from the coating layer for the cases of bias voltages of -20V and -30V. The specimens that are coated under the bias voltages of -50V shows the critical result of fatigue life enhancement compared to bias voltages of -20V and -30V, thereby it is identified as the higher bias voltage on or above which fatigue strength is improved. The compressive residual stress obtained in the coating layer is higher for the specimens coated with the bias voltage of -50V and higher than that, which is significantly influence the higher ratio of Ni/Nf in Figure 2.9 for the specimens coated with -50V and above, in which the higher value of compressive residual stress supresses the fatigue crack to initiate from the coating layer. On the other hand, the Ni/Nf values for the bias voltages of -50V, -75V and -100V are larger than that of the uncoated specimen, which means the fatigue crack cannot appear on the surface until longer cycles than Ni for the uncoated specimen, while a fatigue crack nucleates and propagates in the subsurface substrate before the crack appears on the surface, as discussed based on the fracture surface observations . Especially for the case of bias voltage of -100V, no cracks could be observed on the specimen surface until final fracture, but fatigue fracture feature was observed on the fracture surface, as shown in Fig. 2.11. This result clearly suggests that a fatigue crack nucleates and propagates in the substrate and the coating layer suppresses fatigue crack propagation and/or fracture of the coating layer until final fracture. The similar suppression of fatigue crack propagation due to hard surface layer with compressive residual stress in titanium alloys has been reported [45] and [46].

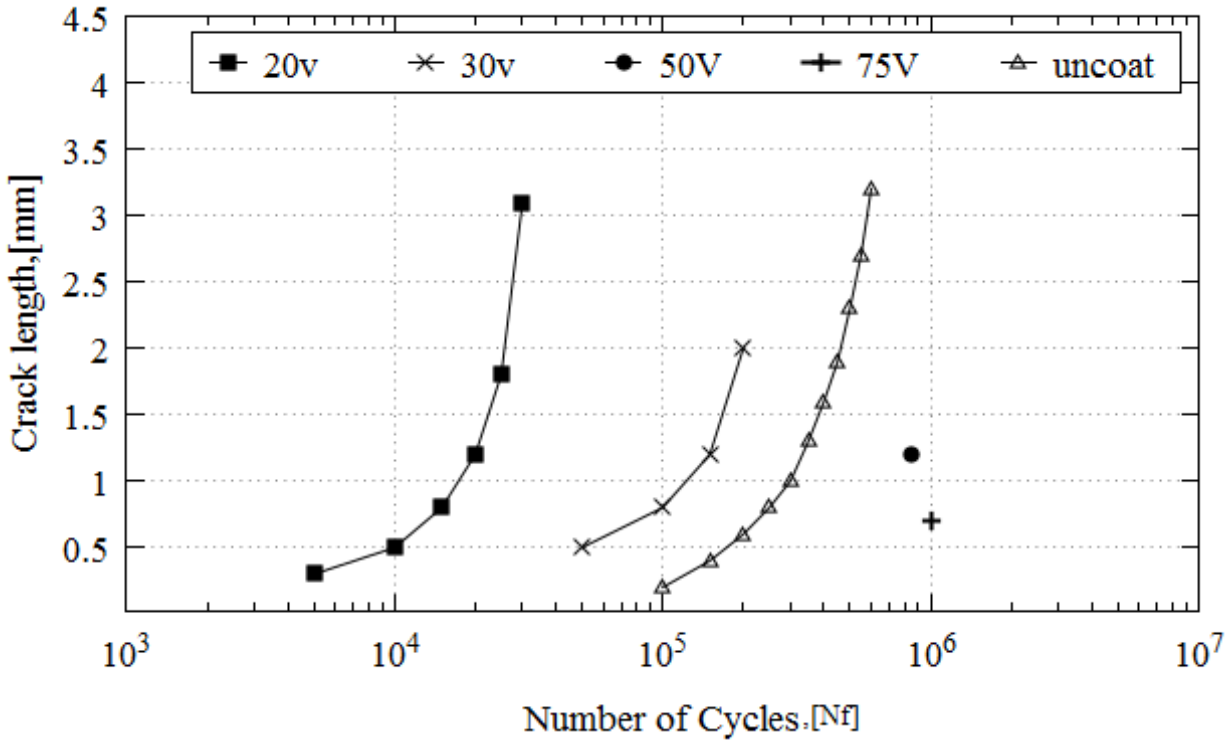

Fig. 2.12 Relationship between crack length on the specimen surface and number of cycles.

2.7 Discussion

2.7.1 Effect of coating growth defect on fatigue crack nucleation

Based on the coating surface observations, the average size and maximum size of the growth defects increased with decreasing bias voltage and the maximum size was about 97.2 μm at the bias voltage of -20V, as shown in Figure2.4 . In this section, it is discussed whether these growth defects could influence fatigue fracture behavior by assuming that the growth defect is a semi-circular surface crack with a same projected area of growth defect. The maximum size of an assumed semi-circular surface crack in the TiAlN coating layer under the lowest bias voltage of -20V can be estimated to be about 48.6μm from the projected area of 50 μm2 which is given by the maximum growth defect size of 97.2 μm and the coating layer thickness of 5 μm. On the other hand, the critical crack size for fatigue crack propagation is given by ElHadded et al equation [47]:

$$a = \frac{1}{\pi}\left(\frac{\Delta K_{th}}{\Delta \sigma_w}\right)^2 \quad \cdots\cdots (2.1)$$

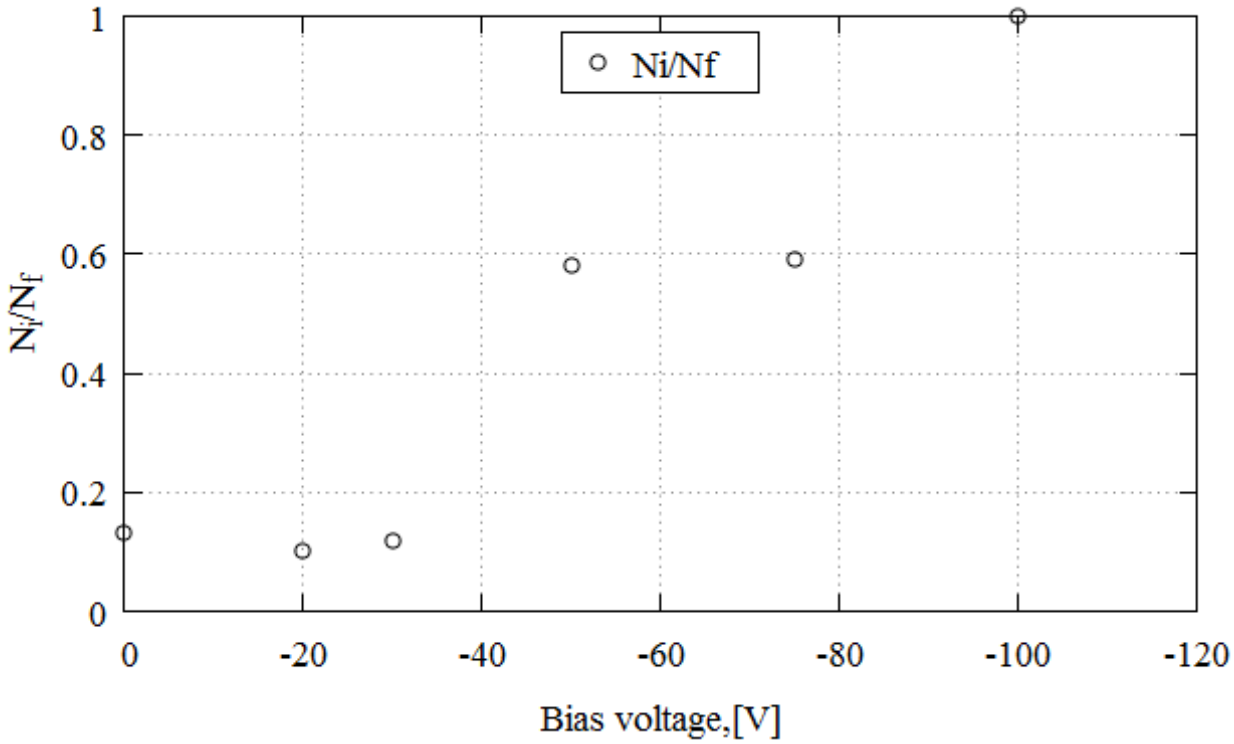

Fig. 2.13 Relationship between the ratio of crack initiation life and fatigue life, Ni /Nf and bias voltage, where the ratio for the uncoated specimen is shown at the bias boltage of 0V.

Fatigue limit σw for Ti6242S substrate material was obtained as 200 MPa under R is 0.1, as shown in Fig. 2-7. Therefore, fatigue limit range σw is given as 400 MPa. The threshold stress intensity factor range δKth for STA-treated Ti6242S alloy was obtained as 5 MPa$m^{0.5}$ under stress ratio 0.1 in [48]. Substituting these values into Eq. 2.1, the critical defect size a for fatigue crack propagation can be evaluated as:

$$a = \frac{1}{\pi}(\frac{5}{400})^2 = 49.7\mu m \cdots (2.2)$$

Therefore, it can be found that the assumed semi-circular surface crack size is closer to the critical crack size for crack propagation, where the fatigue strength would be influenced by the growth defects. If considering the applied stress amplitude of 260 MPa instead of the fatigue limit of 200 MPa, the critical crack size is given as 25.4 μm, which is smaller than the assumed semi-circular surface crack size of 48.6 μm. Therefore, the growth defects existed in the present coating layer would significantly influence the fatigue crack nucleation behavior and then the strength.

2.7.2 Influence of bias voltage on fatigue fracture mechanism

From the foregoing results, fatigue fracture mechanisms for the coated specimens deposited under lower and higher bias voltages could be schematically illustrated as shown in Fig.2.14 . For the case of the bias voltages lower than -30V, the fatigue lives of the coated specimens were shorter than the uncoated specimen and the crack on the specimen surface could be observed in the early stage of life, earlier than the uncoated specimen. Since the subsurface material of the coated specimen is the same as the uncoated specimen, fatigue crack growth behavior in the subsurface region of the coated specimen and the uncoated specimen would be similar. Therefore, this early crack nucleation of the coated specimen would be the main reason for the degraded fatigue life of the coated specimen compared to the uncoated specimen. The early crack nucleation for the coated specimens deposited under lower bias voltages is suggested to result from the low compressive residual stress as shown in Fig. 2.6., which would be not enough to suppress the crack nucleation from the coating surface. The lower hardness for the lower bias voltage shown in Fig. 2.7 may have some marginal effects on the early surface crack nucleation. On the other hand, for the case of the bias voltages higher than -50V, the fatigue lives of the coated specimens were longer than the uncoated specimen. In these coated specimens, the crack on the specimen surface could be observed in the late stage of life. As discussed in the section 2.3.3, a fatigue crack would be nucleated not from the coating layer but in the subsurface and then propagate toward the specimen center, while the crack is difficult to propagate into the coating layer with high compressive residual stress shown in Fig.2.6. When the fatigue cracking area in the subsurface increases to increase the K-value at the interface between coating layer and substrate enough for break of the coating layer, the surface crack can be observed on the coating surface. Consequently, the high compressive residual stress suppresses the crack nucleation in the coating layer and enhance subsurface crack nucleation and propagation. This subsurface crack nucleation due to the high compressive residual stress induced in the surface coating layer would be the main reason for the late nucleation of surface crack and then longer fatigue life in the coated specimens deposited under higher bias voltages. The higher hardness shown in Fig.2.7 may have

some marginal effects on the late surface crack nucleation.

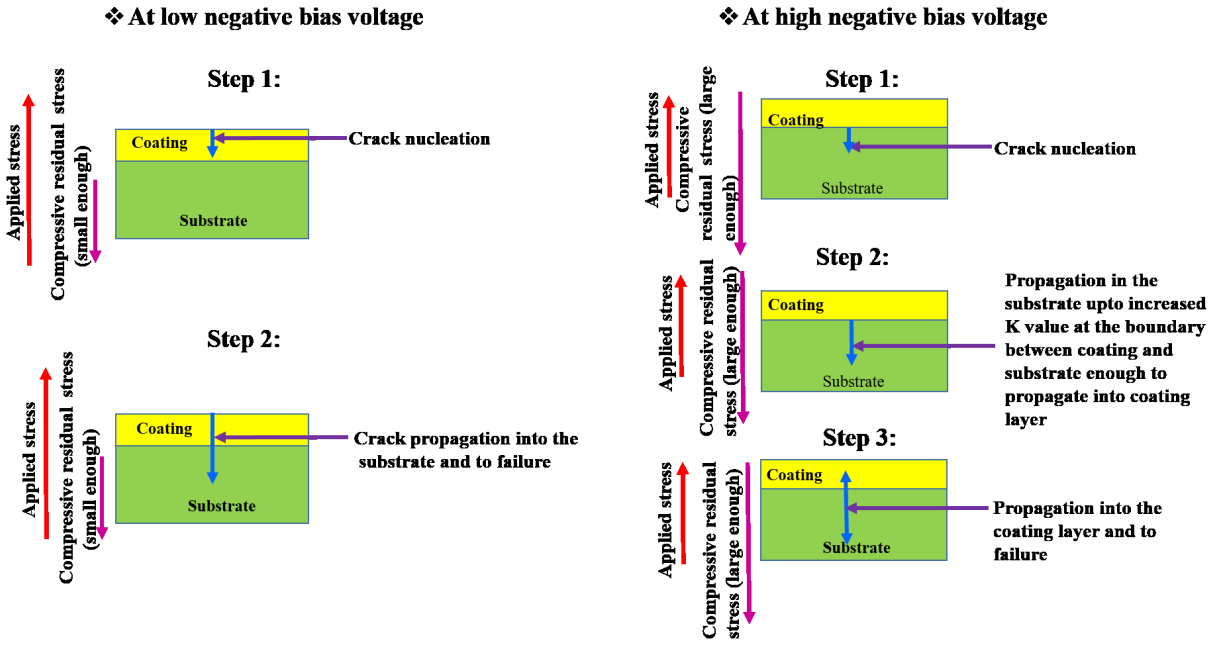

Fig. 2.14 Schematic illustration of fracture mechanism occurred in the coated specimens deposited under lower and higher bias voltages.

2.8 Conclusion

In the present chapter, the fatigue strength tests of the STA-treated Ti6242S specimens and those with TiAlN surface coating layer deposited under various bias voltages were carried out to investigate effect of bias voltage on fatigue strength and mechanism of the coated specimen. The main conclusions obtained are summarized as follows:

1. TiAlN surface coatings deposited under higher bias voltages of -50V, -75V and -100V significantly improved fatigue life compared to the uncoated specimen, while those deposited under lower bias voltages of -20V and -30V significantly degraded fatigue life compared to the uncoated specimen.

2. From the detailed fracture surface observations, fatigue crack seemed to nucleate from the coating layer for the coated specimens deposited under lower bias voltages of -20V and -30V.

Whereas for the coated specimens deposited under higher bias voltages of -50V, -75V and -100V, the crack seemed to nucleate from the subsurface in the Ti6242S substrate.

3. From the detailed surface crack observations, the surface crack of the coated specimens deposited under bias voltages of -20V and -30V was found to be nucleated in the early stage of life, earlier than the uncoated specimen. This early crack nucleation would result in the degraded fatigue lives of the coated specimens deposited under lower bias voltages.

4. The surface crack was observed in the very late stage of life for the coated specimens deposited under bias voltages of -50V, -75V and -100V compared to the uncoated specimen, which suggested that a fatigue crack nucleated in the subsurface and propagated toward the specimen center. When the fatigue cracking area increases to break the coating layer, the surface crack can be observed in the late stage of life. The coating layer could suppress the crack nucleation for the coated specimens deposited under higher bias voltages.

5. The compressive residual stress in the coating layer significantly increased with increasing bias voltage. The high compressive residual stress in the coating layer for the coated specimens deposited under higher bias voltages would take a dominant role in suppression of crack nucleation from the specimen surface and consequently induce the subsurface crack nucleation. On the other hand, low compressive residual stress for the coated specimens deposited under lower bias voltages could not suppress the crack nucleation and propagation in the coating layer but enhance them to degrade their fatigue lives.

Chapter 3 Effect of coating thickness on fatigue behavior of TiAlN coated Ti alloys

3.1 INTRODUCTION

In the previous chapters, effects of bias voltage on fatigue strength and fatigue mechanisms of the TiAlN coated titanium alloy (STA-treated Ti6242S) have been investigated to understand the basic fatigue behavior of the TiAlN coated titanium alloy. From the results, it has been clarified as: (1) Fatigue life increases with increasing bias voltage. (2) For the specimens coated under lower bias voltage with shorter fatigue life, the fatigue crack initiates from coating surface and propagated into substrate. (3) For the specimen coated under higher bias voltage with longer fatigue life, the fatigue crack initiates subsurface in the substrate and propagates into the substrate further as well as toward the coating layer. (4) The compressive residual stress increases with increasing bias voltage. This higher residual stress at higher bias voltage suppresses the crack initiation in the coating layer, forces the crack initiation location into subsurface and then enhances fatigue life. In the previous chapter, the coating thickness is controlled to be 5 μm regardless of bias voltage. As the next step, effect of coating thickness on fatigue behavior is investigated in the present chapter to know the optimal coating thickness. Some works on the effect of coating thickness on fatigue behavior have been reported and the results can be briefly summarized as: For the cases that fatigue life of the coated material is longer than the uncoated material: (1) For fatigue of Zr-based metallic glass thin film coating on A7075 alloy [49], during fatigue cycling, slip bands are formed in the crystalline substrate. When the slip bands propagate to the film/substrate interface, a step-like protrusion is created on the surface of the film, which eventually forms a crack in the film. The thinner film is flexible and beneficial to fatigue resistance, while thicker film tends to induce delamination. The residual stress is almost the same regardless of coating thickness. (2) For fatigue of TiCN coating on 1Cr-1Mo-0.25V steel [50], since plastic deformation of substrate surface is restricted due to hard film, crack initiation is

delayed and then fatigue life becomes longer. Crack initiation occurs subsurface in the substrate. There is no discussion about effect of film thickness in the paper but the optimum thickness can be observed from the figure. The residual stress is not measured. (3) For fatigue of TiN, TiCN and TiAlN coatings on 1Cr-1Mo-0.25V steel [51], fatigue strengths and lives are superior compared to the uncoated specimen. However, systematic trend among three coating thicknesses is not clear and the data points are in a wide range of scatter. Crack initiation occurs subsurface in the substrate due to suppression of crack initiation from the coating layer by high hardness and compressive residual stress in the coating layer. For the case that fatigue life of the coated material is shorter than the uncoated material: For fatigue of CrN coating on SCM435 steel [52], fatigue life of the coated specimen is shorter than the uncoated specimen regardless of coating thickness and stress level. Thickness hardly affects fatigue strength of coating material. The residual stress is almost the same with some scatter for all three thicknesses. For the case that fatigue behavior straddles above two cases: For fatigue of TiAlN coating on TiAl intermetallic compound [53], the maximum fatigue strength and life are obtained at the thickness of 3 μm, where a crack initiates subsurface in the substrate. The minimum fatigue strength and life are obtained at the thickness of 1μm, where a crack initiation is induced by failure of coating layer due to deformation of substrate. Fatigue life of the specimen with coating thickness of 10 μm is shorter than the uncoated specimen, where deep cracks in the coating layer perpendicular to the loading direction are formed and then propagate into substrate. The residual stress is not measured. As summarized above, for the effect of coating thickness on fatigue behavior, it has been hardly understood whether there is the optimum thickness to give the maximum fatigue strength and what is the reason for it, etc. Furthermore, whether the difference of crack initiation mechanism influences effect of coating thickness on fatigue strength has been not yet clarified. In the present chapter, as substrate materials, γ-TiAl intermetallic compound and STA-treated Ti6242S titanium alloy were used for fatigue strength tests. As the target of the present study is to determine the fatigue strength of high temperature titanium alloys that are extensively used in aircraft engine components, γ-TiAl intermetallic compound in addition to STA-treated Ti6242S titanium alloy used in the previous chapter was used as a substrate material to validate the fatigue

behavior of these two substrate materials with TiAlN coating. As the bias voltage for coating, -30V under which fatigue life becomes shorter than the uncoated material and -100V under which fatigue life becomes longer than the uncoated material were selected. Under each bias voltage the coating thickness was varied from 1 μm to 15 μm. Before fatigue tests, residual stress, hardness and Young's modulus of the coating layer were measured and after fatigue tests, fatigue fracture surfaces and cracks on the coating surface near the fracture region were also observed. From the results, the optimum coating thickness and the reason for it were discussed for each crack initiation mode of surface crack initiation and subsurface crack initiation.

3.2 EXPERIMENTAL PROCEDURE

3.2.1 Material

In the present chapter, two Ti-alloys were used as the substrate materials: one was STA-treated Ti6242S titanium alloy and the other was γ -TiAl intermetallic compound. Chemical composition, microstructure with transformed β and primary α phases, and mechanical properties of the STA-treated Ti6242S have been shown in Chapter 2. For γ -TiAl, the high purity ingot was produced by the induction skull melting and then heat-treated to form a microstructure with lamellar and equiaxed gamma phases. Chemical composition is Ti-48Al-2Nb-2Cr (at %). Microstructure of the γ -TiAl has been shown in Fig. 4.1.of Chapter 4. The yield strength and ultimate tensile strength of the γ -TiAl material are considered as 439MPa and 534MPa, respectively[54].

3.2.2 Fatigue test specimen

The specimen used for fatigue test was a round bar tension type with dog-born shape. The gage diameters of the specimens were 3.5mm and 3.0mm for STA-treated Ti6242S and γ-TiAl, respectively, and the gage length was 20mm. The specimen surface was polished by using SiC abrasive papers up

to #4000 and then followed by buff-polishing with diamond pastes of particle sizes up to 1μm. Before fatigue tests, ultrasonic cleaning was applied to the specimens.

3.2.3 Coating Procedure

TiAlN coatings with different thicknesses were deposited by a cathodic arc ion plating system (AIP-SS002, Kobe Steel Ltd.) with a target Ti50Al50 (at %). Detail deposition conditions were the same as those in the previous study [54]. By controlling the deposition time, the coating thicknesses of approximately 1 μm, 5 μm and 15 μm for each bias voltage were achieved.

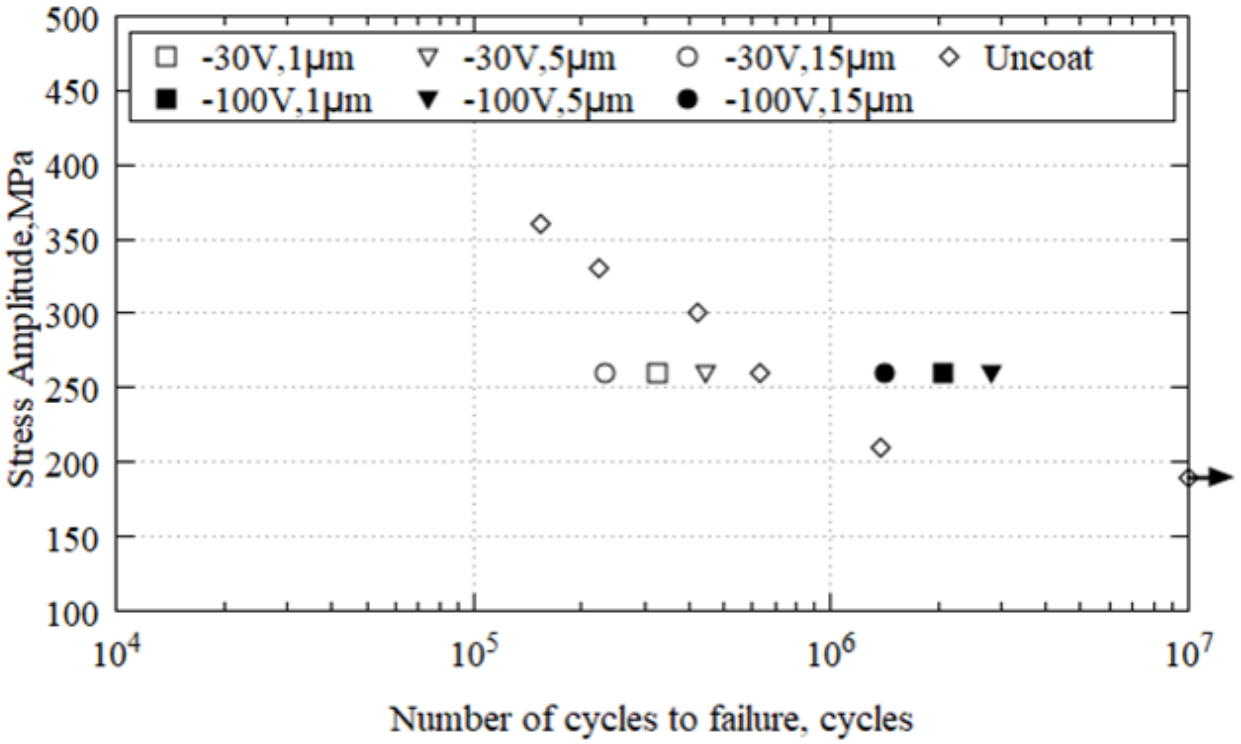

Fig. 3.1 S-N curves for the uncoated specimens with the test results of the coated specimens with different coating thicknesses for STA-treated Ti6242S.

3.2.4 Fatigue test

The fatigue strength tests of STA-treated Ti6242S and γ -TiAl specimens without and with TiAlN coating (hereafter referred as the uncoated specimen and the coated specimen, respectively) were carried out by using a servo-hydraulic fatigue test machine with a load capacity of 10 kN. Detail of

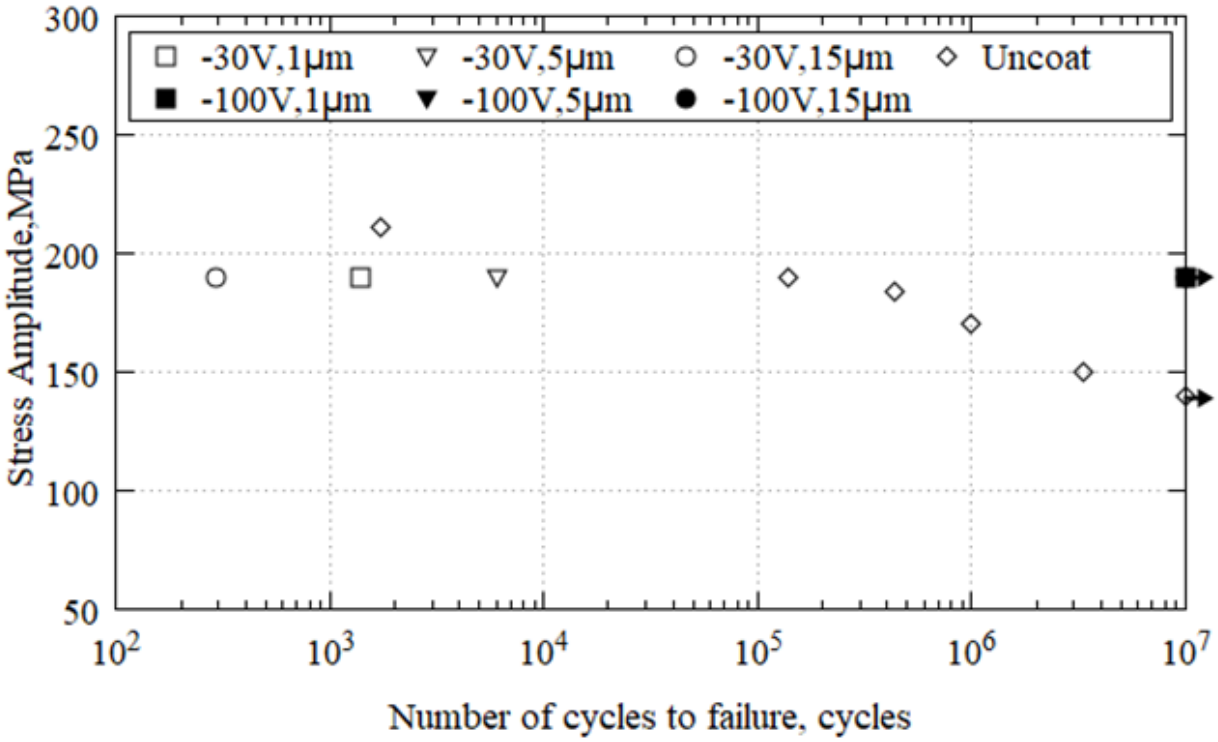

Fig. 3.2 S-N curves for the uncoated specimens with the test results of the coated specimens with different coating thicknesses for γ -TiAl.

fatigue test method and conditions were the same as those in the previous chapters. The selected stress amplitude for the fatigue tests to investigate the effect of coating thickness on fatigue life was 260MPa for STA-treated Ti6242S, which was the same as for the fatigue test to investigate effect of bias voltage in Chapter 2. That for γ -TiAl was 190MPa, which was selected by referring the S-N curve of the uncoated γ -TiAl specimen. The fracture surfaces were observed by using a scanning electron microscope (SEM) to clarify the fatigue crack nucleation location. The cracks on the coating surface near the fracture region were also observed by using an SEM for further discussion about reasons for coating thickness effect.

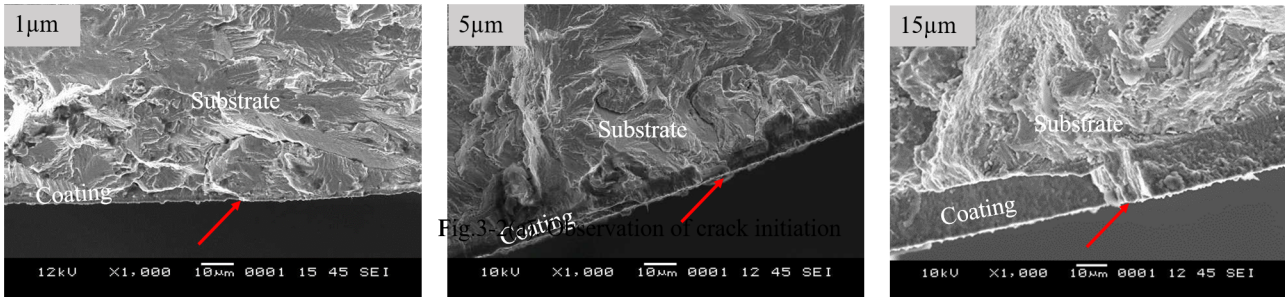

Fig. 3-3 Observation of crack initiation

Fig. 3.3 Observation of crack initiation region of the coated specimens deposited under -30V and tested at 260MPa for the substrates of STA-treated Ti6242S.

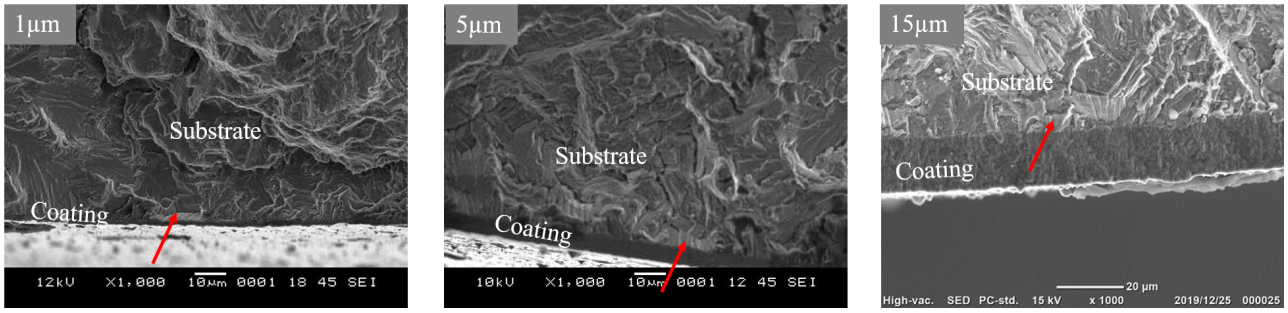

Fig. 3.4 Observation of crack initiation region of the coated specimens deposited under -100V and tested at 260MPa for the substrates of STA-treated Ti6242S.

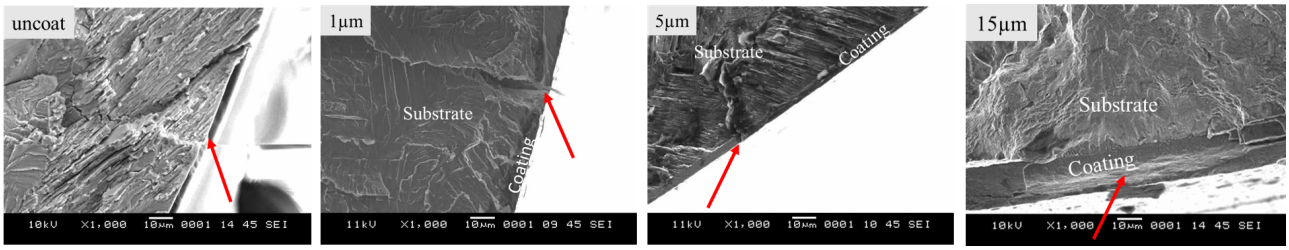

Fig. 3.5 Observation of crack initiation region of the coated specimens deposited under -30V and tested at 190MPa for the substrates of γ -TiAl.

3.2.5 Measurements of hardness, Young's modulus and residual stress of coating layer

Nano-indenter (Dynamic ultra-microhardness tester) was used for measuring the hardness and Young's modulus of the coating layer under an indentation load of 400 mN and a loading duration of 10 s. The hardness and Young's modulus were evaluated as the average value of ten measurements.

The residual stress of the coating layer was measured by the X-ray diffractometer multiple HKL method [55] using X-ray tube of Cu(Kα).

3.3 RESULTS

3.3.1 S-N curves

S-N curves of the coated specimens deposited under -30V and -100V with various thicknesses for the STA-treated Ti6242S and γ -TiAl substrate materials are shown in Fig 3.1. and Fig.3.2 , respectively. As seen from Fig.3.1, the fatigue lives of the coated specimens deposited under bias voltage of -30V were shorter than the uncoated specimen. On the other hand, the coated specimens

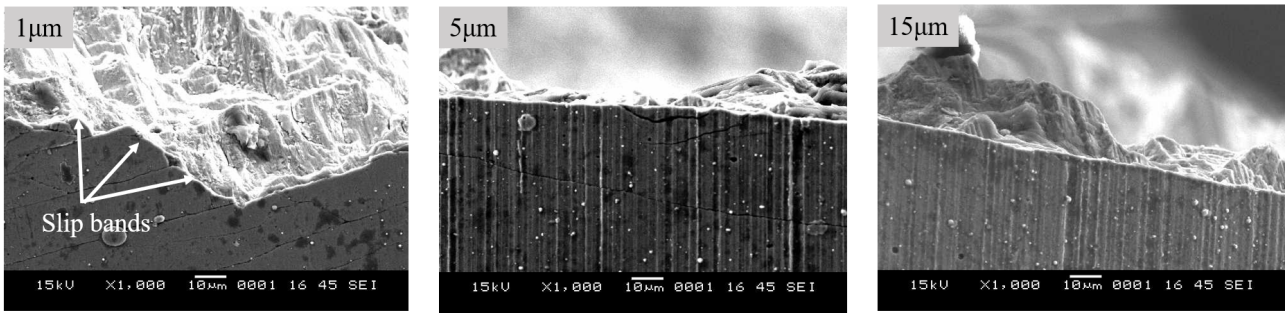

Fig. 3.6 Observation of surface crack of the coating near the fracture region for Ti6242S specimen (a) -30V.

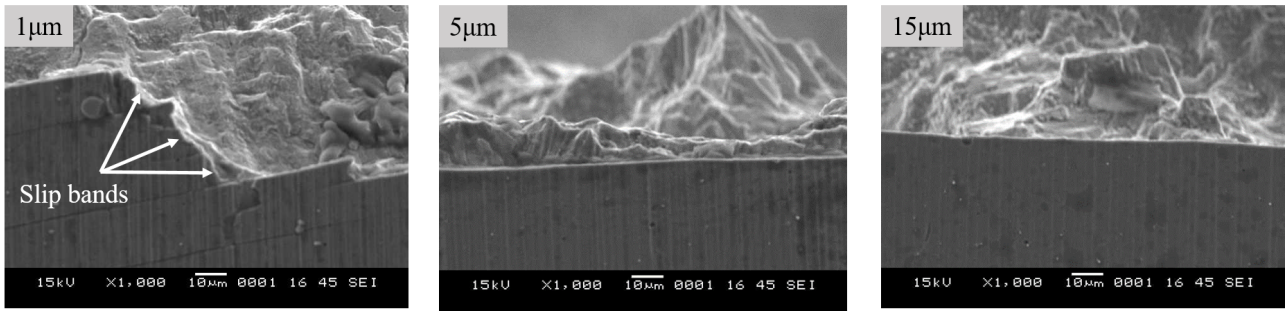

Fig. 3.7 Observation of surface crack of the coating near the fracture region for Ti6242S specimen (b) -100V.

deposited under bias voltage of -100V exhibited the enhanced fatigue lives compared to that of the uncoated specimen. The fatigue life of the specimen with coating thickness of 5 μm was the longest among the three coating thicknesses for both bias voltages of -30V and -100V.

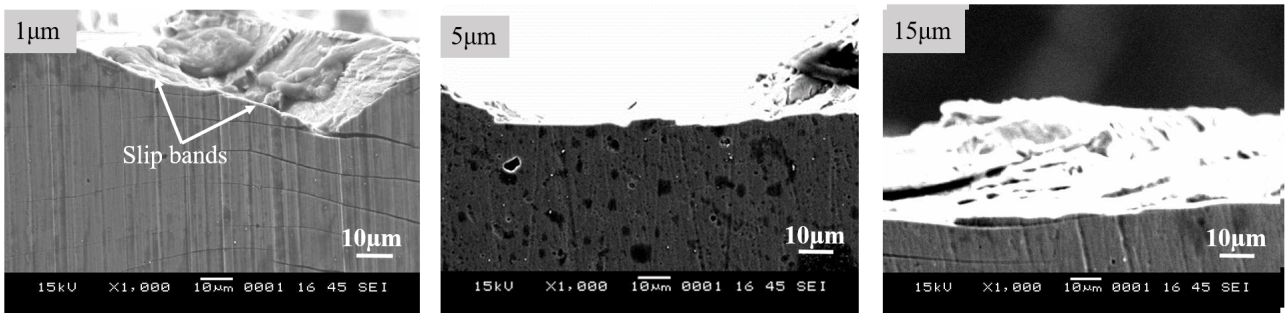

Fig. 3.8 Observation of surface crack of the coating near the fracture region for γ -TiAl (-30V).

As found from Fig..3.2 for γ -TiAl substrate, the fatigue lives of the coated specimens deposited under bias voltage of -30V were shorter than that of the uncoated specimen. On the other hand, the coated specimens deposited under bias voltage of -100V could not fracture up to 10^7 cycles and exhibited the enhanced fatigue lives compared to that of the uncoated specimen. The fatigue life of the specimen with coating thickness of 5 μm was the longest among the three coating thicknesses for

bias voltage of -30V. On the other hand, in case of bias voltage of -100V, since the fatigue lives of the three coating thicknesses excessed 10^7 cycles, coating thickness effect could not be discussed.

3.3.2 Fracture surface observations

To obtain information about fatigue crack nucleation mechanism, the fatigue crack nucleation regions on the fracture surfaces were observed in detail by using an SEM, as shown in following figures..

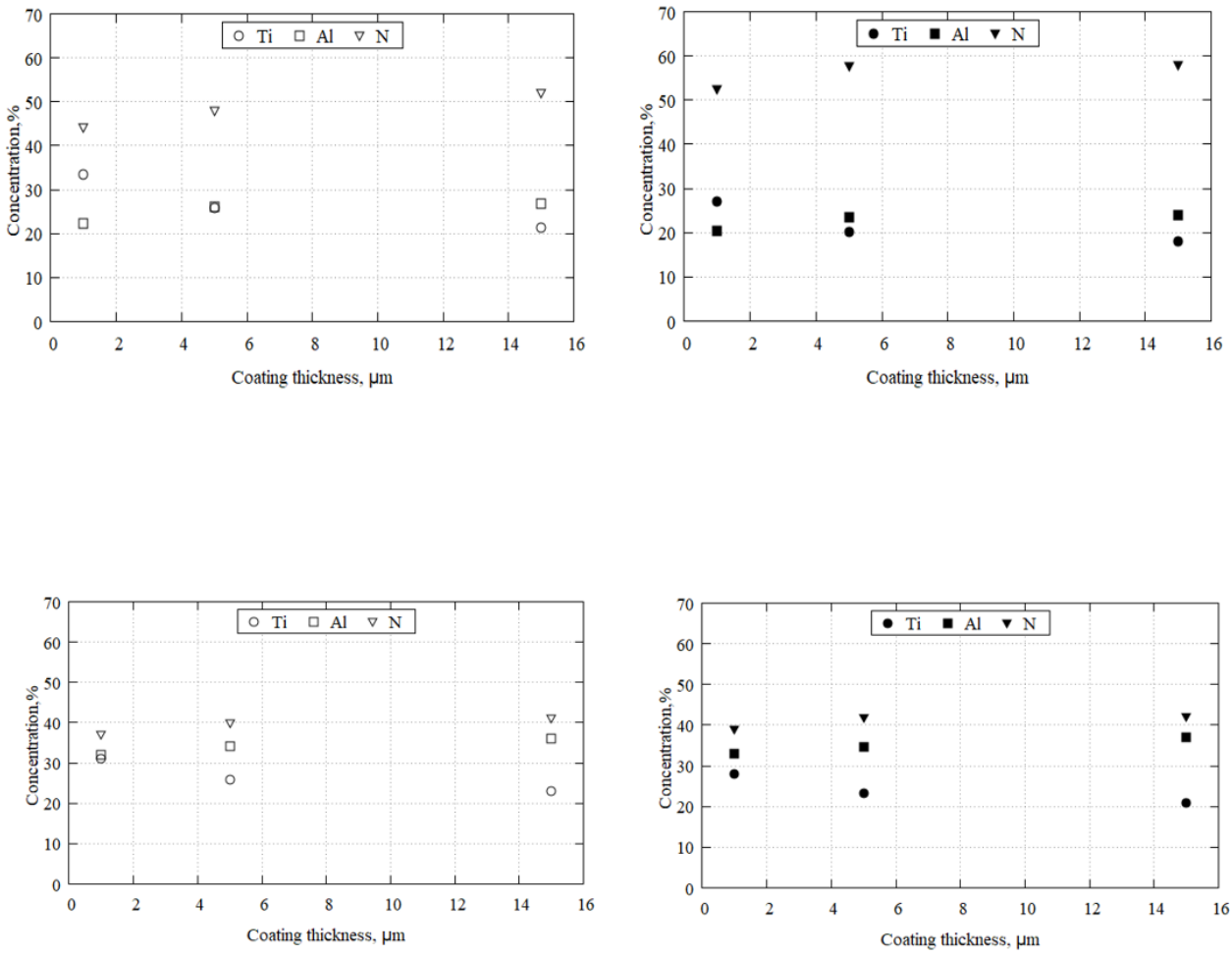

Fig. 3.9 Relationship between distribution of elemental concentration and coating thickness for two substrates.

For the STA-treated Ti6242S uncoated specimen at stress amplitude of 260MPa, a fatigue crack nucleated from specimen surface without any marks or defects, as seen from Fig.2.11 in Chapter 2. For the coated specimens, smooth surface without step could be observed in case of bias voltage of -30V regardless of coating thicknesses, as seen from Fig.3.3. On the other hand, in case of bias voltage of -100V, a step at the interface between coating layer and substrate could be observed re-

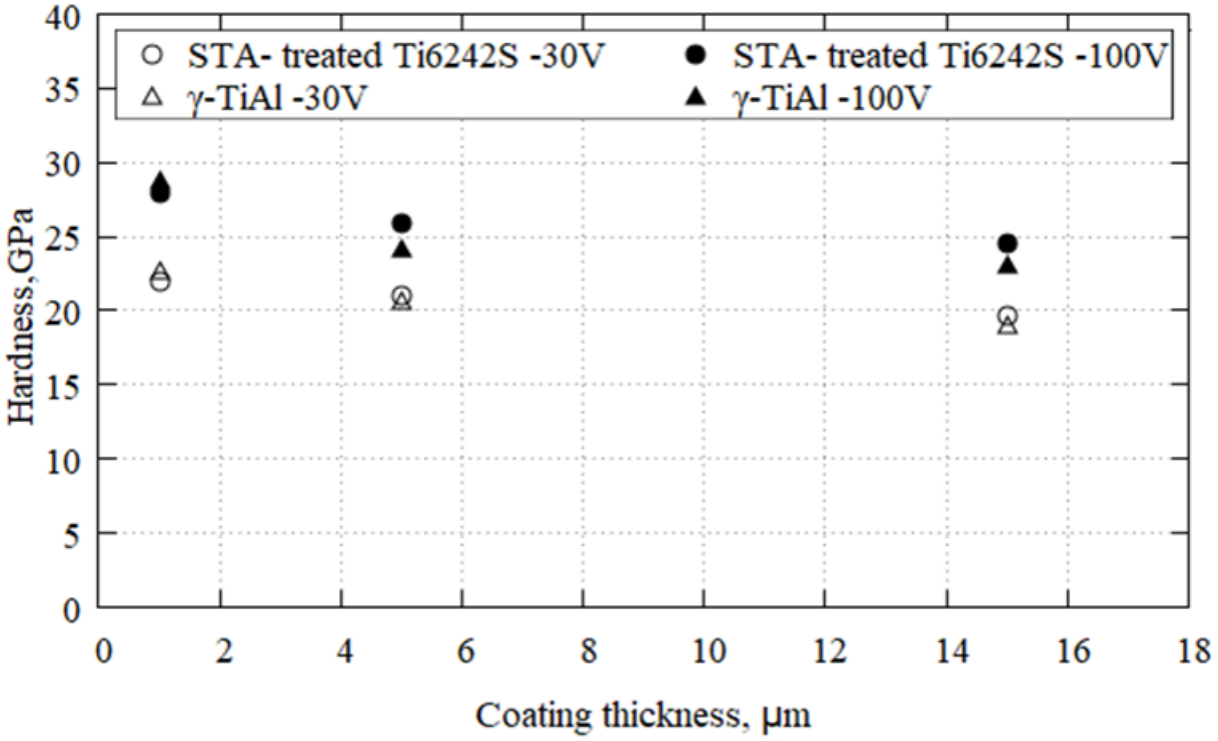

Fig. 3.10 Relationship between hardness and coating thickness for two substrates.

gardless of coating thicknesses, as seen from Fig. 3.4. For the γ-TiAl uncoated specimen tested at stress amplitude of 190MPa, a fatigue crack nucleated from specimen surface without any defects or particles, as found from Fig.3.5. For the γ -TiAl coated specimens deposited under -30V, smooth surface without step at the interface between coating layer and substrate could be observed regardless of coating thicknesses, as seen from Fig.3.5. In case of bias voltage of -100V, the specimen could not fracture until 10^7 cycles and any surface crack could not be observed on the specimen surface regardless of coating thicknesses.

As discussed in Chapter 2 based on detailed observation of crack nucleation region on the fracture surfaces as well as crack nucleation and propagation behavior observed on the surface of the coated specimens during the fatigue tests, in case of smooth surface without step at the interface, fatigue cracks would initiate from the specimen surface and propagate into substrate. While in case of fracture surface with a step at the interface, fatigue cracks would initiate subsurface and propagate into substrate and also toward coating layer. Therefore, based on the present fracture surface observations, it was found that the fatigue crack would initiate from the coating surface for the bias voltage of -30V and from subsurface in the substrate for the bias voltage of -100V regardless of coating thickness and

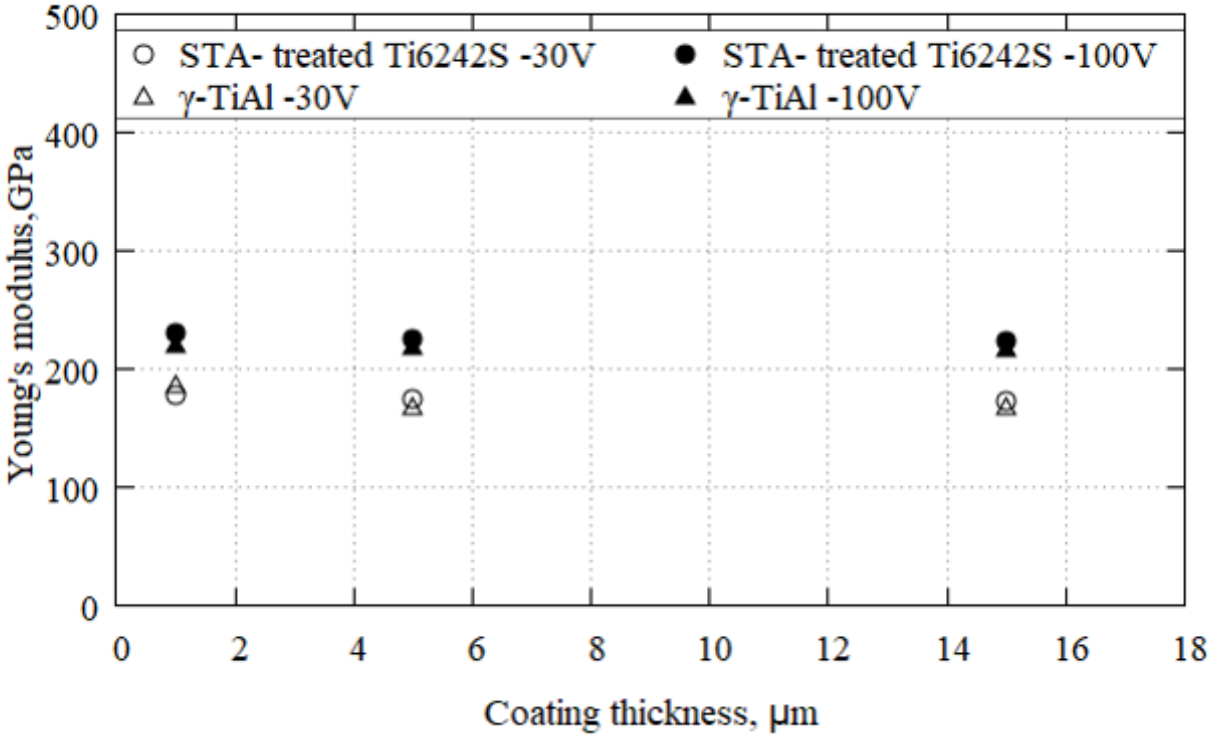

Fig. 3.11 Relationship betwen Young ' s modulus and coating thickness for two substrates.

substrate material.

3.3.3 Surface crack and fracture morphology observed on the coating surface near the fracture region

Surface cracks and fracture morphology observed on the coating surface near the fracture region for the STA-treated Ti6242S coated specimen and the γ -TiAl coated specimen are shown in Figs.3.6,3.7. and .3.8, respectively. As seen from the figures, for all cases of the coating thickness of 1 μm regardless of bias voltage and substrate material, surface cracks and fracture path morphology were zigzagged and seemed to be significantly influenced by the deformation of substrate crystals such as slip bands. Similar zigzagged fracture path of coating layer under an influence of the deformation of substrate crystal has been reported for the TiAlN coating with 1 μm thickness [53]. On the other hand, for the cases of coating thicknesses of 5 μm and 15 μm regardless of bias voltage and substrate material, surface cracks and fracture path morphology were linear and perpendicular to the loading direction.

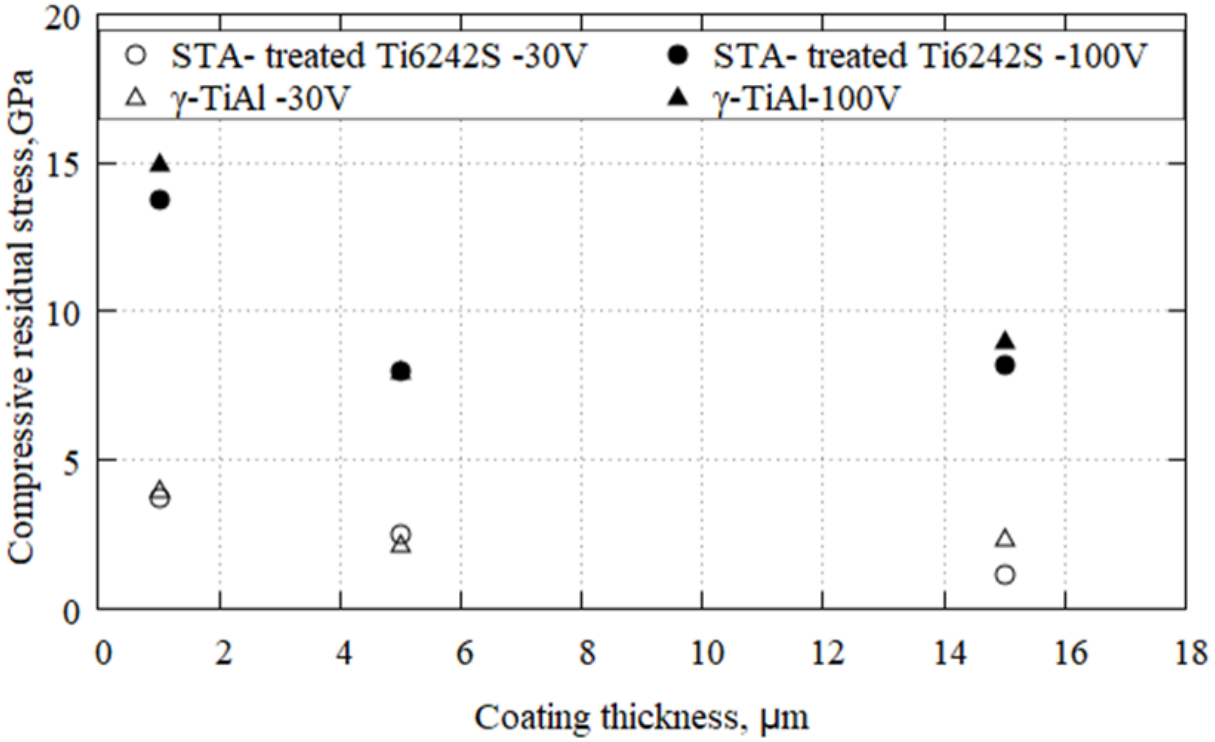

Fig. 3.12 Relationship between compressive residual stress and coating thickness for two substrates.

3.3.4 Chemical composition of coating layer

The concentrations of the most abundant three elements (Ti, Al and N) were evaluated by using EDS analysis. From the results, relationships between element concentration (at.%) of the TiAlN coating and coating thickness for the STA-treated Ti6242S coated specimens deposited under bias voltages of -30V and -100V and the γ -TiAl coated specimens deposited under bias voltages of -30V and -100V are shown in Fig.3.9, respectively. As seen from the figure, for all four cases, concentrations of Al and N elements are slightly decreasing with decreasing coating thickness, which would be mainly induced by an increase of Ti concentration with decreasing coating thickness. The increase in Ti concentration would be induced by detection of more Ti in the substrate when the coating thickness decreases. Therefore, element concentrations of Ti, Al and N elements are speculated to be almost the same regardless of coating thickness.

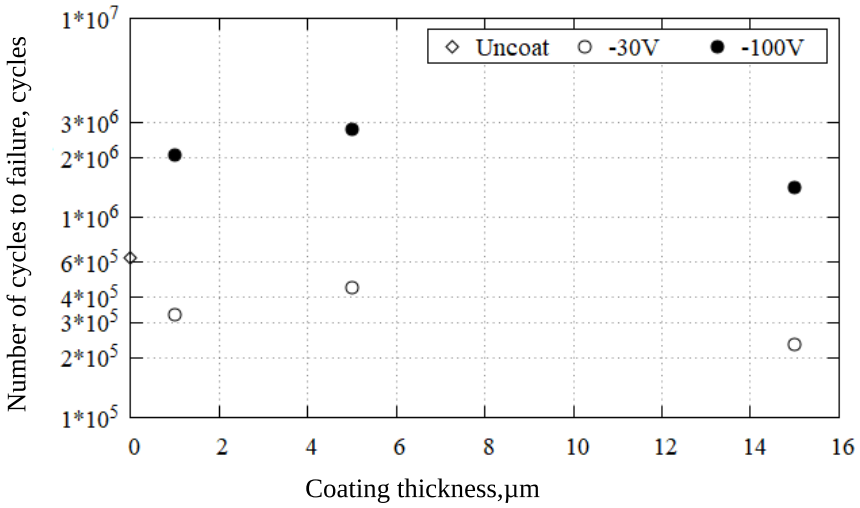

Fig. 3.13 Relationship between coating thickness and fatigue life for the coated STA-treated Ti6242S specimen.

3.3.5 Hardness and Young ' s modulus of the coating layer

Hardness and Young ' s modulus of the TiAlN coatings were evaluated by using a nano indentation method. From the results, relationships between hardness and coating thickness, and between Young's modulus and coating thickness for the two kinds of substrate materials are shown in Fig..3.10 and.3.11, respectively. As found from these figures, the values of both hardness and Young ' s modulus for coating thickness of 1 μm was high compared to those for coating thicknesses of 5 μm and 15 μm and those for higher bias voltage were higher compared to those for lower bias voltage. Since these measurements were conducted by using an indenter, these behavior would mainly resulted from the residual stress variation with coating thickness and bias voltage shown in the following section, where the compressive residual stress was higher for the coating thickness of 1μm and was higher for higher bias voltage. It is also found that the substrate material hardly influence the values of hardness and Young ' s modulus.

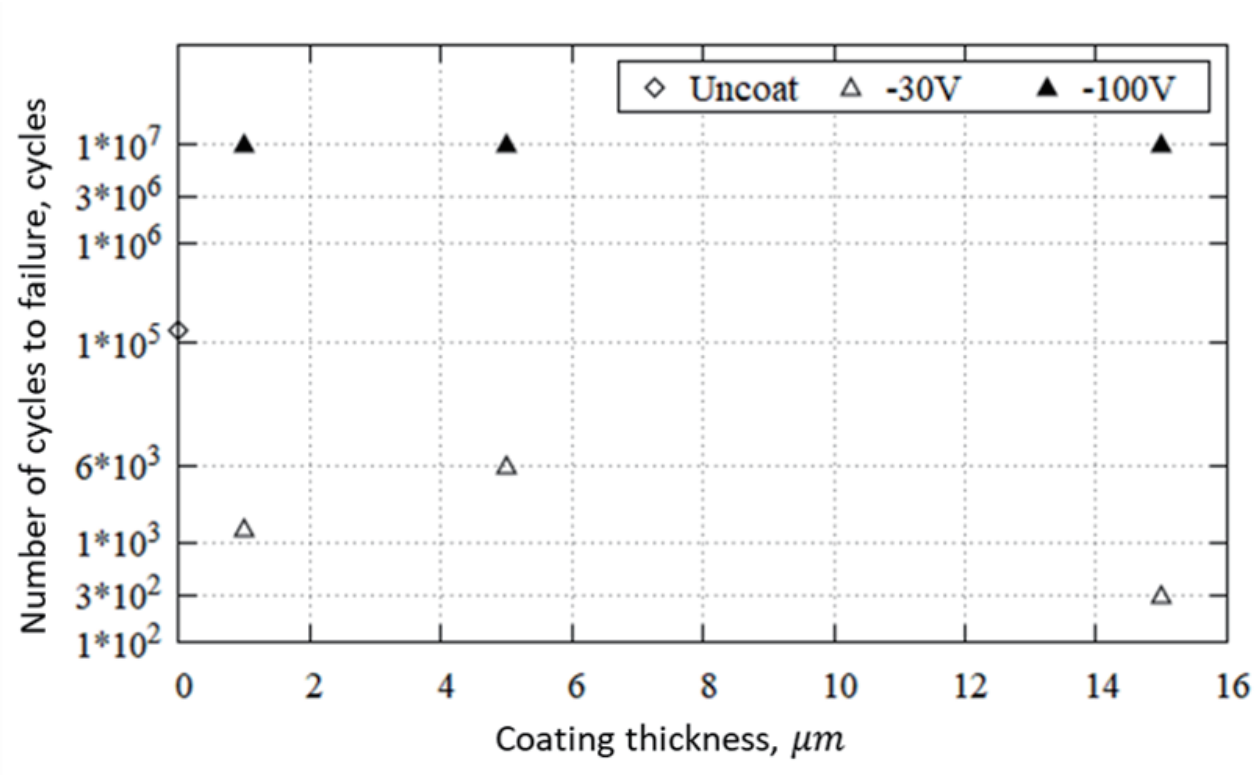

Fig. 3.14 Relationship between coating thickness and fatigue life for the coated γ-TiAl specimen.

3.3.6 Residual stress in the coating layer

Relationships between coating thickness and compressive residual stress of the coating layer for the STA-treated Ti6242S and γ -TiAl coated specimens are shown in Fig.3.12. As seen from the figure, the compressive residual stresses for the coated specimens with coating thickness of 1μmwere high compared to those for coating thicknesses of 5 μm and 15 μmregardless of bias voltage and substrate material. For the coating thicknesses of 5 μm and 15 μm, the residual stresses showed almost the same. The substrate material didn ' t significantly affect the residual stress

3.4 DISCUSSION

3.4.1 Fatigue crack initiation mechanisms and effect of coating thickness

For further discussion about effect of coating thickness on fatigue life, the relationships between fatigue life and coating thickness for the substrates of STA-treated Ti6242S and γ -TiAl are shown in Fig.3.13 and 3.14 , respectively, based on S-N curves shown in Fig.3.1 and .3.2. As seen from the

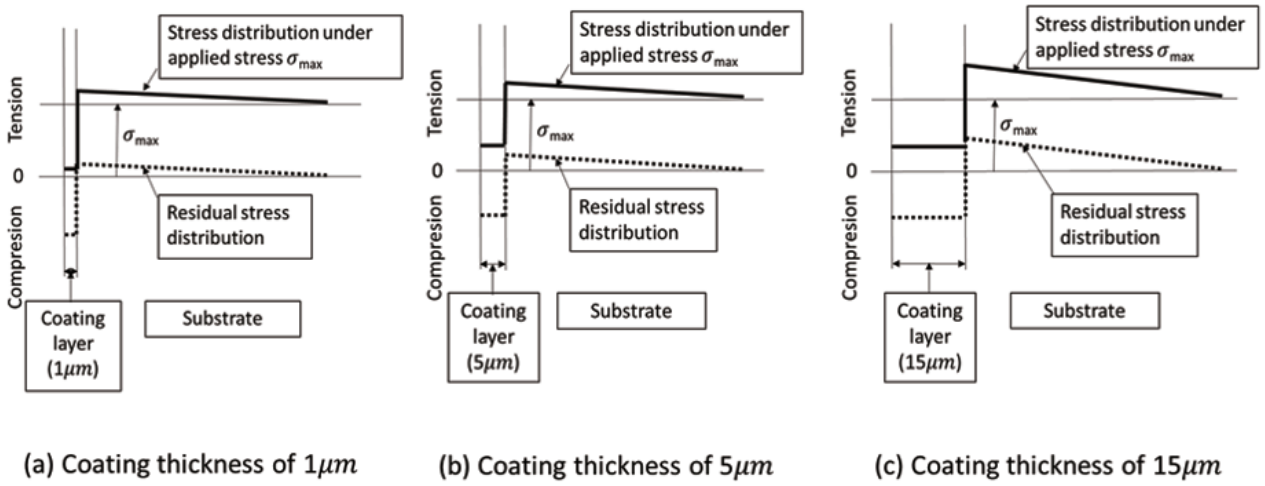

Fig. 3.15 Schematic stress distributions under applied stress σ_a for the coated specimens deposited under bias voltages of -30V.

figure, the maximum fatigue life was achieved at the optimum coating thickness of 5 μm for both the substrates. The same optimum coating thickness could be observed for both cases of fatigue crack initiation mode: one is the surface crack initiation and the other is the subsurface crack initiation. Similar effect of coating thickness with optimum coating thickness has been reported for CrN coated SCM435 specimen[52], TiCN coated 1Cr-1Mo-0.25V steel specimen [50]and TiAlN coated TiAl specimen [53].

To consider dominant factors inducing this effect of coating thickness with the optimum coating thickness, schematic residual stress distribution without applied stress and stress distribution with applied stress for the bias voltages of -30V and -100V are shown in Figs. 3.15 and 3.16, respectively.

For the case of bias voltage of -30V, the fatigue lives of coated specimens were shorter than the uncoated specimen and the fatigue crack initiated from the coating surface regardless of coating thickness. The compressive residual stresses for the coating thicknesses of 5 μm and 15 μm were almost same magnitudes, while that for the coating thickness of 1μm was larger than them, as seen from Fig. 3.12. The compressive residual stress in the coating layer substrate should be balanced by the tensile residual stress in the substrate to maintain the equilibrium of forces, as reported by Kolkman [56]. Therefore, the magnitude of tensile stress depends on both the magnitude of compressive stress and the thickness of coating layer, as schematically shown by the dotted line in Fig. 3.15. Since the compressive residual stress for the coating thickness of 1μm is about two times larger than that for

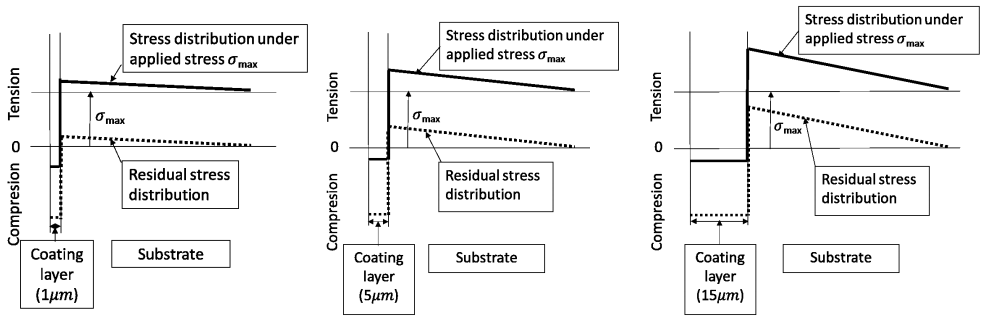

(a) Coating thickness of 1micron (b) Coating thickness of 5micron (c) Coating thickness of 15micron

Fig. 3.16 Schematic stress distributions under applied stress σ_a for the coated specimens deposited under bias voltages of -100V.

the coating thickness of 5 μm but the coating thickness of 5 μm is five times larger than the coating thickness of 1μm , the tensile residual stress induced in the substrate for the coating thickness of 1μm is smaller than that for the coating thickness of 5 μm. In cases of the coating thicknesses of 5 μm and 15 μm, since the compressive residual stress is almost the same, the tensile residual stress for the coating thickness of 15 μm becomes larger than that for the coating thickness of 5 μm, as seen from Fig.3.15 . When the maximum cyclic stress σ max is applied to the specimen, the stress increases by the magnitude of σ max and the stress in the coating layer would become tensile, as shown by the solid line in Fig.3.15 . As seen from the figure, although the maximum tensile stress for the coating thickness of 1μm is lower than the coating thicknesses of 5 μm , the fatigue life for the coating thickness of 1μm is shorter than that for the coating thickness of 5 μm . The reason for shorter fatigue life for the coating thickness of 1μm would be considered as: Failure behavior of the coated specimen with the coating thickness of 1μm was significantly influenced by the plastic deformation of substrate crystals, such as slip bands, as seen from Fig. 3.6 for STA-treated Ti6242S and Fig. 3.8 for γ-TiAl, which would enhance the fatigue crack initiation compared to the case of thicker coating thickness without influence of plastic deformation of substrate. Similar early fatigue failure of thin coating

layer of 1 μm under influence of deformation of substrate crystal compared to the thicker coating has been reported [53]. On the other hand, the reason for shorter fatigue life of the coated specimen with the coating thickness of 15 μm compared to that for the coating thickness of 5 μm has been not always clarified. P.H. Tsai et al.[49] reported that thinner coating thickness resulted in longer fatigue life and thinner coating layer shows flexibility compared to thicker coating layer, which is beneficial to fatigue resistance. However, this would not be the reason for the present case, since the present coating thickness range from 1μm to 15 μm is much thicker than the range of thickness from 200nm to 500nm for Tsai ' s experiments. As shown in Fig..3.15, although the stress level in the coating layer is almost the same between two coating thicknesses, the stress at the interface for the coating thickness of 15 μm is higher than that for the coating thickness of 5 μm . A fatigue crack initiation mechanism of thin film based on the stress and strain concentration at the interface of film/substrate under the influence of slip band formation in the substrate has been proposed [57]. Therefore, the higher tensile stress in the substrate near interface for the coating thickness of 15 μm induces more significant slip bands, which may contribute to earlier fatigue crack initiation in the coating layer and reduce the fatigue life of the specimen with the coating thickness of 15 μm. For the case of bias voltage of -100V, the fatigue lives of the coated specimens were longer than the uncoated specimen and the crack initiated subsurface in the substrate regardless of coating thickness. The compressive residual stress for the coating thickness of 1μm was about two times larger than those for the coating thicknesses of 5 μm and 15 μm, which were almost the same, as seen from Fig 3.12. From the same consideration based on the equilibrium of forces, the residual stress distributions including compressive residual stress in the coating layer and tensile residual stress in the substrate for the three coating thicknesses are schematically shown in Fig. 3.16. As seen from the figure, the compressive residual stresses for the case of bias voltage of -100V are large and the stresses in the coating layer even under the maximum cyclic stress σ max are still compressive, which can suppress the crack initiation from the coating surface and induce subsurface crack initiation. Although the maximum tensile stress at the interface for the coating thickness of 1μm is smaller than that for the coating thickness of 5 μm , the fatigue life for the coating thickness of 1μm is shorter than that for the coating thickness of 5

μm thicker coating thickness. The reason for the shorter fatigue life of the coating thickness of 1μm compared to the coating thickness of 5 μmwill be that the fatigue crack initiates subsurface at the maximum tensile location and propagates towards the center of the specimen and at the same time the plastic deformation induced near interface in the substrate would induce failure of the thin coating and lead to earlier fatigue failure of the specimen. On contrary, the thicker coating layer of 5 μm with compressive stress is hard to fracture until late stage of fatigue failure and could achieve longer fatigue life. The reason for shorter fatigue life of the coated specimen with the coating thickness of 15 μm compared to that for coating thickness of 5 μm can be speculated as follows: The compressive residual stresses for both the coating thicknesses are similar as seen from Fig.3.12. As schematically shown in Fig.3.16, the maximum tensile stress in the substrate for the coated specimen with thicker coating layer becomes higher compared to that for the coated specimen with thinner coating layer, which enhances earlier crack initiation in the substrate and then shorter fatigue life for thicker coating thickness. Since the values of hardness and Young ' s modulus for both two coating thicknesses are almost the same, as discussed in section 3.3.5, effects of mechanical properties of coating layer would be not significant.

The foregoing results and discussion are summarized in Fig. 3.17 for clarification. As seen from the table, the fatigue crack initiation mechanism for the coating thickness of 1μm is different from those for the coating thicknesses of 5 μm and 15 μm and is strongly affected by the plastic deformation of substrate crystal, which would be the main reason for the degraded fatigue life compared to the coating thickness of 5 μm. It is also understood that the higher tensile stress near the interface in the substrate for the coating thickness of 15 μm would be the main reason for the degraded fatigue life compared to the coating thickness of 5 μm , while the crack initiation modes are different between bias voltages of -30V and -100V.

There is no special consideration to select each value of the coating thicknesses of 1μm, 5 μm and 15 μm. However, referring the former studies reviewed in Introduction, to find the optimum thickness with the longest fatigue life among various coating thicknesses, the coating thickness of 1μm is taken as a thinner side thickness, 15 μm as a thicker side thickness and 5 μm as an intermediate thickness.

	Coating thickness				
	$1\mu m$		$5\mu m$		$15\mu m$
Bias voltage of -30V (Fatigue life is shorter than the uncoated specimen.)					
Fatigue life, N_f	N_f^1	<	N_f^5	>	N_f^{15}
Crack initiation mode	Surface				
Compressive residual stress, σ_{com}	$\sigma_{com}{}^1$	>	$\sigma_{com}{}^5$	=	$\sigma_{com}{}^{15}$
Tensile residual stress, σ_{ten}	$\sigma_{ten}{}^1$	<	$\sigma_{ten}{}^5$	<	$\sigma_{ten}{}^{15}$
Crack initiation mechanism of coating layer	Coating layer failure due to deformation of substrate crystal		Crack initiation due to stress concentration at interface, σ^5	<	Crack initiation due to stress concentration at interaface, σ^{15}
Bias voltage of -100V (Fatigue life is longer than the uncoated specimen.)					
Fatigue life, N_f	N_f^1	<	N_f^5	>	N_f^{15}
Crack initiation mode	Subsurface in the substrate				
Compressive residual stress, σ_{com}	$\sigma_{com}{}^1$	>	$\sigma_{com}{}^5$	=	$\sigma_{com}{}^{15}$
Tensile residual stress, σ_{ten}	$\sigma_{ten}{}^1$	<	$\sigma_{ten}{}^5$	<	$\sigma_{ten}{}^{15}$
Crack initiation mechanism in the substrate	Crack initiation due to high tensile stress in the substrate and then cracking of the coating layer due to deformation of substrate crystal		Crack initiation due to high tensile stress in the substrate, σ^5	<	Crack initiation due to high tensile stress in the substrate, σ^{15}

Fig. 3.17 Fatigue crack initiation mechanisms and the related factors.

If the intermediate thickness other than 5 μm would be selected, this intermediate thickness will show the longest fatigue life instead of the coating thickness of 5μm. However, the conclusion obtained in the present study is that there exists the optimum thickness and the reason for this is explained based on the variation of fatigue crack initiation mechanisms of the coated specimen depending on the coating thickness. The specimen coated with the thickness of 5 μm exhibits improved fatigue strength regardless of bias voltages, as the thickness is optimum enough to withstand the plastic deformation of the substrate with less tensile residual stress at the substrate/coating interface.to large extent compared to the specimens coated with 1μm and 15 μm. Thus, the optimum coating thickness of 5 μm with the longest fatigue life can be appeared.

3.5 CONCLUSIONS

In the present chapter, effect of coating thickness on fatigue strength for TiAlN coated STA-treated Ti6242S and γ -TiAl deposited under bias voltages of -30V and -100V was investigated in the range of coating thickness from 1 μm to 15 μm. The effect of coating thickness on fatigue strength was discussed in detail for both cases of surface crack nucleation mode and subsurface crack nucleation mode. The main conclusions obtained are summarized as follows:

1. Fatigue lives of the coated specimens with various coating thicknesses deposited under -30V were shorter than that of the uncoated specimen. The optimum thickness with the longest fatigue life was 5 μm. From the detailed fracture surface observation, it was found that fatigue crack initiated from specimen surface.

2. Fatigue lives of the coated specimens with various coating thicknesses deposited under -100V were longer than that of the uncoated specimen. The optimum thickness with the longest fatigue life was also 5 μm. From the detailed fracture surface observation, it was found that fatigue crack initiated subsurface in the substrate..

3. The reason why the shorter fatigue life for the coating thickness of 1μm compared to those for thicker coatings will be that thin coating layer of 1μm can be affected by plastic deformation of substrate crystal and then earlier cracking of the coating layer takes place compared to thicker coating layer, while thicker coating layers of 5 μm and 15 μm are much rigid and hardly affected by deformation of substrate..

4. The reason why the shorter life for the coating thickness of 15 μm compared to that for the coating thickness of 5 μm will be that the tensile residual stress in the substrate near the interface between coating layer and substrate is larger for the coating thickness of 15 μm compared to the coating thickness of 5 μm and this higher tensile residual stress results in earlier fatigue crack initiation.

Chapter 4 Suitability of bias voltage for avoiding fatigue strength degradation by coating

4.1 INTRODUCTION

In the chapter 2, taking up an STA-treated Ti6242S as a substrate material used for turbine components, etc., fatigue behavior of TiAlN coated specimen deposited under various bias voltages has been investigated in detail. It was found from the results that the fatigue crack nucleated from the specimen surface and the fatigue life was shorter than the uncoated specimen for the case of lower bias voltages. On the other hand, for the case of higher bias voltages it nucleated from subsurface in the substrate by supressing crack nucleation from specimen surface due to higher compressive residual stress and the fatigue life was longer than the uncoated specimen. However, the detail conditions for avoiding the fatigue life degradation due to TiAlN coating on Ti alloy substrates have not yet been clarified. In the present chapter, to find the process conditions for avoiding the fatigue life degradation of TiAlN coated Ti-alloys, fatigue strength tests of TiAlN coating deposited under various bias voltages on the substrate materials of a γ -TiAl intermetallic compound, an as-rolled Ti6242S and STA-treated Ti6242S were carried out. Fatigue behavior of these specimens was investigated in detail and the compressive residual stress of the coatings on different substrate materials was also measured to clarify the effect of substrate material on residual stress. From the results, the critical relationship between applied stress and bias voltage was proposed to find the process condition for avoiding the fatigue life degradation of TiAlN coated Ti-alloy was discussed.

4.2 EXPERIMENTAL PROCEDURE

4.2.1 Material

In the present chapter, three Ti-alloys were used as the substrate materials. STA-treated Ti6242S titanium alloy used in the chapters 2 and 3, as-rolled Ti6242S titanium alloy, which was prepared from the same starting material of STA-treated Ti6242S as a material with different strength and hardness and γ -TiAl intermetallic compound used in the chapter 3 as one of the different kinds of high temperature Ti-alloys. For γ -TiAl, the high purity ingot was produced by the induction skull melting and then heat-treated to form a microstructure with lamellar and equiaxed gamma phases. Chemical composition of the material used is Ti-48Al-2Nb-2Cr (at%). Microstructure of γ -TiAl is shown in Fig. 4.1. Chemical composition of the as-rolled Ti6242S is Al 6%, Sn 2%, Zr 4%, Mo 2%, Si 0.1% and Ti balance (in mass %), which is the same as that of the STA-treated Ti6242S used in the previous study. Microstructure of the as-rolled Ti6242S is shown in Fig. 4.1, which consists of transformed β (dark) and primary α (white) phases with different morphology from the STA-treated Ti6242S shown in the previous chapter.

The physical and mechanical properties of the substrate and coating materials are stated as follows: The young ' s modulus of γ -TiAl, as-rolled Ti6242S and TiAlN are 160-175 GPa,120GPa [58] and 450GPa respectively. The yield stress of γ -TiAl and as-rolled Ti6242S TiAlN are 459MPa [59] and 866MPa respectively. Tensile strength of γ -TiAl and as-rolled Ti6242S are 541MPa and 931MPa respectively. The hardness values of γ -TiAl, as-rolled Ti6242S and TiAlN are 470HV (4.6GPa), 330HV (3.2GPa) and (20 – 26GPa) respectively. The coefficient of thermal expansion, 1/°C of γ -TiAl, as-rolled Ti6242S and TiAlN are $10.8\text{x}10^{-6}$ [60], $9.3\text{x}10^{-6}$ [58] and $7.5\text{x}10^{-6}$ [61] respectively. The fatigue limit of γ -TiAl and as-rolled Ti6242S are 140 and 200 MPa respectively.

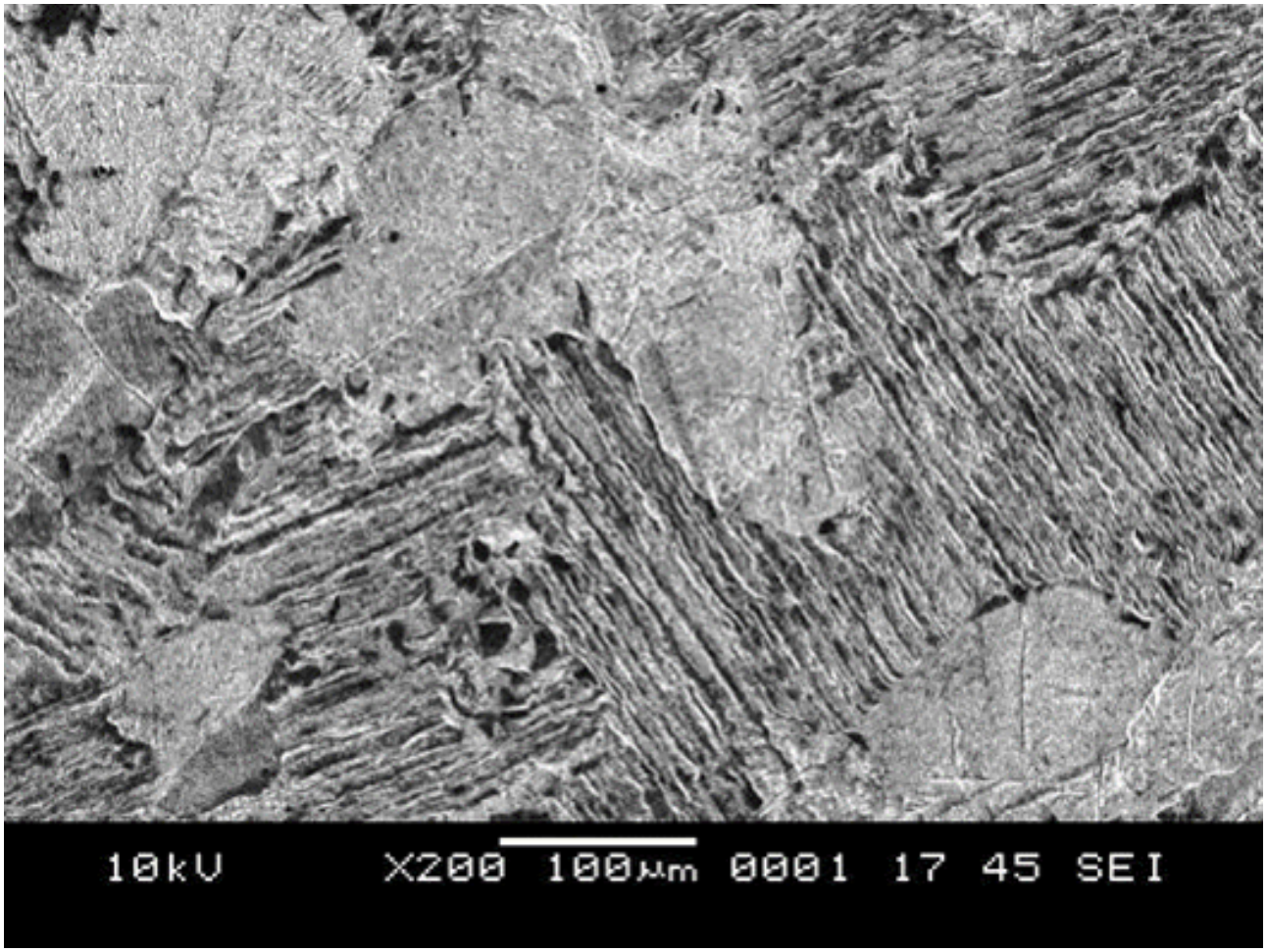

Fig. 4.1 Microstructures of (a) γ -TiAl and (b) as-rolled Ti6242S.

4.2.2 Fatigue test specimen

Shape and dimensions of a round bar tension type specimen used in the fatigue test are shown in Fig.4.2. The diameters of the specimen gage part are 3.0mm and 3.5mm for γ -TiAl and Ti6242S, respectively. However, the difference of the diameter is not due to special purpose and influence of diameter in the present range of difference would be negligible since the fatigue test is performed not by rotating-bending but tension-tension axial loading. The specimen surface was successively polished by using SiC abrasive papers up to #4000 and then buff-polished using diamond pastes with particle sizes up to 1μm to obtain mirror-like surface. One group of the polished specimens was forwarded to the coating process. The other group of the polished specimens was used for fatigue tests without coating. Before fatigue tests, ultrasonic cleaning was applied to the specimens.

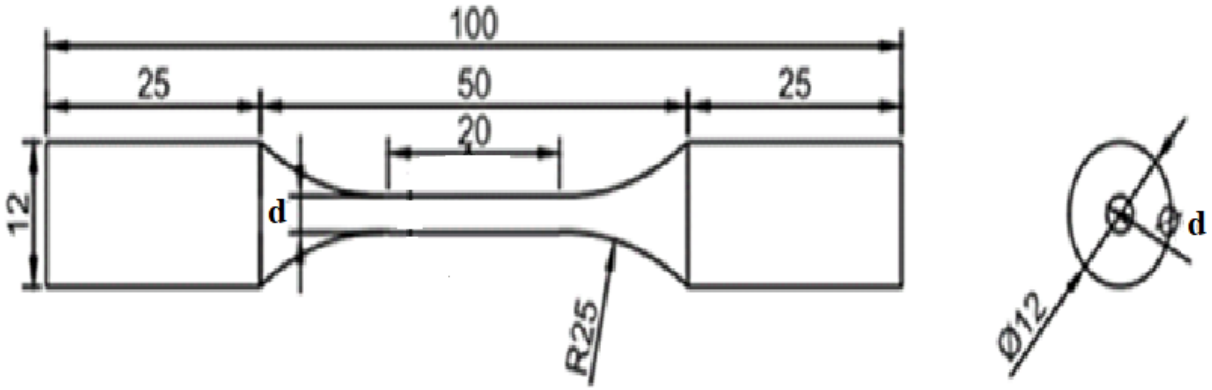

Fig. 4.2 Fatigue test specimen (All dimensions are in mm.) (d=3.0mm for γ-TiAl; d=3.5mm for Ti6242S).

4.2.3 Coating Procedure

TiAlN coating was deposited by using a cathodic arc ion plating system (AIP-SS002, Kobe Steel Ltd.) with a target Ti50Al50 (at %). Prior to deposition, the substrate specimens were heated and ion-etched. During the deposition process, pure reactive nitrogen atmosphere and temperature of substrate were kept to be 4Pa and 500°C, respectively. The bias voltages were varied from -20V to -100V for investigating influence of bias voltage on fatigue strength. The coating thickness of approximately 5 μm for each bias voltage was achieved by controlling time for deposition. The resultant coating layer thickness of about 5 μm was confirmed by the cross-sectional observations of the coated specimens. Some examples of the observations are shown in Fig.4.3. The coating thickness of TiAlN coating layer on the STA-treated Ti6242S substrate was also controlled to be about 5 μm, as in the previous chapter.

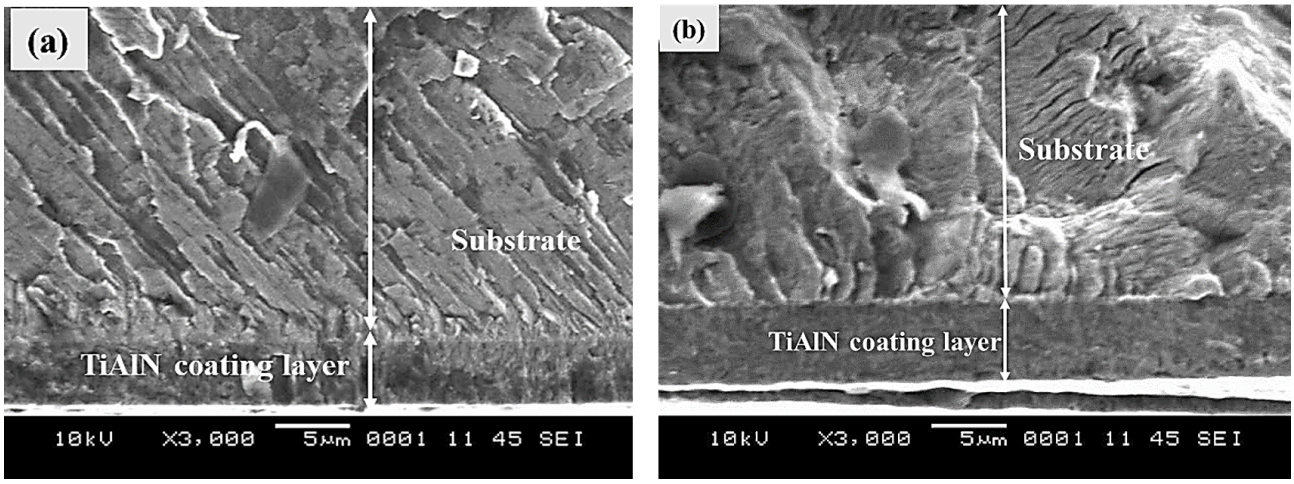

Fig. 4.3 Coating thickness observations through secondary electron imaging for (a) γ -TiAl coated specimen and (b) as-rolled Ti6242S coated specimen).

4.2.4 Fatigue test

A servo-hydraulic fatigue test machine with a load capacity of 10 kN was used for the fatigue strength tests of γ -TiAl and as-rolled Ti6242S specimens without and with TiAlN coating (hereafter referred as the uncoated specimen and the coated specimen, respectively). The fatigue tests were conducted at room temperature under a stress ratio of 0.1 and a frequency of 20 Hz. The fatigue test was continued up to specimen failure, while the test was stopped when the specimen was not fractured up to 10^7 cycles. The basic S-N curves of the uncoated specimens were obtained by conducting fatigue tests under various stress amplitudes. The fatigue tests at the same stress amplitude were carried out for the coated specimens deposited under various bias voltages to discuss the effect of bias voltage on fatigue life as well as to compare their fatigue lives with those of the uncoated specimens. Fatigue fractured surfaces were observed by using a scanning electron microscope (SEM) to clarify the fatigue crack nucleation location.

4.2.5 Measurements of residual stress and hardness

NX-ray diffractometer multiple HKL method [55] was applied to measure the residual stress of the coating by using X-ray tube of Cu(Kα).

Nano-indenter (Dynamic ultra-microhardness tester) was used to measure the hardness of the coating layer under an indentation load of 400 mN and a loading duration of 10 s. The hardness value was evaluated as the average value of ten measurements.

4.3 RESULTS

4.3.1 S-N curves

From the fatigue test results, S-N curves for the γ -TiAl and as-rolled Ti6242S uncoated specimens are shown in Fig. 4.4 and 4.5. For γ -TiAl, the fatigue strength defined at 10^7 cycles was about 140MPa based on the S-N curve of the uncoated specimen. Based on the S-N curve of the uncoated specimen, the stress amplitudes for fatigue tests of the coated specimens deposited under various bias voltages were selected as 190MPa and 210MPa. The fatigue test results of the coated specimens are also shown in Fig.4.4. As found from the figure, at the stress amplitude of 190MPa, the coated specimen deposited under -75V and -100V exhibited enhanced fatigue life compared to the uncoated specimen. The coated specimen deposited under -100V bias voltage did not fail until 10^7 cycles, which showing significant improvement of fatigue life. On the other hand, the fatigue lives of the coated specimens deposited under bias voltages of -20V, -30V and -50V were significantly decreased. At the higher stress amplitude of 210MPa, the resultant fatigue lives of the coated specimens were in the narrow range from 100 to 800 cycles, which were shorter than that of the uncoated specimen. It is suggested that fatigue lives of the coated specimens deposited even under higher bias voltages become shorter than that of the uncoated specimen at higher stress amplitudes. For as-rolled Ti6242S, the fatigue strength defined at 10^7 cycles was about 200MPa based on the S-N curve of the uncoated specimen. The fatigue test results of the coated specimens tested at 235 MPa,

which was selected by referring the S-N curve of the uncoated specimen, are also shown in Fig. 4.5. As seen from the figure, the fatigue lives of the coated specimens deposited under low bias voltage of -20V significantly degraded compared to that of the uncoated specimen. On the other hand, the coated specimens deposited under higher bias voltages of -30V, -50V, -75V and -100V exhibited the enhanced fatigue lives compared to that of the uncoated specimen. For STA-treated Ti6242S, the fatigue strength of the uncoated specimen defined at 10^7 cycles was about 200MPa based on the S-N curve shown in the previous chapter. Based on the fatigue test results of the coated specimens tested at 260 MPa, which was selected by referring the S-N curve of the uncoated specimen, the fatigue lives of the coated specimens deposited under low bias voltages of -20V and -30V significantly degraded compared to that of the uncoated specimen. On the other hand, the coated specimens deposited under higher bias voltages of -50V, -75V and -100V exhibited the enhanced fatigue lives compared to that of the uncoated specimen. From the foregoing results, the fatigue lives of the coated specimens would increase with increasing bias voltage regardless of substrate materials. However, whether the fatigue life of the coated specimen is longer than that of the uncoated specimen is not decided only by the bias voltage, which may be also affected by other factors, such as applied stress level.

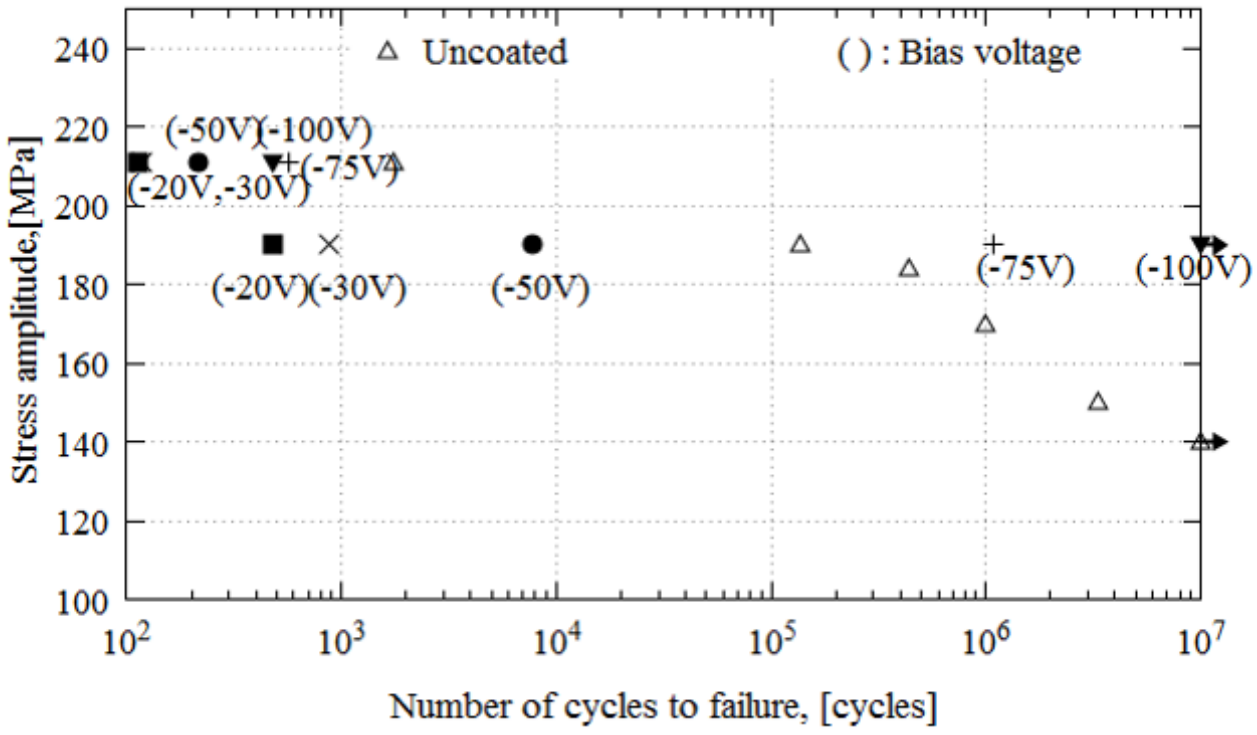

Fig. 4.4 S-N curves of the uncoated specimens and the coated specimens for γ -TiAl.

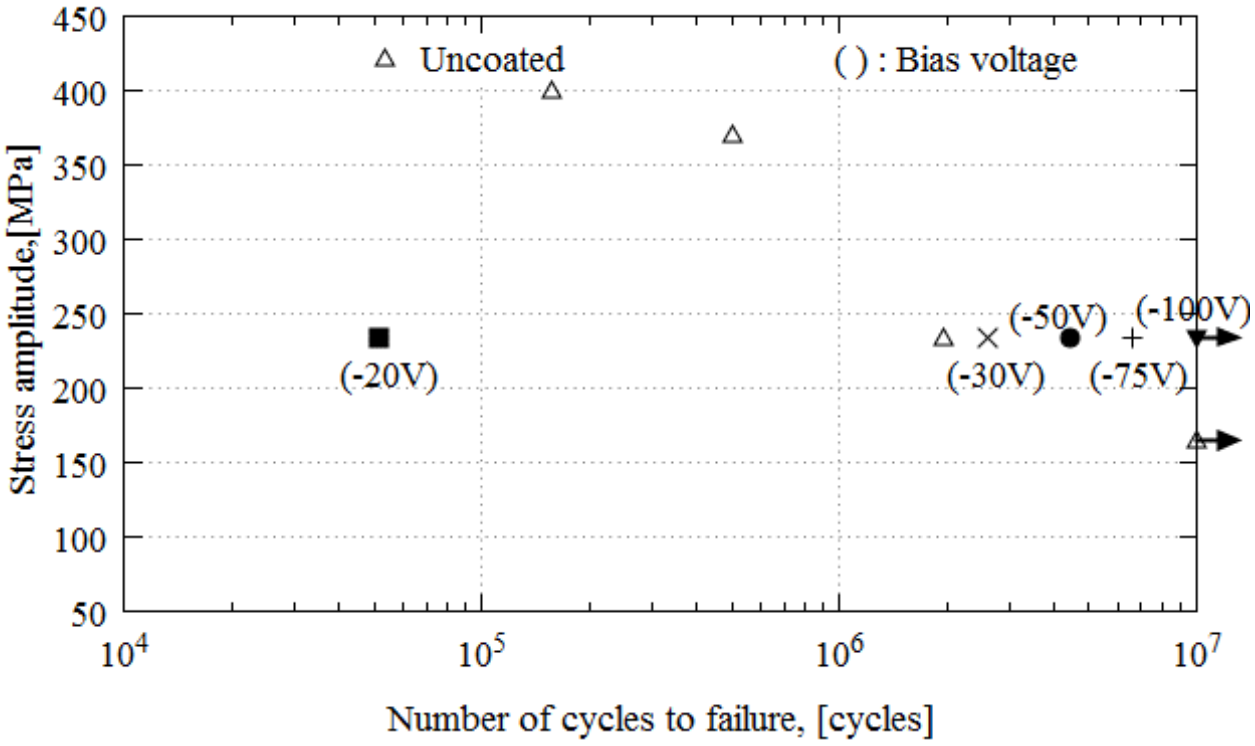

Fig. 4.5 S-N curves of the uncoated specimens and the coated specimens for as-rolled Ti6242S.

In the present study, for three materials with four levels of stress amplitude including the results of the previous study, fatigue tests of five specimens with different bias voltages were conducted at each stress amplitude. The fatigue test results clearly showed the same trend of bias voltage dependence of fatigue life, where the fatigue life increases with increasing bias voltage, regardless of material and stress amplitude. Therefore, this trend would be highly reliable, while some scatter will exist around each data point of fatigue life. Consequently, the authors believe the reliable conclusion could be obtained, while more data points will be preferable.

4.3.2 Fracture surface observations

Fatigue crack nucleation regions of the fatigue fractured specimens were observed in detail by using an SEM to obtain information about fatigue crack nucleation mechanism.. For the γ -TiAl uncoated specimen tested at 210MPa, as can be seen from Fig. 4.6, a fatigue crack nucleates from specimen surface without any marks or defects for a crack to start. For the coated specimen, smooth surface without step at the interface between coating layer and substrate could be observed regardless

of bias voltage. On the other hand, for the γ -TiAl coated specimen tested at a lower stress amplitude of 190MPa, as seen from Fig.4.7, smooth surface could be also observed in case of bias voltage of -20V. Similar smooth surface without step was also observed in case of bias voltages of -30V and -50V. On the other hand, a step at the interface between coating layer and substrate could be observed in case of bias voltage of -75V. In case of bias voltage of -100V, the specimen could not be fractured until 10^7 cycles and any surface crack could not be observed on the specimen surface.

For the as-rolled Ti6242S uncoated specimen tested at 235MPa, a fatigue crack nucleates from specimen surface without any marks or defects for a crack to start, as seen from Fig 4.8. For the coated specimens, smooth surface without step could be observed in case of bias voltage of -20V, similar smooth surface without step was also observed in case of bias voltage of -30V for the as-rolled Ti6242S coated specimen. On the other hand, a step at the interface between coating layer and substrate could be observed in case of bias voltage of -75V, as seen from Fig.4.8. Similar step at the interface between coating layer and substrate was observed in case of bias voltages of -30V and -50V. In case of bias voltage of -100V for the as-rolled Ti6242S substrate, the specimen could not be fractured until 10^7 cycles and any surface crack could not be observed on the specimen surface. For the STA-treated Ti6242S uncoated specimen, similar fracture surface morphology to that of the as-rolled Ti6242S uncoated specimen was observed, as shown in the previous chapter. For the STA-treated Ti6242S coated specimen, similar fracture surface evolution depending on bias voltage as found for the as-rolled Ti6242S coated specimen was also observed, as shown in the previous chapter.

As mentioned above, smooth surface in the interface region between coating layer and substrate was observed in case of higher applied stress amplitude and lower bias voltage, which suggests that the fatigue crack starts from surface and propagates into substrate on the same fracture plane (surface crack nucleation mode). On the other hand, a step at the interface between coating layer and substrate was observed in case of lower applied stress amplitude and higher bias voltage, which suggests that fatigue propagation plane would be different between coating layer and substrate and the fatigue crack would nucleate in the substrate and propagate to the coating layer and then fracture or fatigue fracture of coating layer would be induced (subsurface crack nucleation mode). It is noteworthy that

fatigue lives of the coated specimens with surface crack nucleation mode are shorter than the uncoated specimen, while those of the coated specimens with subsurface crack nucleation mode are longer than the uncoated specimen. The longer lives of the coated specimens would be induced by suppression of crack nucleation from specimen surface. In the previous chapter, from the results of surface crack observation on the coated specimen and fatigue fracture surface observation, typically for the bias voltage of -100V, fatigue fracture in the substrate was visible on the fracture surface, while a crack couldn ' t be observed on the coating surface until final fracture. Therefore, it is clear that a crack nucleates subsurface in the substrate and propagates to the coating layer to break in case of the coated specimens deposited under higher bias voltages, as schematically shown in Fig.2.11 of the previous chapter .

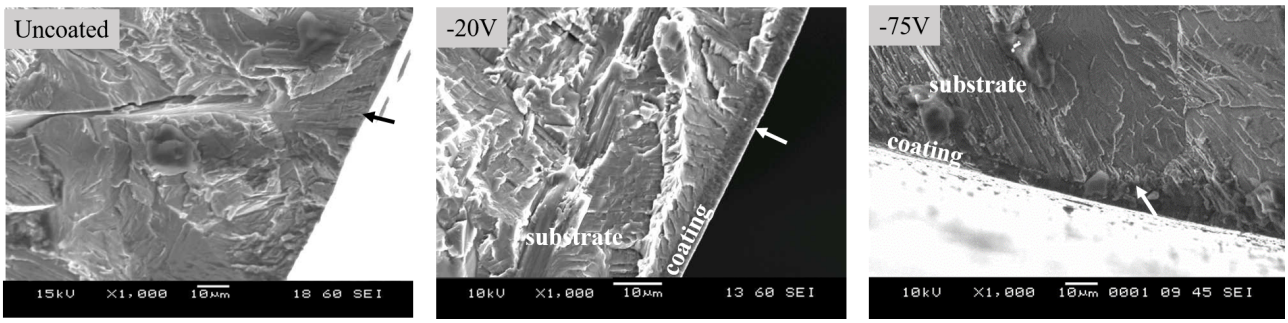

Fig. 4.6 Crack initiation region of the uncoated specimen and the coated specimens deposited under -20V and -75V for the substrates of γ -TiAl at stress amplitude σ_a =210MPa.

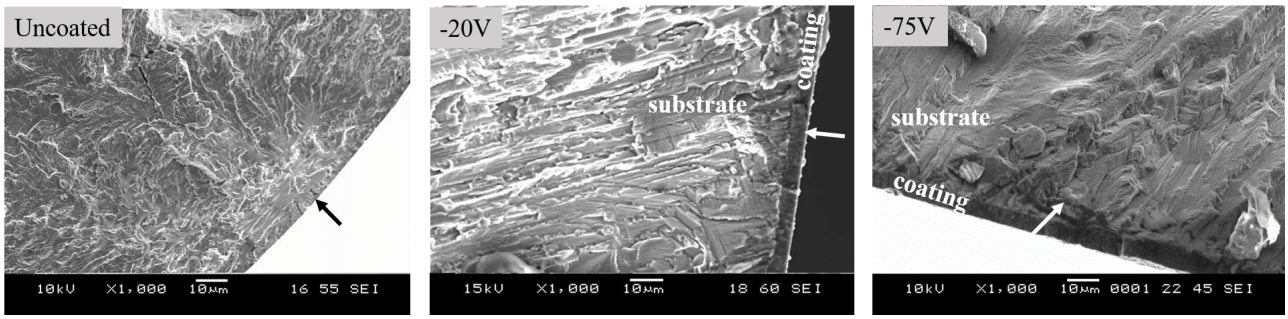

Fig. 4.7 Crack initiation region of the uncoated specimen and the coated specimens deposited under -20V and -75V for the substrates of γ -TiAl at stress amplitude σ_a =190MPa.

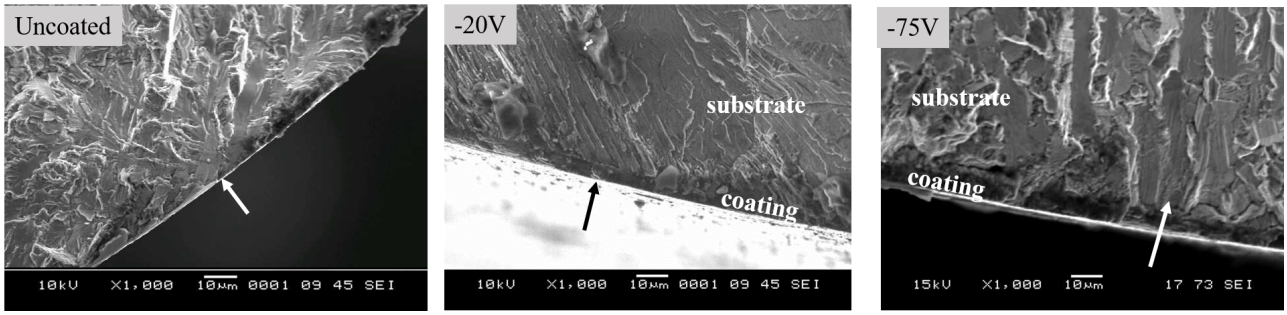

Fig. 4.8 Crack initiation region of the uncoated specimen and the coated specimens deposited under -20V and -75V for the substrates of as-rolled Ti6242S at stress amplitude σ_a =260MPa.

4.3.3 Observations of the coating surface

The surface observations of the coating on the γ -TiAl and the as-rolled Ti6242S substrate materials deposited under -20V bias voltage are shown in Fig. 4.9. As seen from the figure, the coating growth defects are visible and their maximum defect sizes are in the range from 36.4 μm to 46.8 μm for both substrate materials. In the previous chapter, it was confirmed based on the fracture mechanics approach that the stress intensity factor range of the growth defect was near to the threshold stress intensity factor range of the substrate material and then the defects with this range of sizes could become fatigue crack nucleation sites.

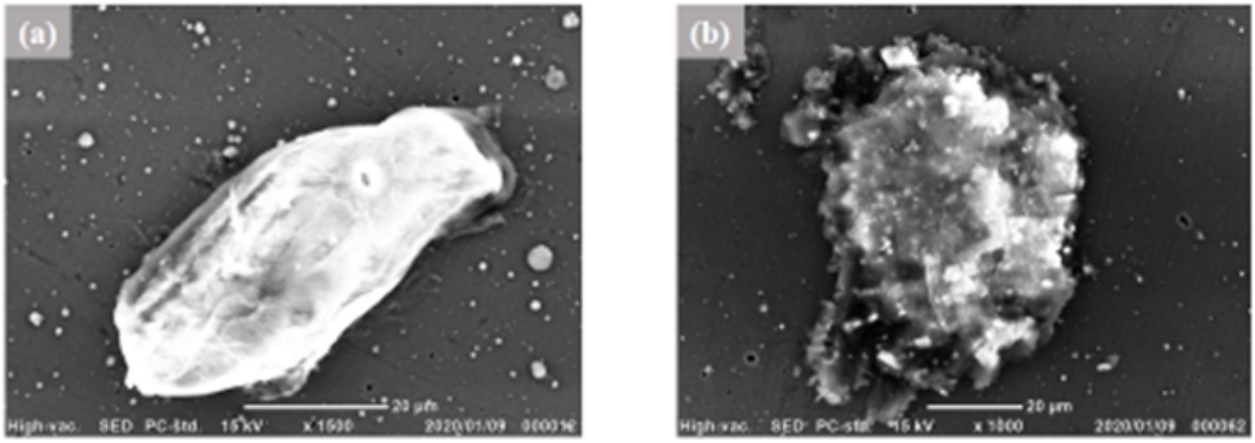

Fig. 4.9 Observation of the defects on coating surface deposited under bias voltage of -20V for the substrates of (a) γ -TiAl and (b) as-rolled Ti6242S.

4.3.4 Residual stress in the coating layer

Relationships between bias voltage and compressive residual stress of the coating layer on the γ -TiAl and as-rolled Ti6242S substrate materials are shown in Fig.4.10. The same relationship was obtained for the STA-treated Ti6242S substrate material as shown in the previous chapter. As seen from the figure, the compressive residual stress for three kinds of the coated specimens significantly increased with increasing bias voltage. It was also found that the compressive residual stress values for the coated specimens with as-rolled and STA-treated Ti6242S substrates were almost same, while those for the coated specimens with γ -TiAl substrate were rather high compared to the case of Ti6242S substrates. It is reported that the ion peening effect induced the increase of residual stress in the cathodic arc TiC [39] and magnetron sputtered TiN [40] and TiC [41] coatings. It would be speculated that similar ion peening effect also induces the increase of residual stress in the present CA-PVD TiAlN coating. With increasing bias voltage, the input energy of irradiate ion increases and then the intrinsic stress in the coating increases. The main reason for the increased residual stress with increasing bias voltage would be due to this increased intrinsic stress.

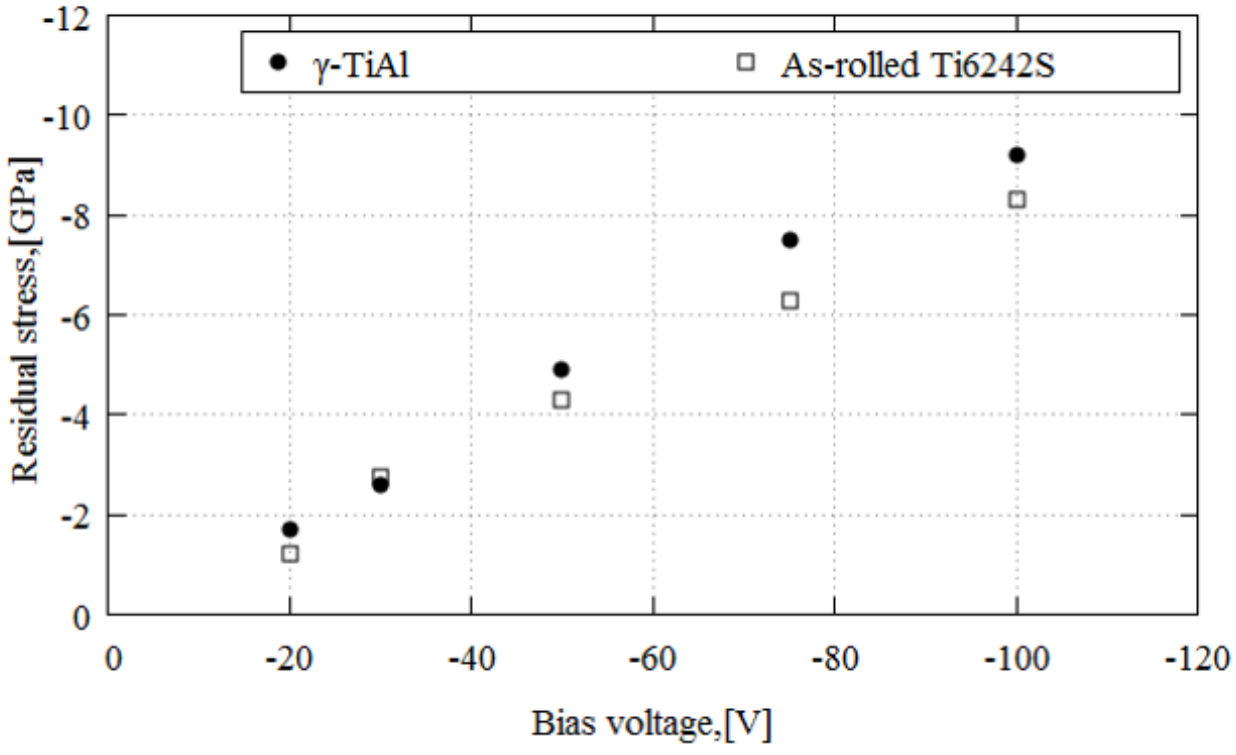

Fig. 4.10 Relationship between bias voltage and residual stress.

The estimation of true stress distribution of coating layer is estimated as follows: During the tensile deformation of the metal, the shear stress is created at the interface between the substrate and the coating layer and normal tensile stress is transferred into the film. While the tensile strain in the metal substrate adverses during the testing, cracks transverse to the tension direction start to appear in the ceramic coating layer. The strain present in the substrate at the first appearance of the transverse cracks is related to the tensile fracture strength of the coating layer. The crack spacing at the saturated crack density is related to the interfacial shear strength of the ceramic-metal interface. The key finding lies in the relationship between the interfacial shear strength ($\tau\hat{}$), film thickness (δ), average saturated crack spacing (λ), maximum crack spacing at saturation (($\lambda_{max} = 1.5\lambda$), the applied tensile stress (σ), and the tensile strength of the ceramic film (σ), as shown below [59]: Oettel and Wiedemann [62] proposed an equation for estimating residual stress in PVD hard coatings by considering the ion peening effect, the hetero-epitaxy misfit at the interface and thermal expansion misfit during cooling as:

$$\sigma_r = \sigma_{ep} + \sigma_g + \sigma_c \cdots\cdots (4.1)$$

where

- σ_{ep}: stress induced by hetero-epitaxy misfit at interface between coating and substrate
- σ_g: intrinsic stress induced during growth of coating, where atom or ion peening into lattice defects induces volume expansion.
- σ_c : stress induced by the difference of thermal expansion between coating material and substrate material during cooling after deposition.

They considered that the first term can be assumed to be a priori negligibly small or will be relaxed by misfit dislocation networks. The second term is related only to growth of coating film and not dependent on substrate material. The third term is related to the thermal expansion misfit between coating and substrate materials. Therefore, the inclination of the relationship between bias voltage

and residual stress shown in Fig.4.10 will be the same and independent of substrate material, while the third term will be influenced by the substrate material. The coefficient of thermal expansion for STA –treated Ti6242S is same as that of as-rolled Ti6242S. As found from the table, difference of coefficient of thermal expansion between TiAlN and γ -TiAl is larger than that between TiAlN and Ti6242S, which indicates the residual stress due to the third term for the γ -TiAl substrate is larger than that for the Ti6242S substrate. This will contribute to the higher residual stress for γ -TiAl substrate compared to Ti6242S substrate. The third term is given as [62]:

$$\sigma_C = \frac{E_L}{(1-\nu)}(\alpha_L - \alpha_S)(T_d - T) \cdots (4.2)$$

where E_L is the Young ' s modulus of the coating, ν the Poisson ratio of the coating, $\alpha_L$and α_S the coefficient of thermal expansion for the coating and the substrate, respectively, and T_d the deposition temperature. Since the difference of the values of $(\alpha_L - \alpha_S)$ between γ -TiAl and Ti6242S is 2.7×10^{-6}, the difference of residual stress between γ -TiAl and Ti6242S substrates can be estimated to be about 0.83 GPa according to Eq.4.2 by assuming the Poisson ratio ν is 0.3 and T is 20°C, which is similar order to the difference of residual stress observed in Fig. 4.10. The second term is given as [29]:

$$\sigma_g = -\frac{1}{3}\frac{E_L}{(1-\nu)}\Sigma\Omega_i c_{Di} \cdots (4.3)$$

whereΩ_i is the specific volume change caused by defect i and c_{Di} is the defect concentration. However, it seems to be difficult to estimate σ_g value, since detailed information about the characteristics of the defects is not available.

4.3.5 Hardness of the coating layer

The relationship between bias voltage and hardness of the coating layer on the γ -TiAl and as-rolled Ti6242S substrate materials are shown in Fig. 4.11 . The same relationship was obtained for the STA-treated Ti6242S substrate material in the previous chapter. As seen from the figure, the hardness value of the coating layer was increased with increasing bias voltage. It is also found that the substrate material does not influence the hardness of the coating layer. It is known that the hardness of the TiAlN coating is generally influenced by the grain size, the texture and the residual stress [38, 42] . However, as concluded in the previous chapter as well as in the reports [28] , the higher hardness under higher bias voltage would be dominantly induced by higher compressive residual stress at higher bias voltage, while some other factors during coating process may contribute to an increase of hardness. The compressive residual stress for the γ -TiAl substrate was rather high compared to those for Ti6242S substrates . However, since the difference of residual stress between two kinds of substrates is small compared to the variation of residual stress with bias voltage, an influence of the difference of residual stress could not be observed.

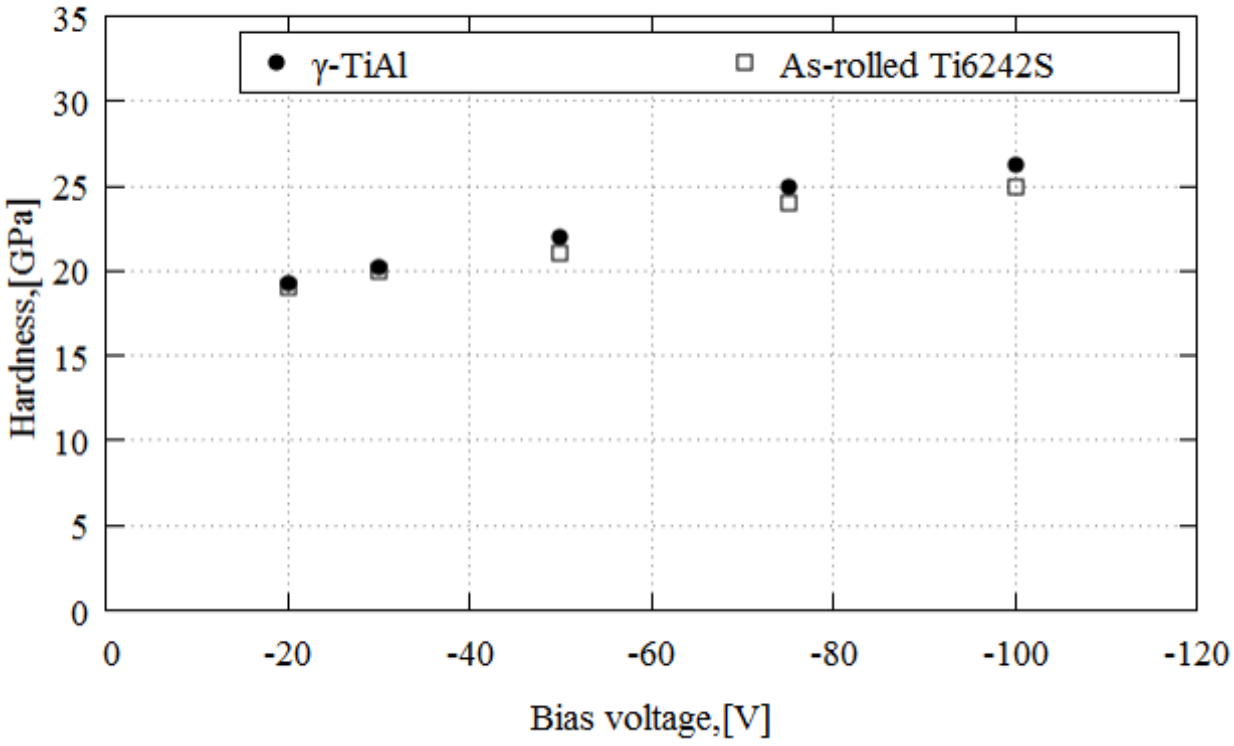

Fig. 4.11 Relationship between bias voltage and hardness.

4.3.6 Fracture toughness of the coating layer

Fracture toughness of the coating layer would influence cracking behavior of the coating layer and then fatigue behavior of the coated material. Fracture toughness of the present TiAlN coated Ti alloys could not be measured by the indentation fracture toughness test due to large plastic deformation of the substrate before cracking of the coating layer. Therefore, the dependence of fracture toughness on bias voltage has been speculated based on the fracture toughness estimating equation for the indentation fracture toughness test method, which is given as:

$$K_{IC} = 0.016(\frac{E}{HV})^{0.5}\frac{P}{c^{1.5}} \cdots\cdots (4.4)$$

for Vickers indenter [63], where E is Young's modulus, HV the hardness, P the indentation load and c the crack length. When the bias voltage is increasing, the hardness is not significantly but slightly increasing as discussed in the previous section. Therefore, the fracture toughness of the coating layer is speculated to slightly decrease with increasing bias voltage based on Eq. 4.4, which may be also induced mainly by the increased compressive residual stress

4.4 DISCUSSION

4.4.1 Critical relationship between applied stress and bias voltage

Relationship between applied stress amplitude normalized by fatigue limit and bias voltage is shown in Fig 4.12 , where the symbols ● and ○ represent the fatigue life shorter than the uncoated material and the fatigue life longer than the uncoated material, respectively. As seen from the figure, when the normalized applied stress amplitude decreases, the fatigue life of the coated material becomes longer than the uncoated material even under lower bias voltages, while the fatigue life of the coated material becomes shorter even under higher bias voltages when the normalized applied stress amplitude increases. When the bias voltage increases, the compressive residual stress also increases. The higher compressive residual stress at higher bias voltage suppresses the crack nucleation from

surface and then a crack tends to nucleate from subsurface,. The similar fatigue crack propagation retardation due to hard surface layer with compressive residual stress in titanium alloys has been reported [45] and [46]. The critical condition for avoiding the fatigue life degradation of the coated material compared to the uncoated material can be estimated based on Fig. 4.12 . In the figure, the boundary between shorter and longer fatigue lives of the coated material compared to the uncoated material is presented by the broken line, which is given by the following equations in the bias voltage range from -20V to -100V:

$$\frac{\sigma_a}{\sigma_w} = 1.12–0.00375BV$$

$$BV = \frac{1}{0.00375}(1.12–\frac{\sigma_a}{\sigma_w}) \cdots\cdots (4.5)$$

where BV is the bias voltage. The region upper the broken line is the region of shorter fatigue life than the uncoated material, while the region below the broken line is the region of longer fatigue life than the uncoated material. As found from Eq. 4.5) as well as from Fig. 4.12 , when the normalized stress level is lower than 1.12, fatigue life of the coated material would be longer than the uncoated material regardless of substrate material and bias voltage. This means that if the design stress amplitude is equal to or lower than the fatigue limit of the substrate material, fatigue strength and life of TiAlN coated material would be superior compared to those of the uncoated material. On the other hand, when the normalized stress level is higher than 1.12, larger bias voltage (negative sign) depending on the applied stress level has to be selected according to Eq. 4.5 for avoiding the degraded fatigue life compared to the uncoated material. For example, if the design stress amplitude is given and is higher than 1.12, the bias voltage should be selected to be larger than the BV value obtained by Eq. 4.5 for avoiding the degraded fatigue life. These information and procedure for avoiding the degraded fatigue life of the coated material would be useful for reliable and safe design of TiAlN coated Ti-alloy components.The compressive residual stress for γ -TiAl substrate was rather high compared to those for Ti6242S substrates. However, since the difference of residual stress is small compared to the variation of residual stress with bias voltage, it might be considered that Eq. 4.5 is

still effective in the range of the present study.

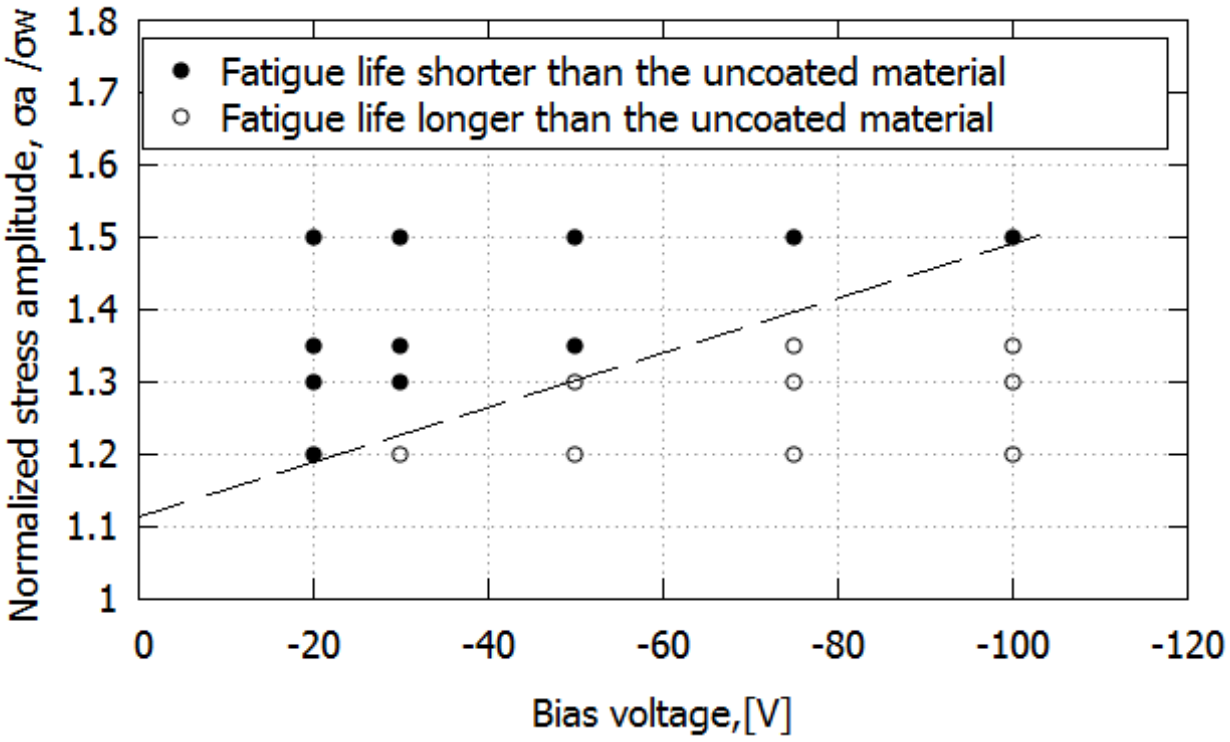

Fig. 4.12 Relationship between normalized applied stress amplitude σ_a / σ_w and bias voltage.

In the present study, the following parameters were selected: TiAlN as a coating material, three kinds of Ti-alloys as substrate materials including the material used in the previous paper, 5 μm as a coating thickness, five bias voltages as coating process parameters and stress ratio of 0.1. Based on the proposed critical relationship, which is effective in the range of the present study, when the normalized stress level is lower than 1.12, fatigue life of the coated material would be longer than the uncoated material regardless of substrate material and bias voltage.

4.4.2 Transition behavior of crack nucleation mode from surface to subsurface

From Fig.4.12, it can be found that at the same bias voltage the surface crack nucleation mode changes to the subsurface crack nucleation mode when the applied stress amplitude is reduced. The fatigue life for the subsurface crack nucleation mode is longer than that of the uncoated specimen. Therefore, Fig. 4.12 can estimate the condition for the fatigue life of the coated specimen longer than the uncoated specimen. The region upper the one-dotted line is the region of shorter fatigue life

than the uncoated specimen, while that lower the one-dotted line is the region of longer fatigue life than the uncoated specimen. Finally, the figure suggests that fatigue lives of the coated specimens are longer than the uncoated specimen at fatigue limit level of the substrate material regardless of substrate material and bias voltage. The current study has limitations in ignoring frequency effect (Dwell fatigues) and creep (time effects) at high temperature etc.,

4.5 CONCLUSIONS

In the present chapter, the fatigue strength tests of the TiAlN coating deposited on γ -TiAl and as-rolled Ti6242S substrates in addition to STA-treated Ti6242S substrate used in the previous chapter were carried out. Based on the results, the critical condition of bias voltage for avoiding the fatigue strength degradation due to TiAlN coating was discussed. The main conclusions obtained are summarized as follows:

1. The compressive residual stress of the coating layer increased with increasing bias voltage for three substrate materials. The relationships between bias voltage and compressive residual stress for three substrate materials were almost coincided each other, while the compressive residual stress for the γ -TiAl substrate was rather high compared to those for the as-rolled and STA-treated Ti6242S substrates, which could be explained based on the difference of thermal expansion coefficient.

2. At the same applied stress amplitude, with increasing bias voltage, the fatigue life of the coated specimen becomes longer due to increased compressive residual stress. While at the same bias voltage, the fatigue life of the coated material becomes longer than that of the uncoated material with decreasing applied stress amplitude. .

3. TBased on the proposed critical relationship, Eq. 4.5, when the normalized stress level is lower than 1.12, fatigue life of the coated material would be longer than the uncoated material regardless of substrate material and bias voltage. On the other hand, when the normalized

stress level is higher than 1.12, larger bias voltage depending on the applied stress level has to be selected according to Eq. (6) for avoiding the fatigue life degradation due to TiAlN coating.

Chapter 5 Conclusions

Titanium alloys have been intensively used as structural materials for turbine components, jet engine components, etc. Ti6242S and γ-TiAl Titanium alloys are selected as two substrate materials in this work to investigate their influence on the properties of coating which affects the performance of the substrates.As it is well known that the substrate materials plays an important role in determining the mechanical properties and wear resistance of coatings. and thereby its influence on fatigue behavior of coated titanium alloys, the study has been carried out by coating TiAlN on different substarte materials.Ti6242S and γ-TiAl Titanium alloys are selected as two different kinds of turbine blade materials, where γ-TiAl can be applied at much higher service temperature compared to Ti6242S.Under the present test conditions, the maximum applied stress levels are lower than yield stress for both the materials. If much high applied stresses are selected, low-cycle fatigue behavior should be considered, which will be future work. TiAlN coating has been recently applied on the titanium alloy to improve wear and erosion resistance. However, fatigue strength as well as fatigue mechanism of the TiAlN coated titanium alloys have not yet been clarified fully, while they are crutial for strauctural design and maintenance. In the present work, as the basic study on fatigue of TiAlN coated titanium alloys, the following issues have been worked on: (1) fatigue characteristics, fatigue behavior and mechanisms, (2) critical condition of bias voltage, which is one of main process parameters, for avoiding fatigue strength degradation compared to the uncoated specimen, (3) effect of coating thickness and the optimum thickness. Based on the results, following conclusions were obtained.

1. Fatigue strengths of the TiAlN coated STA-treated Ti6242S alloy specimens deposited under higher bias voltages were significantly improved compared to the uncoated specimens, where a fatigue crack nucleated in the subsurface. On the other hand, the TiAlN coated STA-treated Ti6242S alloy specimens deposited under lower bias voltages exhibited degraded fatigue strengths compared to the uncoated specimens, where a fatigue crack nucleated from the coated surface.

2. The compressive residual stress induced in the coating layer was significantly increased with increasing bias voltage, which dominantly influence the fatigue behavior and fatigue mechanism of the coated specimen, where fatigue life of the TiAlN coated STA-treated Ti6242S alloy specimen increased with increasing bias voltage.

3. At the same applied stress amplitude, fatigue lives for the substrates of as-rolled Ti6242S and γ -TiAl became shorter than the uncoated specimen with decreasing bias voltage, while they became longer than the uncoated specimen with increasing bias voltage, similar to the case of STA-treated Ti6242S substrate. This phenomenon observed for the case of as-rolled Ti6242S and γ -TiAl substrates also resulted from the increase of compressive residual stress with increasing bias voltage, same as to the case of STA-treated Ti6242S substrate.

4. From the foregoing fatigue test results, the critical relationship between applied stress normalized by each fatigue limit of uncoated specimen and bias voltage to give the boundary between shorter and longer lives could be obtained. It was found from this relationship that at fatigue limit level, fatigue life of the TiAlN coated Ti-alloy specimen would be not degraded but enhanced compared to the uncoated specimen regardless of bias voltage. While, the higher bias voltage was required for avoiding the degraded fatigue life at stress amplitudes higher than the fatigue limit.

5. From the fatigue strength tests of TiAlN coated Ti-alloys with coating thicknesses of 1μm, 5 μm and 15 μm , the optimum thickness with the longest fatigue life could be found to be around the intermediate coating thickness of 5 μm.

6. It was found from the detailed observations and discussion that the lower fatigue life of coating thickness of 1μm results from fracture of coating layer under strong influence of deformation of substrate crystal. On the other hand, the lower fatigue life of 15 μm coating thickness results from the higher tensile residual stress induced in the substrate near coating layer and at the substrate interface. The fatigue behavior and properties of coated materials would be influenced by

many parameters, such as coating process conditions, coating thickness, combination of coating material and substrate material, mechanical properties of coating layer, residual stress, etc. There have been lots of reports on the effects of these parameters on performance of coatings. In the present work, the authors have selected TiAlN as a coating material, three kinds of Ti-alloys as substrate materials, 5 μm as a coating thickness and five bias voltages as coating process parameters to investigate the critical process condition for avoiding degradation of fatigue performance due to application of coating. Within these ranges of parameter, relation could be obtained to estimate the critical condition of bias voltage for enhancing fatigue performance of the coated specimen more than the uncoated specimen.

The effects of multiaxial stress state of residual stress for fatigue crack initiation and propagation mechanism plays a vital role as the residual stress will be in multiaxial state, while the applied stress is uniaxial in the loading direction. Furthermore, the residual stress is a static stress, while the applied stress is a cyclic stress.Therefore, the residual stress in the loading direction will dominantly influence fatigue crack initiation and propagation behavior.as a mean stress. Above mentioned conclusions summarized based on the present work have revealed basic fatigue behavior and fatigue mechanisms of the TiAlN coated titanium alloys, the coating process parameter of bias voltage for avoiding fatigue strength degradation and effect of coating thickness, which were not clarified fully until now. These findings and conclusions would significantly contribute to structural design of turbine components with TiAlN coated titanium alloy as well as process design of TiAlN coating on titanium alloy. However, there are still various parameters remained, which influence fatigue behavior of TiAlN coated titanium alloys, such as composition of TiAlN coating which influences mechanical properties and then fatigue property, coating process parameters which may influence residual stress of the coating layer, etc. Effects of these parameters needs to be clarified in the future investigations. High temperature fatigue behavior of the TiAlN coated titanium alloy is an important issue remained and the related investigations are required in the next step of research. These investigations would significantly contribute the reliable structural design of high temperature components such as gas turbines and jet engines. The residual stress maintains the same level as at room temperature

upto certain temperature which has to be investigated. Therefore, it is expected that even at high temperatures , the residual stress can suppress crack initiation and propagation in the similar manner at room temperature.The sustainability of TiAlN coating in high temperature environment has to be investigated as a future study to investigate the effect of TiAlN coating on fatigue behavior of Titanium alloys under high temperature for suitability to high temperature applications. The effects of elastic-plastic shake down of substrate on residual stress distribution of coating has to be carried out as future investigation as it holds the following significance:If the applied stress is high enough to induce elastic-plastic deformation of substrate near the interface between coating layer and substrate, the residual stress will be released up to some level at the first cycle under stress control fatigue test. However, after the second cycle, the deformation behavior will become elastic due to cyclic hardening. On the other hand, under strain control fatigue test the plastic deformation near the interface will be cyclically induced, which significantly release the residual stress and influence the fatigue behavior of the coated materials. Investigation on detail of residual stress relaxation due to cyclic plastic deformation will be carried out as future work.

In the case of high temperature applications such as gas turbine engine components,creep is the dominant failure factor which has to be considered as a major issue.Regarding to this failure issue,the study on how TiAlN coating behave under creep at high temperature also has to be studied as future work.

References

1) A Chamanfar, T Pasang, A Ventura, and WZ Misiolek. Mechanical properties and microstructure of laser welded ti–6al–2sn–4zr–2mo (ti6242) titanium alloy. *Materials Science and Engineering: A*, 663:213–224, 2016.

2) Toshimitsu TETSUI. Development of a new tial turbocharger for high temperature use. In *Third International Workshop on γ-TiAl Technologies, Bamberg, Germany*, pages 29–31, 2006.

3) RE Schafrik. A perspective on intermetallic commercialization for aero-turbine applications. *Minerals, Metals and Materials Society/AIME, Structural Intermetallics 2001(USA),*, pages 13–17, 2001.

4) Ian Mellor, Lucy Grainger, Kartik Rao, James Deane, Melchiorre Conti, Greg Doughty, and Dion Vaughan. Titanium powder production via the metalysis process. In *Titanium powder metallurgy*, pages 51–67. Elsevier, 2015.

5) Matthew J Donachie. *Titanium: a technical guide*. ASM international, 2000.

6) Olayinka Oluwatosin Abegunde, Esther Titilayo Akinlabi, Oluseyi Philip Oladijo, Stephen Akinlabi, and Albert Uchenna Ude. Overview of thin film deposition techniques. *AIMS Mater. Sci*, 6(2):174–199, 2019.

7) HW Wang, MM Stack, SB Lyon, P Hovsepian, and W-D Münz. Wear associated with growth defects in combined cathodic arc/unbalanced magnetron sputtered crn/nbn superlattice coatings during erosion in alkaline slurry. *Surface and Coatings Technology*, 135(1):82–90, 2000.

8) Tony Pilkington. *Development and Evaluation of Plasma Assister Alumina Based Coatings*. PhD thesis, University of Sheffield, Department of Materials Science and Engineering, 2014.

9) H Jiménez, DM Devia, V Benavides, A Devia, YC Arango, PJ Arango, and JM Velez. Thermal protection of h13 steel by growth of (tial) n films by papvd pulsed arc technique. *Materials Characterization*, 59(8):1070–1077, 2008.

10) Jeon G Han, Joo S Yoon, Hyung J Kim, and Keon Song. High temperature wear resistance of (tial) n films synthesized by cathodic arc plasma deposition. *Surface and Coatings Technology*, 86:82–87, 1996.

11) L Cunha, M Andritschky, L Rebouta, and R Silva. Corrosion of tin,(tial) n and crn hard coatings produced by magnetron sputtering. *Thin Solid Films*, 317(1-2):351–355, 1998.

12) CP Constable, DB Lewis, J Yarwood, and W-D Münz. Raman microscopic studies of residual and applied stress in pvd hard ceramic coatings and correlation with x-ray diffraction (xrd) measurements. *Surface and Coatings Technology*, 184(2-3):291–297, 2004.

13) J Vetter and AJ Perry. Advances in cathodic arc technology using electrons extracted from the vacuum arc. *Surface and Coatings Technology*, 61(1-3):305–309, 1993.

14) O Knotek, F Löffler, and G Krämer. Arc-deposited ti-zr-n coatings on cemented carbides for use in interrupted cutting. *Surface and Coatings technology*, 49(1-3):325–329, 1991.

15) Gerhard Welsch, Rodney Boyer, and EW Collings. *Materials properties handbook: titanium alloys*. ASM international, 1993.

16) Seog-Young Yoon, Kwang O Lee, Sung Soo Kang, and Kwang Ho Kim. Comparison for mechanical properties between tin and tialn coating layers by aip technique. *Journal of materials processing technology*, 130:260–265, 2002.

17) JH Hsieh, C Liang, CH Yu, and W Wu. Deposition and characterization of tialn and multi-layered tin/tialn coatings using unbalanced magnetron sputtering. *Surface and Coatings Technology*, 108:132–137, 1998.

18) Kazuki Kawata, Hiroyuki Sugimura, and Osamu Takai. Characterization of (ti, al) n films deposited by pulsed dc plasma-enhanced chemical vapor deposition. *Thin solid films*, 386(2):271–275, 2001.

19) Paul H Mayrhofer, Christian Mitterer, Lars Hultman, and Helmut Clemens. Microstructural design of hard coatings. *Progress in materials science*, 51(8):1032–1114, 2006.

20) MMM Bilek, DR McKenzie, and W Moeller. Use of low energy and high frequency pbii during thin film deposition to achieve relief of intrinsic stress and microstructural changes. *Surface and Coatings Technology*, 186(1-2):21–28, 2004.

21) D Rafaja, Ch Wüstefeld, C Baehtz, V Klemm, M Dopita, M Motylenko, C Michotte, and M Kathrein. Effect of internal interfaces on hardness and thermal stability of nanocrystalline ti 0.5 al 0.5 n coatings. *Metallurgical and Materials Transactions A*, 42(3):559–569, 2011.

22) JM Andersson, J Vetter, J Muller, and J Sjoen. Structural effects of energy input during growth of ti1- xalxn (0.55 ≤ x≤0.66) coatings by cathodic arc evaporation. *Surface and Coatings Technology*, 240:211–220, 2014.

23) Donghai Yu, Chengyong Wang, Xiaoling Cheng, and Fenglin Zhang. Optimization of hybrid pvd process of tialn coatings by taguchi method. *Applied Surface Science*, 255(5):1865–1869, 2008.

24) K-D Bouzakis, G Skordaris, S Gerardis, G Katirtzoglou, S Makrimallakis, M Pappa, E LilI, and R M'Saoubi. Ambient and elevated temperature properties of tin, tialn and tisin pvd films and their impact on the cutting performance of coated carbide tools. *Surface and Coatings Technology*, 204(6-7):1061–1065, 2009.

25) SK Wu, HC Lin, and PL Liu. An investigation of unbalanced-magnetron sputtered tialn films on skh51 high-speed steel. *Surface and Coatings Technology*, 124(2-3):97–103, 2000.

26) R Wuhrer and WY Yeung. Grain refinement with increasing magnetron discharge power in sputter deposition of nanostructured titanium aluminium nitride coatings. *Scripta Materialia*, 50(6):813–818, 2004.

27) SCDS PalDey and SC Deevi. Single layer and multilayer wear resistant coatings of (ti, al) n: a review. *Materials Science and Engineering: A*, 342(1-2):58–79, 2003.

28) Amina Zouina Ait-Djafer, Nadia Saoula, Hamid Aknouche, Bendiba Guedouar, and Noureddine Madaoui. Deposition and characterization of titanium aluminum nitride coatings prepared by rf magnetron sputtering. *Applied Surface Science*, 350:6–9, 2015.

29) Masahiro Kawate, Ayako Kimura Hashimoto, and Tetsuya Suzuki. Oxidation resistance of cr1-xalxn and ti1- xalxn films. *Surface and Coatings Technology*, 165(2):163–167, 2003.

30) O Knotek and T Leyendecker. On the structure of (ti, al) n-pvd coatings. *Journal of Solid State Chemistry*, 70(2):318–322, 1987.

31) T Leyendecker, O Lemmer, S Esser, and J Ebberink. The development of the pvd coating tialn as a commercial coating for cutting tools. *Surface and Coatings Technology*, 48(2):175–178, 1991.

32) TK Heckel, A Guerrero Tovar, and H-J Christ. Fatigue of the near-alpha ti-alloy ti6242. *Experimental mechanics*, 50(4):483–489, 2010.

33) Sudha Joseph, Trevor C Lindley, and David Dye. Dislocation interactions and crack nucleation in a fatigued near-alpha titanium alloy. *International Journal of Plasticity*, 110:38–56, 2018.

34) S Fujishiro and D Eylon. Improvement of ti alloy fatigue properties by pt ion plating. *Metallurgical Transactions A*, 11(8):1259–1263, 1980.

35) Paul S Prevey. A method of determining the elastic properties of alloys in selected crystallographic directions for x-ray diffraction residual stress measurement. *Adv. in X-ray Analysis*, 20:345–354, 1977.

36) BL Boyce, X Chen, JW Hutchinson, and RO Ritchie. The residual stress state due to a spherical hard-body impact. *Mechanics of Materials*, 33(8):441–454, 2001.

37) Peter Panjan, M Čekada, M Panjan, and D Kek-Merl. Growth defects in pvd hard coatings. *Vacuum*, 84(1):209–214, 2009.

38) H Elmkhah, TF Zhang, A Abdollah-Zadeh, KH Kim, and F Mahboubi. Surface characteristics for the tialn coatings deposited by high power impulse magnetron sputtering technique at the different bias voltages. *Journal of Alloys and Compounds*, 688:820–827, 2016.

39) Hao Du, Ji Xiong, Haibo Zhao, Yuemei Wu, Weicai Wan, and Linlin Wang. Structure and properties of tiallan films deposited at various bias voltages. *Applied surface science*, 292:688–694, 2014.

40) Grzegorz Greczynski, Jun Lu, MP Johansson, Jens Jensen, Ivan Petrov, Joseph E Greene, and Lars Hultman. Role of tin+ and aln+ ion irradiation (n= 1, 2) during ti1-xalxn alloy film growth in a hybrid hipims/magnetron mode. *Surface and Coatings Technology*, 206(19-20):4202–4211, 2012.

41) Huili Wang, Sam Zhang, Yibin Li, and Deen Sun. Bias effect on microstructure and mechanical properties of magnetron sputtered nanocrystalline titanium carbide thin films. *Thin Solid Films*, 516(16):5419–5423, 2008.

42) K Chu, PW Shum, and YG Shen. Substrate bias effects on mechanical and tribological properties of substitutional solid solution (ti, al) n films prepared by reactive magnetron sputtering. *Materials Science and Engineering: B*, 131(1-3):62–71, 2006.

43) G.P. Zhang, G.J. Gao, X.Q. Wang, G.H. Lv, L. Zhou, H. Chen, H. Pang, and S.Z. Yang. Influence of pulsed substrate bias on the structure and properties of ti−al−n films deposited by cathodic vacuum arc. *Applied Surface Science*, 258(19):7274 – 7279, 2012.

44) Magnus Odén, Claes Ericsson, Greger Håkansson, and Henrik Ljungcrantz. Microstructure and mechanical behavior of arc-evaporated cr–n coatings. *Surface and Coatings Technology*, 114(1):39–51, 1999.

45) JA Ruppen, D Eylon, and AJ McEvily. Subsurface fatigue crack initiation ofβ-annealed ti-6al-4v. *Metallurgical Transactions A*, 11(6):1072–1075, 1980.

46) AJ McEvily, S Ishihara, and Y Mutoh. 1989 dc-10 crash: A cold case mystery solved. *Engineering Fracture Mechanics*, 157:154–165, 2016.

47) MH El Haddad, KN Smith, and TH Topper. Fatigue crack propagation of short cracks. 1979.

48) W Shen, WO Soboyejo, and ABO Soboyejo. An investigation on fatigue and dwell-fatigue crack growth in ti–6al–2sn–4zr–2mo–0.1 si. *Mechanics of materials*, 36(1-2):117–140, 2004.

49) PH Tsai, TH Li, KT Hsu, JH Ke, JSC Jang, and JP Chu. Coating thickness effect of metallic glass thin film on the fatigue-properties improvement of 7075 aluminum alloy. *Thin Solid Films*, 677:68–72, 2019.

50) Chang Min Suh, Kyung Ryul Kim, Yong Goo Kang, Duck Young Suh, and Chang Keun Kim. Fatigue behavior of tin and ticn coated a rotor turbine steel. *International Journal of Modern Physics B*, 17(08n09):1527–1533, 2003.

51) KR Kim, CM Suh, RI Murakami, and CW Chung. Effect of intrinsic properties of ceramic coatings on fatigue behavior of cr–mo–v steels. *Surface and Coatings Technology*, 171(1-3):15–23, 2003.

52) Daisuke Yonekura, Atsushi Tsukuda, Ri Ichi Murakami, and Koji Hanaguri. Fatigue properties of nitride cr-mo steel with crn thin film deposited by aip method. *International Journal of Modern Physics B*, 17(08n09):1554–1559, 2003.

53) Takeshi Kasuya and Hideto Suzuki. Effect of film thickness on fatigue strength of tial alloy coated with tialn film at elevated temperature. In *Key Engineering Materials*, volume 297, pages 1446–1451. Trans Tech Publ, 2005.

54) WO Soboyejo, W Shen, J Lou, C Mercer, V Sinha, and ABO Soboyejo. A probabilistic framework for the modeling of fatigue in cast lamellar gamma-based titanium aluminides. *Mechanics of materials*, 36(1-2):177–197, 2004.

55) K Tuffy, G Byrne, and D Dowling. Determination of the optimum tin coating thickness on wc inserts for machining carbon steels. *Journal of Materials Processing Technology*, 155:1861–1866, 2004.

56) HJ Kolkman. Effect of tin/ti gas turbine compressor coatings on the fatigue strength of ti− 6al−4v base metal. *Surface and Coatings Technology*, 72(1-2):30–36, 1995.

57) FX Liu, Peter K Liaw, WH Jiang, CL Chiang, YF Gao, YF Guan, JP Chu, and PD Rack. Fatigue-resistance enhancements by glass-forming metallic films. *Materials Science and Engineering: A*, 468:246–252, 2007.

58) RR Boyer, JD Cotton, M Mohaghegh, and RE Schafrik. Materials considerations for aerospace applications. *MRS Bulletin*, 40(12):1055–1066, 2015.

59) Dinesh C Agrawal and R Raj. Measurement of the ultimate shear strength of a metal-ceramic interface. *Acta metallurgica*, 37(4):1265–1270, 1989.

60) P Bartolotta, J Barrett, T Kelly, and R Smashey. The use of cast ti- 48al- 2cr- 2nb in jet engines. *Jom*, 49(5):48–50, 1997.

61) Seol Jeon, Chester J Van Tyne, and Heesoo Lee. Degradation of tialn coatings by the accelerated life test using pulsed laser ablation. *Ceramics International*, 40(6):8677–8685, 2014.

62) H Oettel and R Wiedemann. Residual stresses in pvd hard coatings. *Surface and coatings technology*, 76:265–273, 1995.

63) PGRBR Chantikul, GR Anstis, Brian R Lawn, and DB Marshall. A critical evaluation of indentation techniques for measuring fracture toughness: Ii, strength method. *Journal of the American Ceramic Society*, 64(9):539–543, 1981.

Acknowledgement

First of all, I would like to thank for my advisor, Associate Prof. Yuichi Otsuka for his kind support, advice and all of the contributions for me during my studying and doing the research work in the doctoral program.

My pleasure to thank Prof. Emeritus Yoshiharu Mutoh, who gave me the opportunity to study in a doctoral program in Nagaoka University of Technology (NUT). His various kinds of supports and help are essential to complete my PhD works. I would like to thank Associate Prof. Yukio Miyashita for his kind support, comments and discussions on my research work and presentations at seminars. I also wish to express my sincere thanks to the doctoral examination committee members for their time, valuable comments and useful suggestions on my thesis work. I also wish to express my gratitude to Kobe Steel Co., Ltd and Mr. Kenji Yamamoto for providing me sufficient specimens to conduct my experimental work. I am thankful to all officers of machine center for their assistance in making specimens in time and cooperation during my fabrication work.I would like to thank Mr. Hoshino and all of machine shop staff for everything that they kindly supported for experimental works. For all of the lab members, I would like to thank for giving me a warm welcome, kindness and good memories while I was spending my life in Japan. I will be grateful to all of you. I am grateful to Kokusaika (Division of International Affairs) for sincerely taking care of us and arranging events throughout the year which helped me to experience Japanese culture, tradition, innovation and technology.

Special thanks to the all member of this laboratory for creating a friendly atmosphere and giving meaningful suggestions.

I am thankful to all of my family members for giving me the morale support.